FIELD INSTRUMENTATION AND LIVE LOAD TESTING TO EVALUATE BEHAVIORS OF THREE REINFORCED CONCRETE BRIDGE DECKS

by

Peter James Smolenski

A thesis submitted in partial fulfillment
of the requirements for the degree

of

Master of Science

in

Mechanical Engineering

MONTANA STATE UNIVERSITY
Bozeman, Montana

May 2004

APPROVAL

of a thesis submitted by

Peter James Smolenski

This thesis has been read by each member of the thesis committee and has been found to be satisfactory regarding content, English usage, format, citations, bibliographic style, and consistency, and is ready for submission to the College of Graduate Studies.

Dr. Jerry Stephens

Dr. Douglas Cairns

Approved for the Department of Mechanical Engineering

Dr. Vic Cundy

Approved for the College of Graduate Studies

Dr. Bruce McLeod

STATEMENT OF PERMISSION TO USE

In presenting this thesis in partial fulfillment of the requirements for a master's degree at Montana State University, I agree that the Library shall make it available to borrowers under rules of the Library.

If I have indicated my intention to copyright this thesis by including a copyright notice page, copying is allowable only for scholarly purposes, consistent with "fair use" as prescribed in the U.S. Copyright Law. Requests for permission for extended quotation from or reproduction of this thesis in whole or in parts may be granted only by the copyright holder.

Peter James Smolenski

May 17, 2004

ACKNOWLEDGEMENTS

This thesis would never have been completed without the wealth of support offered by so many people. First and foremost, I acknowledge God for the blessings of a good mind and a good attitude, which have brought me to this point. He has blessed me with a loving wife, Casey, who has stood by my side throughout these two years, and devoted parents who have always encouraged me to do my personal best and loved me regardless of the outcome.

I extend my thanks to Jerry Stephens and Eli Cuelho for their patience, guidance, encouragement and friendship throughout the Saco Bridge Project. None of this would be possible without their expertise or their oversight. Each of them has encouraged me toward excellence and bestowed gracious acknowledgements for a job well done. I would also like to thank Jeff Johnson for the intelligence, hard work, and quick wit he has brought to the many hours we've spent together on this project.

My gratitude is also extended to the Western Transportation Institute for funding my research through a graduate fellowship and offering me the opportunity to learn and grow in ways I might never have imagined.

TABLE OF CONTENTS

TABLE OF CONTENTS

LIST OF TABLES

LIST OF FIGURES

Figure Page

LIST OF FIGURES

LIST OF FIGURES

ABSTRACT

The deterioration of reinforced concrete bridges in Montana has prompted the Montana Department of Transportation (MDT) to investigate alternative bridge deck designs which minimize concrete cracking and subsequent steel corrosion. Construction was completed during the summer of 2003 on three new bridges near Saco, Montana that afford an unusually good opportunity to investigate the performance of different bridge decks. Notably, the bridges are in close proximity, and are of the same geometric design. The only differences between the bridges is the deck construction: one deck has a conventional concrete and conventional reinforcement layout; the second deck has a conventional concrete with a reduced amount of reinforcing steel; and the third deck has a high performance concrete (HPC) with conventional reinforcement layout. MDT contracted with Western Transportation Institute (WTI) at Montana State University to install strain instrumentation within each deck prior to pouring the deck concrete and to subsequently perform analyses on collected data. As part of the project, live load testing was performed on each bridge prior to opening them to traffic. The goal of this study was to evaluate and compare baseline performance of the three new bridge decks under live load demands. Data from the transversely-oriented strain gages cast in the decks were used for this purpose. This analysis found that all three decks performed equally well under vehicle loads, with only minor differences observed between them. None of the decks showed evidence of longitudinal cracking. The position of the neutral axis revealed that in-plane axial tension forces occurred in the decks during testing; internal compression arching was not observed at the load levels used in the tests. Transverse strains over the girders show no indication that cracking has occurred, nor do they suggest future cracking from vehicle loads. Using the geometry of each deck's cross-section and Girder Distribution Factors (GDFs), the relative stiffness of the three decks was compared. As expected, the deck with reduced reinforcing steel was determined to be the least stiff, both longitudinally and transversely. Based upon the applicability of superposition, all three decks were determined to behave linear-elastically. These observations serve as a baseline measure of performance for future analyses on these bridge decks.

CHAPTER 1

INTRODUCTION

The deterioration of transportation infrastructure in the United States is of great concern for bridge designers and researchers. Reinforced concrete bridges are among the most severely affected, and bridge decks are one of the primary components found to be deficient (Cao 1996). It is generally acknowledged across the country that the service life of bridge decks designed by traditional procedures is often shorter than desired, yet little research has been done to specifically address bridge deck performance. A majority of past research has focused on the behavior and performance of the girders in the superstructure.

The primary mechanism leading to deterioration of bridge decks is cracking of the deck concrete. Further damage results from seepage of corrosive agents through the cracks, causing corrosion in the reinforcing steel. Cracks are also susceptible to freeze-thaw damage: water enters the cracks and expands when frozen, thus widening the crack and increasing susceptibility to corrosion. Several methods have been devised to mitigate damage to reinforced concrete bridge decks. Among them are the uses of epoxy-coated rebar, the use of fiber-reinforced polymer (FRP) concrete, reducing the amount of reinforcing steel, sealing the surface of the concrete, and using concretes with special properties. Instrumented field testing on the performance of these measures has been sparse.

The Montana Department of Transportation (MDT) recently recognized a unique opportunity to directly compare the durability of bridge decks having different deck designs. Three bridges were scheduled for routine replacement along Route 243 north of Saco, Montana. Due to their close proximity along the same roadway, all three bridge decks are subjected to identical environmental conditions and identical traffic demands. All three bridges have the same global dimensions and were constructed by the same contractor. As such, all three bridges were completed in the summer of 2003 within two weeks of one another with similar quality of construction. The primary difference among them was the composition of the reinforced concrete deck. In this way, the variability in conditions that often surrounds field investigation of bridge performance is minimized for this case.

All three bridges utilize a concrete-slab-on-prestressed-girder configuration, with each bridge incorporating a different deck design. The first deck, referred to as the 'Conventional' deck, is the standard design used by the MDT Bridge Bureau, composed of a standard concrete with a standard layout of reinforcing steel. The second bridge deck, referred to as the 'Empirical' deck, was designed to use the standard concrete mixture, but the volume of steel was reduced throughout the bridge deck. This alternative reinforcement layout was determined using the empirical design guidelines in the American Association of State Highway and Transportation Officials (AASHTO) LRFD Specification for Highway Bridges (*AASHTO* 2000). The third deck design, referred to as the 'HPC' deck, was designed with the same volume and configuration of

reinforcement as the Conventional deck, but utilized a High Performance Concrete (HPC). All three bridge decks used epoxy coated rebar throughout.

Overall, the Saco Bridge Project (being conducted by Western Transportation Institute) aims to identify any differences in structural behavior and durability that might exist due to the incorporation of these different damage mitigation techniques into the deck designs. To realize this goal, a comprehensive study of the three bridges was necessary. Strain gages and temperature sensors were embedded into the bridge decks at the time of their construction to monitor internal conditions over the duration of the Saco Bridge Project. To establish relative performance among the bridges, monitoring will occur over several years in response to ambient changes and traffic usage. Additionally, two live load experiments are being conducted to aid in evaluating the relative response of each bridge deck due to truck loads. The first live load test was conducted in July 2003, before the bridges were open to traffic; the second is scheduled for the summer of 2005. The objective of this thesis is to use strain data from the 2003 live load tests to evaluate and compare the performance of three different concrete bridge decks in their baseline conditions. The three bridge decks studied in this investigation are:

- the Conventional deck: a deck composed of a standard concrete mix and a conventional reinforcement layout, designed and constructed following standard practices of MDT's Bridge Bureau,
- the Empirical deck: a deck composed of a standard concrete mix with a reduction in the volume of steel reinforcement, designed following the empirical design approach presented in AASHTO (2000) and constructed following standard MDT practice, and
- the HPC deck: a deck utilizing a high performance concrete (HPC) developed following FHWA guidelines with a conventional reinforcement layout.

CHAPTER 2

LITERATURE REVIEW

Reinforced concrete has emerged as a highly versatile building material in the modern age. For certain applications, it has several advantages over other building materials. Due to the combination of the steel and the concrete, the structure is effectively strong under both tensile and compressive demands. This strength is offered at a significantly reduced cost from steel alone. Additionally, reinforced concrete may be formed into countless structural and aesthetic forms not readily available when using steel or other building materials. As with all materials, reinforced concrete's benefits are accompanied by handicaps. The concrete matrix is susceptible to brittle fracture, while the steel is susceptible to corrosion damage.

Historically, as the use of reinforced concrete became more widespread, it was important to test and understand its physical properties and behaviors under loading conditions. Due to the deterioration of transportation infrastructure in the United States, a renewed interest has emerged toward understanding reinforced concrete specifically as it applies to highway bridges (Lenett, et al. 2001).

Cao (1996) cites that about one-third of the nation's bridges have deficient decks. In this regard, one of the major problems that bridge decks face is corrosion of the reinforcing steel. This damage is generally initiated by cracking of the concrete in the top of the deck. The cracks allow moisture, deicing chemicals, and air to reach the steel and begin the oxidation process. When steel corrodes, it debonds from the concrete, thereby

losing the structural value of the material's composite nature. Furthermore, due to the expansive nature of the corrosion products, and the relatively low tensile strength of concrete, portions of the deck can subsequently spall as the corrosive activity proceeds. Possible solutions to this problem are under investigation and include the use of epoxy-coated rebar, fiber-reinforced polymer (FRP) reinforcement, fiber-reinforced concretes (FRC), low-permeability concretes, and reduced amounts of reinforcement (Cao 1996; Bakht, et al. 2000). To date, full-scale field testing of these damage mitigation techniques has been sparse.

Bridge Deck Design Considerations

The deck-on-girder design is comprised of a concrete deck supported by two or more girders made of steel, timber, or prestressed concrete, and is one of the most common bridge designs in use today (Cao, et al. 1996). In this configuration, the deck directly supports tire loads, transferring them transversely to the adjacent girders. Using shear connectors, the deck is compositely attached to the girders. The girders act in conjunction with the composite deck to resist longitudinal moments and transfer loads to the supporting substructure.

Traditionally, the AASHTO (2000) bridge deck design method assumes that slab-on-girder deck sections behave as one-way slabs acting in the transverse direction (perpendicular to traffic). Based on the work of Westergaard in 1930, the deck is designed as a continuous beam supported by rigid girders, which are unable to deflect vertically (Mourad and Tabsh 1999; Csagoly and Lybas 1989; Cao, et al. 1996). It is

generally acknowledged that Westergaard's model yields conservative designs relative to strength and safety. More recent research has sought to make deck design more efficient by more accurately modeling the actual load carrying mechanisms. The discovery of a mechanism called "internal arching" offers designers and researchers greater the ability to develop strong designs with a lesser amount of reinforcing steel than is required in conventionally designed decks. In an attempt to mitigate damage as well as improve efficiency, reductions in the amount of reinforcing steel has become a popular concept. Reducing or removing steel, especially in the top mat, reduces the susceptibility of the deck to damage from steel corrosion and the subsequent debonding and spalling of the concrete.

Canada developed a deck design that takes advantage of this arching behavior, commonly referred to as the 'Ontario' deck design. For bridge decks fulfilling certain geometric criteria, the Ontario approach allows the total amount of reinforcing steel to be reduced by approximately 30%. The primary design guideline requires a minimum steel area of 0.3% of the concrete area in both the top and bottom reinforcing mats to help control cracking and maintain confinement within the deck. Based on component testing and finite element analysis (FEA), AASHTO (2000) has included provisions for the 'empirical design', which is similar to the Ontario deck design, except that a further reduction in the top layer of reinforcing steel is allowable, requiring a minimum top-mat steel area of 0.2% of the concrete area. A minimum bottom-mat steel area of 0.3% of the concrete area is required for improved crack control and to maintain confinement within the deck.

Contrary to traditional models, the deck slab does not actually support wheel loads completely in flexure. Instead, a 'compressive dome' forms due to cracking in the positive moment regions (i.e., bottom fibers) of the deck concrete (Csagoly and Lybas 1989; Fang, et al. 1990; *AASHTO* 2000). This 'compressive dome' supports wheel loads by relying upon the lateral restraint provided by the surrounding deck concrete and other structural elements such as girders and diaphragms. Additionally, there remains a small flexural load-carrying component, which is resisted by the prescribed 0.3% steel in the bottom reinforcing mat (Csagoly and Lybas 1989). In-plane compressive membrane forces found in the concrete near the tire generally helped to establish the presence of the arching phenomenon.

To evaluate the validity of the internal arching behavior, Fang, et al. (1990) tested a full-scale bridge specimen at the University of Texas at Austin. The deck concrete had a compressive strength of approximately 29 MPa. At wheel loads up to three times the AASHTO service wheel load of 92.5 kN, no compressive membrane stresses (indicative of internal arching) were observed. However, membrane tension was observed up to this point. Above this load, cracking began to occur in the positive moment regions of the slab, marking the onset of internal arching. Internal arching and failure in punching shear were also observed in the specimen at higher loads, as expected.

To further validate the credibility of the empirical deck design method, Csagoly and Lybas (1989) reviewed several research projects related to internal arching behavior in bridge decks. One laboratory experiment proved that bridge decks with two mats of reinforcement fail in punching shear at loads six times larger than the design wheel load.

All of the reviewed studies confirmed that the ultimate capacity and serviceability of the empirical deck design is comparable to the traditional deck design methods.

Fenwick and Dickson (1989) performed laboratory testing on reinforced concrete slabs to investigate structural benefits from membrane action. Without further testing, they were unable to conclusively establish the relationship between membrane action and increased strength. However, their results indicated increased strength in confined plates, suggesting membrane action was possibly contributing to load carrying capacity.

A more aggressive approach to mitigating steel corrosion is to completely remove all steel from the top mat, as proposed by Cao (1996). The slab theory of Westergaard requires the placement of reinforcing steel near the top of the deck to resist negative moments that occur over the girders. However, Cao (1996) concluded that slab theory alone was not sufficient for use in deck design. Due to the underlying differential deflections between girders, the negative moments incurred in the deck slab were less than those predicted by a slab supported on rigid girders. Cao, et al. (1996) performed live load testing on the South Platte River Bridge near Commerce City, Colorado to evaluate this conclusion. Results showed that the top mat of reinforcing steel was not necessary to withstand the negative bending moment over the girders induced by truck loads. Although the conclusions of Cao (1996) have not been included in the bridge design provisions of AASHTO (2000), Cao's findings have important implications for properly interpreting live load testing results and should be taken into consideration.

Canada has taken the most aggressive approach to steel reduction by designing steel-free decks, which take advantage of arching action to completely eliminate all of the

reinforcing steel within the deck (Bakht and Lam 2000; Sargent, et al. 1999; Bakht and Mufti 1998). In lieu of the internal steel reinforcement, exterior steel 'straps' are connected between adjacent girders to provide the lateral confinement necessary to maintain arching action. Other 'steel-free' deck designs utilize fiber-reinforced polymer (FRP) bars or grids within the deck concrete in place of traditional steel rebar (Bakht, et al. 2002). Both steel-free methods effectively mitigate any damage due to corrosion by complete removal of the corrosive medium (i.e, steel), regardless of concrete integrity.

Live Load Testing of Bridges

For any deck design, it is important to evaluate how that deck responds to loading from vehicles and how that response affects the expected durability of the deck over time. In this regard, a reduction in the amount of steel could have some influence on the load-carrying capacity. Although the susceptibility to cracking and corrosion are reduced, it is not eliminated and the integrity of the concrete under loads is of great importance. One method of evaluating the behavior and integrity of a bridge deck is to perform live load tests. In the past, a majority of bridge tests involving deck-on-girder designs have focused mainly on the girder system and how loads are distributed amongst these members. These studies have generally attempted to quantify the load carrying capacity of the bridge based on properties of the girders, and how loads are globally transferred through the superstructure and the substructure to the ground. In this regard, girder distribution factors (GDFs) are commonly reported as a measure of bridge performance

(Nassif, et al. 2002; Tabsh and Tabatabai 2001; Yang and Myers 2003; Amer, et al. 1999).

Despite the acknowledgment that bridge decks are a primary source of deficiency, very few projects have focused specifically on the internal response and the durability of the bridge deck under live loads and environmental loads. A limited number of projects have investigated the deck, but only as a small part of a larger study. For example, Lenett, et al. (2001) installed instrumentation and conducted live load testing on the HAM-126-0881L bridge near Cincinnati, Ohio. The instrumentation for the project was extensive, monitoring nearly every aspect of the bridge – abutments, piles, stringers, and the deck. Most deck sensors were placed longitudinally and used to construct strain profiles in the deck-girder composite sections. Monitoring was conducted during construction of the bridge to evaluate what effects the bridge experienced prior to being commissioned. Before servicing traffic, the bridge was subjected to live load testing with mostly static truck load tests. Reported results primarily focus on the bending stresses in the girders, and the distribution of longitudinal strains across transverse strips of the deck. The response of the bridge to environmental fluctuations was then monitored over at least one full year.

Stallings and Porter (2002) performed live load testing on the Uphapee Creek Bridge in Alabama, in which some measurements specifically of the deck response were made. This structure is a high performance concrete (HPC) bridge. Comparisons of test results against AASHTO predictions were of greatest interest to the authors. Although deck strains recorded from transverse reinforcing gages were measured and reported, no

analysis was performed and little comment was offered with regard to their meaning. Typical deck strain results reported by Stallings and Porter are shown in Figure 1. The graph shown in this figure represents internal deck strains recorded from gages located at the longitudinal midspan and transversely between two girders; the "TT" and "BT" designations refer to transverse top and bottom gages, respectively; the "TL" and "BL" refer to longitudinal top and bottom gages, respectively.

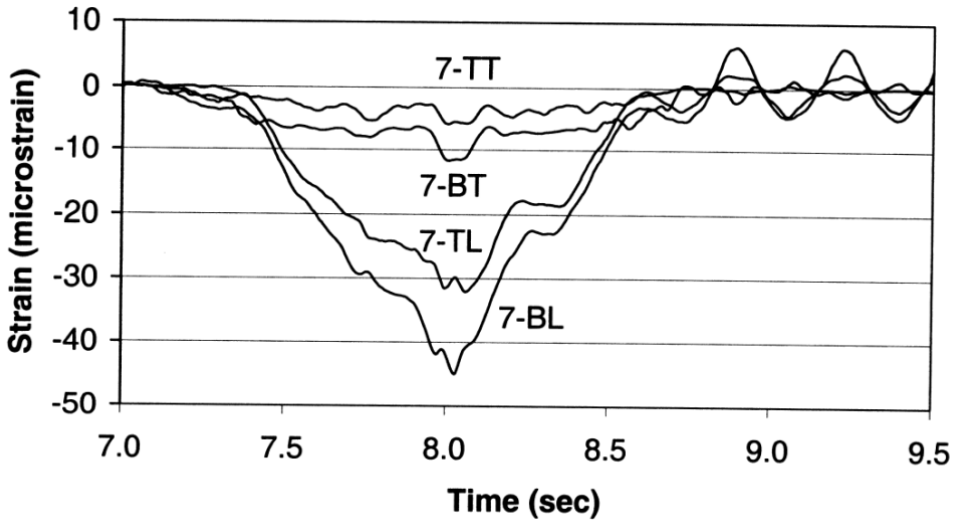

Figure 1 Reported deck strains at midspan (Stallings and Porter 2002)

Cao (1996) performed live load testing on the South Platte River Bridge near Commerce City, Colorado to validate a simplified method for analyzing and modeling the behaviors of reinforced concrete bridge decks. The bending moments incurred in the bridge deck were calculated from strain data. This analysis helped to verify his hypothesis that the negative moments in the bridge deck are reduced due to differential girder deflections.

CHAPTER 3

DESCRIPTION OF BRIDGES

The three new bridges that are the subject of this investigation were constructed on Route 243 approximately one mile north of Saco, Montana. Route 243 is a local route that has an average annual daily traffic count of 220 (1998), with 11.5% being trucks. Much of the structurally significant loading is anticipated to come from heavy farm machinery and commercial trucks, which can impose high demands.

All three bridges are 44.5 meters long and 9.1 meters wide. The superstructure consists of three spans, as shown in the elevation drawing of Figure 2. Each deck is supported by identical superstructure components: four prestressed concrete girders across the width. The girders are standard, Type-I prestressed concrete I-beams spaced at 2.4 meters on center, as shown in the cross-section view of Figure 3. The thickness of each deck is 210 mm. Each deck is continuous over the bents and is compositely integrated with the supporting girders using shear connectors. Integral abutments are utilized in each design, as well.

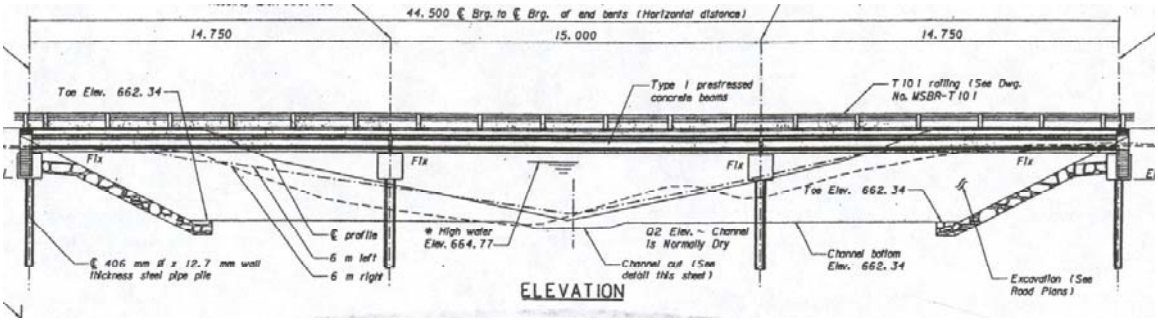

Figure 2 Elevation view of the three Saco bridges (typical)

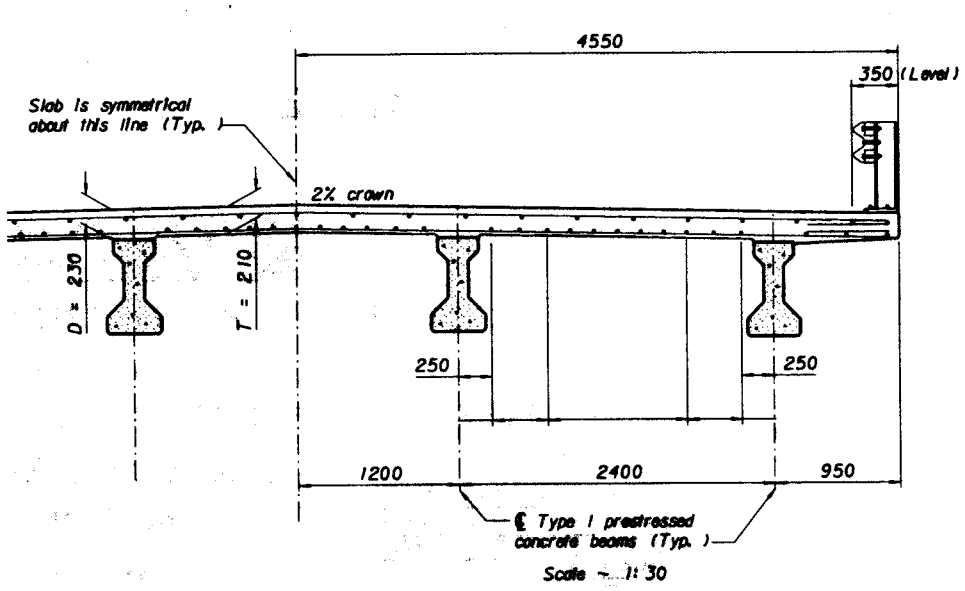

Figure 3 Partial cross-section view of the superstructure of the Saco bridges (typical)

The primary difference between the three bridges is the composition of the deck. Concrete mix design specifications for the Conventional and Empirical decks required 21 MPa strength concrete, while the HPC deck design specified 28 MPa strength concrete. Concrete testing performed after bridge construction was used to determine the actual compressive strength of the concrete for each bridge deck. All tests were performed on standard compression cylinders that were 152 mm in diameter and 305 mm tall. The compressive strength for each bridge is reported in Table 1, tested both 28 days after deck pouring and at the time of the live load testing (approximately 6 weeks after the decks were poured).

Table 1 Average compressive strengths of deck concretes

Deck	28-day Compressive Strength (MPa)	Live Load Testing Compressive Strength (MPa)
Conventional	31.6	37.7
Empirical	27.4	32.9
HPC	46.2	49.2

All three decks use epoxy-coated reinforcing steel, but the layout of the reinforcement varies between the three decks. The Conventional and HPC decks are designed using the traditional strength approach described in the AASHTO bridge specifications (2000). The traditional strength design method treats the deck as if it were a beam in flexure supported by the girders. This design results in the primary reinforcement being oriented transversely to the direction of traffic. As such, the transverse area of steel in the Conventional and HPC decks is 12.33 cm^2/meter in each of the top and bottom mats.

AASHTO (2000) also allows bridge designers to utilize the empirical design approach for monolithic concrete bridge decks that satisfy specific conditions (also referred to as the Ontario bridge deck design). No formal analysis is required when using this design method. Instead, reinforcement ratios for the top and bottom mat in both the longitudinal and transverse directions are simply a function of the depth of concrete and length of span. AASHTO (2000) specifies the longitudinal and transverse reinforcement directions to have identical steel areas, with a specified minimum reinforcement ratio of 0.2 percent steel in both directions for the top mat and 0.3 percent steel in the bottom mat. In this case, these requirements correspond to an area of steel in the cross-section of 3.8 cm^2/meter for the top mat, and 5.7 cm^2/meter for the bottom mat. The amount of steel is

increased in the bottom mat to improve flexural resistance and to control cracking in the positive bending regions of the slab. Comparatively, the Empirical deck requires 3679 kg less steel than the Conventional and HPC decks (approximately 30% less). Besides the obvious initial cost savings, reducing the amount of steel in the Empirical deck, especially in the top layer, decreases the susceptibility to corrosion, thereby decreasing long-term costs associated with maintenance, repair, and replacement.

Another notable modification in the Empirical design is the exclusion of extra longitudinal steel in the continuous deck section over the bents (included in both the Conventional and HPC deck designs). The top fibers of the deck concrete in this region are susceptible to cracking due to negative bending moments in the longitudinal direction. Although the susceptibility to corrosion is diminished by the removal of this steel, the longitudinal stiffness of the deck is also expected to decrease.

CHAPTER 4

INSTRUMENTATION

General Layout

The instrumentation in the Saco Bridge Project was configured to fulfill multiple project goals. The two primary objectives were to observe both long-term environmental and short-term live load deck responses. Also, it was desirable to separately monitor the strains in the concrete and in the reinforcing bars, especially in areas prone to cracking. To meet these objectives, the instrumentation was also developed to be durable, reliable, adaptable, and redundant.

In the early stages of the Saco Bridge Project, a three-dimensional analytical model of the bridges was created using the Visual Analysis finite element package to aid in selecting critical instrumentation locations (French 2002). The bridge deck was represented by 4-node plate elements, while the girders were represented by beam elements. The deck and girder elements were linked together by stiff beam elements to simulate the composite action of the deck-girder superstructure system. The model was loaded with point loads at nodes corresponding to standard tire-spacing dimensions of a three-axle truck. By positioning the truck loads at several longitudinal and transverse locations of interest, locations of critical stresses were identified from stress contour plots. Gage locations were selected to: 1) capture the extreme response, 2) characterize the response in general, and 3) characterize the response at specific features/locations of

interest. For added verification, preliminary instrumentation locations were compared with locations chosen by other researchers in similar bridge test studies. (French 2002).

To identify precise locations for instrumentation, envelopes of extreme fiber stresses were generated for the bridge deck. These stress envelopes were produced for both the longitudinal and transverse directions. Using this information, specific reinforcing bars within these areas were selected to be instrumented with strain gages. If appropriate, embedded instrumentation was placed near these instrumented bars to record concrete strains and to duplicate and augment strain information from the instrumented rebar. Subsequently, a formal instrumentation plan was generated that detailed gage type, location, and expected level of response (Cuelho, et al. 2004).

The final instrumentation suite utilized three types of instrumentation to monitor strains within the bridge decks. Each of the three bridge decks contains 35 strain gages bonded directly to the reinforcement, 9 strain gages embedded in the concrete, and 20 vibrating wire gages embedded in the concrete. The vibrating wire gages are also capable of monitoring local deck temperatures. During live load testing only, 4 Intelliducers™ from Bridge Diagnostics, Inc. (BDI) were temporarily attached to the underside of the girders. A detailed description of each of these technologies is provided in a later section below.

The approximate positions of the longitudinal deck gages and transverse deck gages are indicated by the black rectangles in Figures 4 and 5, respectively. Positions of the BDI gages are shown in the plan view of Figure 6. Generally, the gages have been placed within a single span and within a single traffic lane, covering approximately $1/6^{th}$

of each bridge deck (southwest corner in Figures 4, 5, and 6. The southernmost span of the southbound lane of each bridge is instrumented for this project. This span was selected to minimize dynamic effects from southbound traffic, as it is furthest downstream. Deck gages in the longitudinal direction primarily provide information about global behavior of the bridge. The transverse deck gages are focused in the area between the diaphragm and the bent, providing information about local deck behaviors. Most locations have gages located in the planes of both the upper and lower reinforcing mats. Overall, the selected gage locations provide data regarding:

- girder-bent interaction,
- bending across the bent,
- effects of the diaphragm,
- continuity effects,
- global bending,
- effect of saw cut over the bents, and
- local deck behavior.

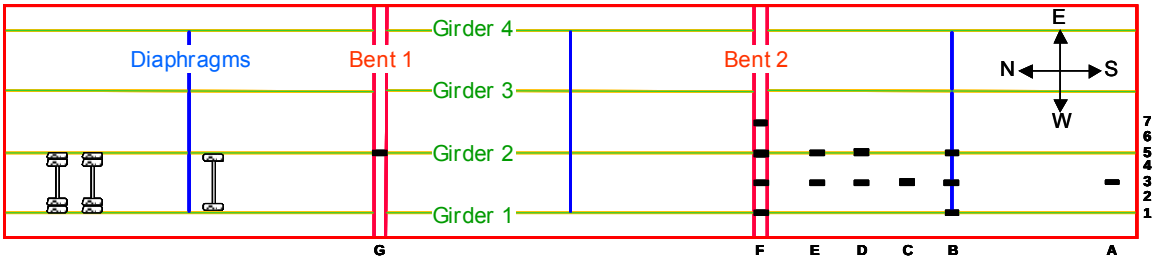

Figure 4 General positioning of longitudinal deck gages (plan view)

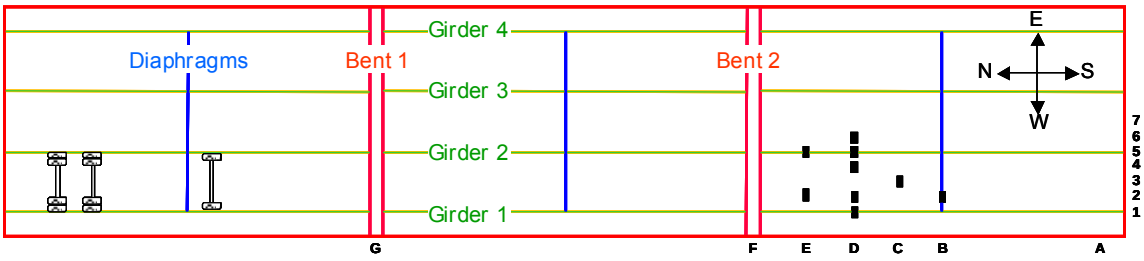

Figure 5 General positioning of transverse deck gages (plan view)

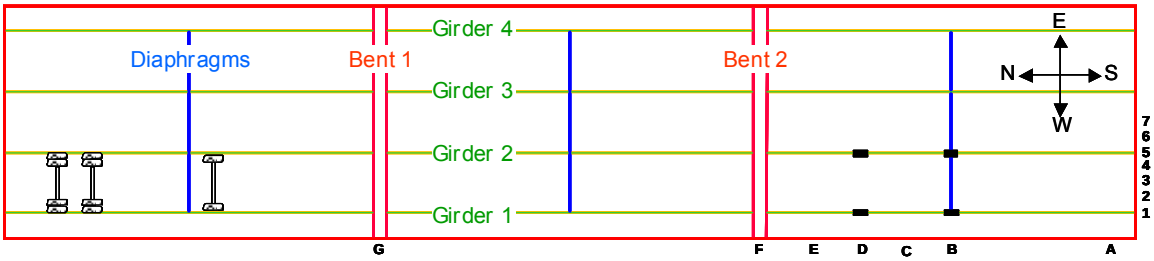

Figure 6 General positioning of BDI gages on the bottom of girders (plan view)

Position-Referencing Nomenclature

A reference numbering system was created to help organize and distinguish each gage based on its location, orientation, type, and relative position. An example of this six-character label is provided in Figure 7. The bridge deck in which the sensor is embedded is denoted by Conventional 'C', Empirical 'E', or HPC 'H'. Gages are oriented either longitudinally 'L' or transversely 'T' with respect to the direction of traffic. The gage type is either a strain gage bonded to the reinforcement 'R', vibrating wire strain gage 'V', or concrete embedment strain gage 'E'. Gage positions are referenced from the southwest corner of the bridge. The letters A through G denote longitudinal distances from the south end of the bridge. The numbers 1 through 7 denote transverse positions of

the gages from the west side of the bridge. Finally, the vertical position of each gage within the deck cross-section is described as bottom 'B', middle 'M', or top 'T'.

Altogether, the gage numbering system consists of six unique characters. The example provided in Figure 7 (C-LV-F-3-B) corresponds to a **L**ongitudinally oriented **V**ibrating wire gage within the **C**onventional bridge deck, located at Gage Line **F** (approximately 14.625 meters from the south end), transverse position **3** (approximately 2.15 meters from the west side), and in the plane of the **B**ottom mat of reinforcement. These unique reference numbers are used throughout the remainder of the report to identify specific gages.

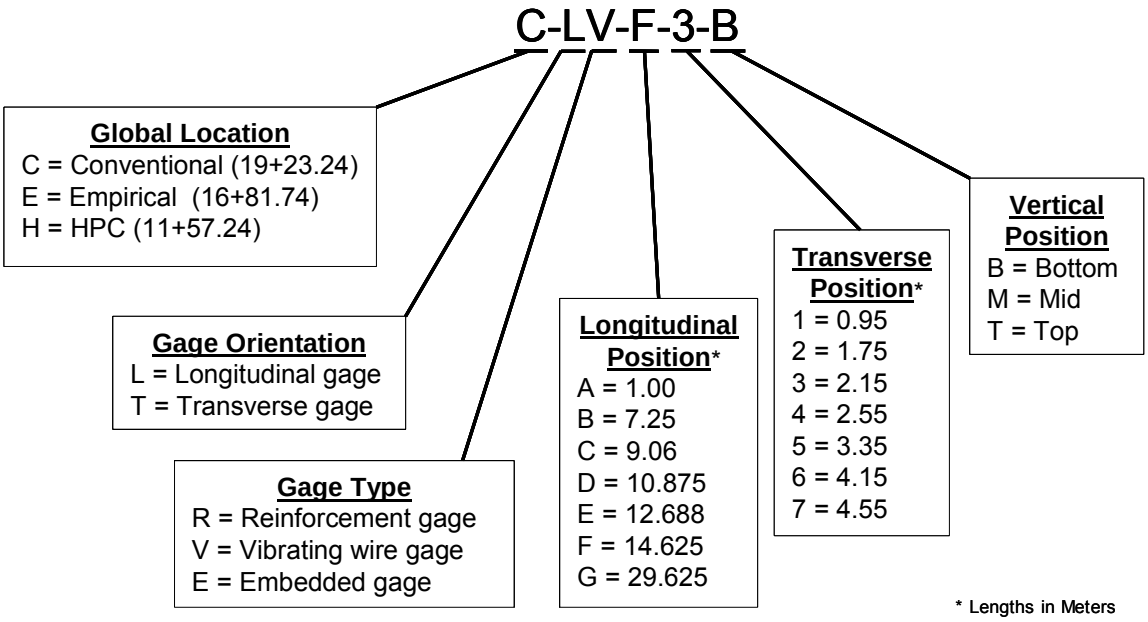

Figure 7 Gage reference numbering system

Sensors

Vibrating Wire Strain Gages

Vibrating wire strain gages are an integral part of the instrumentation system for long-term monitoring of concrete strains. The vibrating wire gages were *not* recorded during live load testing due limitations on the rate at which they can acquire data. The 20 vibrating wire strain gages in each deck are Geokon Model VCE-4200 gages. A typical installation of three gages suspended through the depth of the deck prior to pouring the concrete is shown in Figure 8. They are embedded in the bridge decks for long-term monitoring of concrete strains and temperatures. As shown in Figure 8 (inset), this standard model has a gage length of 153 mm, capped with endplates of diameter 19 mm. The operable range of the gage is 3000 microstrain (με), with a published sensitivity of 1 με. They are designed to be embedded directly in concrete and are typically used to monitor long-term strain in structures such as foundations, piles, bridges, dams, containment vessels, and tunnel liners. As of May, 2004, only 3 vibrating wire strain gages had quit working, giving these sensors a 95% survival rate, the highest of the three internal deck sensor types.

The vibrating wire technology employs a steel wire, stretched in tension between two circular end plates. As the surrounding concrete contracts or expands, the tension in the wire is changed, thereby changing the resonant frequency of vibration of the wire. The wire is excited with a range of frequencies using an electromagnetic coil. The wire then vibrates at its resonant frequency, which is detected by the electromagnetic coil.

Frequencies detected by the coil are converted to a DC voltage (using a Campbell Scientific, Inc. AVW1 unit) and recorded by the datalogger. The AVW1 unit will only accommodate a single vibrating wire gage at one time. Using a multiplexer, up to 16 vibrating wire gages may be sequentially converted and recorded. The time required for the frequency sweep and the slow speed of the multiplexer makes it impractical to log data from the vibrating wire gages during the live load testing with a moving vehicle.

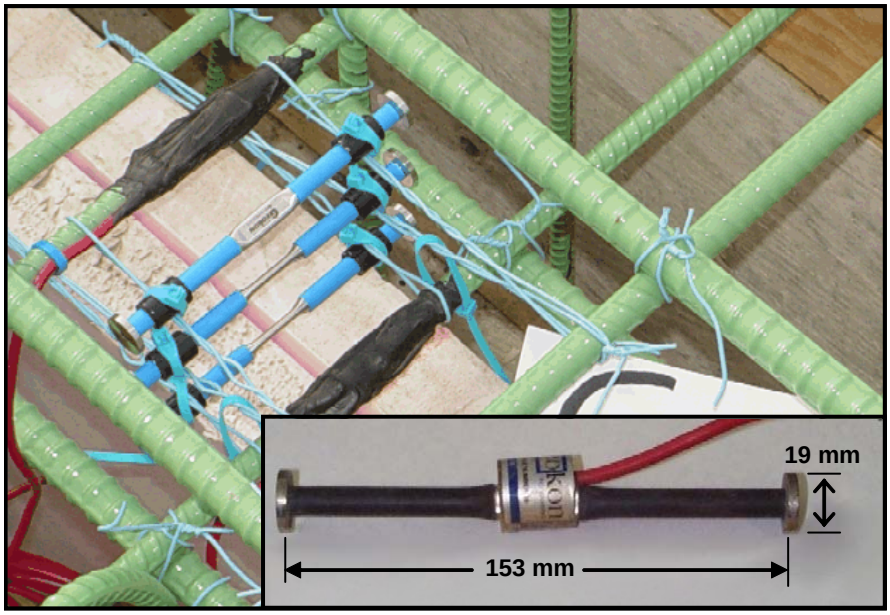

Figure 8 Vibrating wire strain gage (VCE-4200) installation; Inset: dimensions

Each vibrating wire gage is also equipped with a thermistor that measures temperature at the gage. These measurements are used to apply temperature corrections to measured strains. The need for the temperature corrections arises from the disparity between the thermal expansion coefficients of steel and concrete.

Using specially coated steel wire, each vibrating wire strain gage was suspended in the concrete between the reinforcing bars (see Figure 8). A protective rubber padding

was also placed between the gage body and the tying wire. The rubber padding provides damping to minimize resonant vibrations in the steel wire and rebar cage.

Concrete Embedment Strain Gages

The nine embedded gages used to monitor strains in the concrete of each bridge deck are Concrete Embedment Gages (EGP-5-350), fabricated by Micro-Measurements Group, Inc. These gages are specially designed to measure strains inside concrete structures. The outer dimensions of an Embedment strain gage are shown in Figure 9 (inset). Each embedment gage contains a single 350 ohm (Ω) bonded-foil resistance gage, functionally similar to those described in the following section. The sensing grid has an active gage length of 100 mm and is self-temperature-compensated to minimize thermal output when installed in concrete structures. The gage is encased in a proprietary polymer body to protect it from corrosion, moisture and mechanical damage during construction and use. The outer body has a length of 130 mm and is dimpled to ensure proper engagement with the surrounding concrete. Since the sensing gage is also a bonded-foil resistance gage, the Embedment strain gages also require a Wheatstone Bridge circuit for sensing, described later in this chapter.

A typical installation of three embedded gages through the depth of the bridge deck is shown in Figure 9. Similar to the installation of the vibrating wire strain gages, the Embedded gages were suspended in the plane of the appropriate rebar mat using a plastic-coated steel wire.

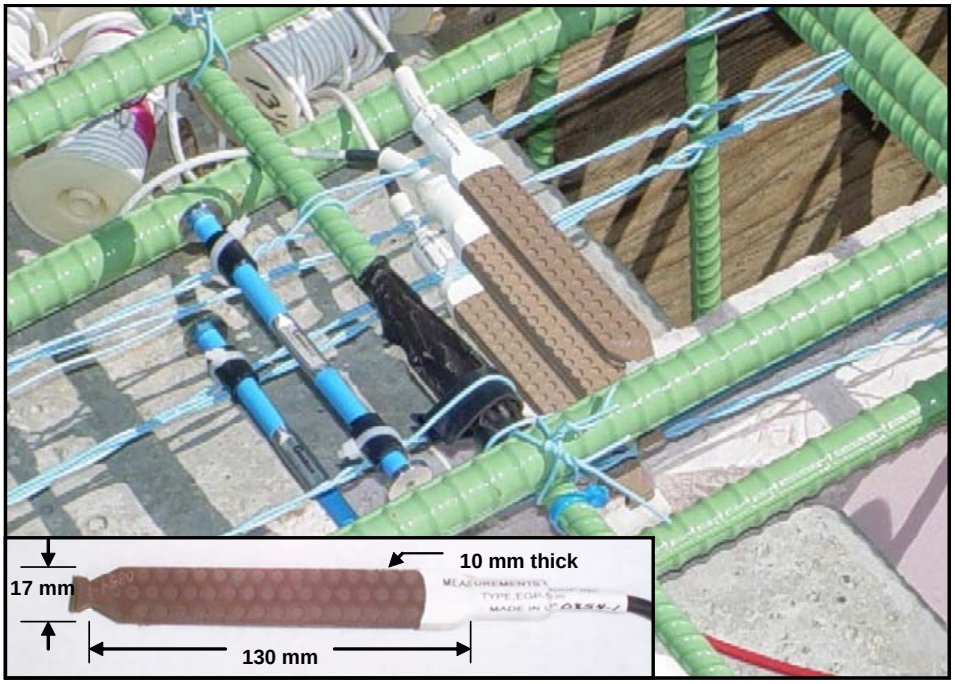

Figure 9 Concrete Embedment stain gage (EGP-5-350) installation; Inset: dimensions

During implementation and usage, the embedment strain gages suffered the worst mortality, having only a 56% survival rate. Many of the Embedment gages were located in the continuous deck over the bent, which cracked in all three decks several days after the deck concrete was poured. Cracking of the continuous deck over the interior bents is not uncommon. The cracking likely occurred due to flexural bending and axial stresses in response to diurnal temperature changes. At the crack, strains exceeded the maximum strain threshold of the Embedment gage, rendering them unusable.

Reinforcement Gages

Local strain in the steel reinforcement was measured using 35 bonded-foil resistance strain gages. These strain gages were bonded directly to the top and bottom surfaces of the reinforcement using a special epoxy. Bonding them to both the top and bottom

surface electronically negates any local bending effects in the bar, such that only pure axial tension strains are recorded.

Bonded-foil resistance strain gages are composed of a thin layer of foil, which is bonded atop a thin polymer backing; the foil acts as an electrical resistor. When applied to a material's surface, changes in the length of the gage result in an identical change of length of the foil. These length changes result in a change in the electrical resistance of the gage. Such changes are quite small and are generally detected using a special circuit arrangement called a Wheatstone Bridge, as discussed below.

The strain gages were Micro-Measurements Group, Inc., type CEA-06-250UN-350. A resistance strain gage prior to installation is shown in Figure 10. CEA gages are general-purpose gages made of constantan that are widely used in experimental stress analysis. The foil grid is fully encapsulated and includes exposed copper-coated integral solder tabs. The temperature range over which these gages will self-temperature-compensate is -75° to +175° C for static measurements on steel. The active gage length of these gages is 0.250 inches and their resistance in is 350Ω ±0.3%. Strain in these gages should not exceed approximately ±5000 με and fatigue life is reported as 10^5 cycles at ±1500 με.

The gages were mounted on the reinforcing steel in laboratories at Montana State University. The instrumented bars were then shipped to the bridge site at Saco, Montana and tied into the decks at the appropriate locations. The strain gage application process followed several steps, including:

- locating and marking the desired location,

- grinding away the epoxy coating and steel ribs on the bars to expose a smooth bonding surface,
- cleaning and neutralizing the area,
- gluing the gage onto the bar,
- soldering the lead wires to the gage,
- cleaning the area of any contaminants, and
- covering the area with a coating to provide environmental and mechanical protection.

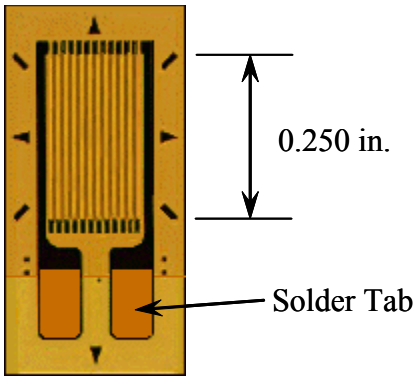

Figure 10 Bonded foil resistance strain gage (CEA-06-250UN-350; not to scale)

A two-part, medium viscosity epoxy (M-Bond AE-10) was used to attach the gages to the reinforcing steel. This epoxy system is highly resistant to moisture and chemicals and is used for general-purpose stress analysis, with improved longevity over other epoxies. After gage application, cure time for the epoxy was about six hours at 24° C.

A two-part polysulfide liquid polymer compound (Micro-Measurements M-COAT J) was used to environmentally protect the strain gages from damage, both during and after construction. This tough, flexible, black coating was mixed and applied over the strain gaged area in the lab and allowed to dry overnight. M-COAT J provides protection

against oil, grease, most acids and alkalis, and most solvents. A strain gage bonded to the reinforcement both before and after the environmental protection was applied is shown in Figure 11.

These particular gages proved to be quite durable, with a survival rate of 85%. Similar to the Embedment gages, the reinforcing gage locations experienced the greatest losses over the bents. Losses were sustained at a few other gage locations, which could have occurred during installation or due to wire breaks.

BDI Intelliducers™

During the live-load experiments only, four Intelliducers™ were temporarily mounted on the bottom of the girders of each bridge using a special quick-drying adhesive. Intelliducers™ are pre-manufactured by Bridge Diagnostics, Inc. (BDI) of Boulder, Colorado, and are used to measure strain at the surface of structural elements. They are made of aluminum and have a 76.2mm (3 inch) effective gage length. In concrete applications, extensions are often used to determine strains over a greater span. For this application, a 228.6mm gage length was used (Figure 12). The extensions are used to obtain an average strain in the event cracking occurs in or near the gaged zone, which would affect the gage response. The dimensions of an Intelliducer™ without an extension are shown in Figure 12 (inset). The internal circuitry consists of a full Wheatstone Bridge with four active 350Ω resistance gages. Thus, no external circuitry is required to operate or monitor them. During use, the datalogger provided a 5V input voltage and read the output on its differential terminals. BDI states that the gages have

an accuracy of ± 2%, a range of ±4000 με, and should not be used below 30 με. The BDI gages suffered no mortality over the duration of the live load tests.

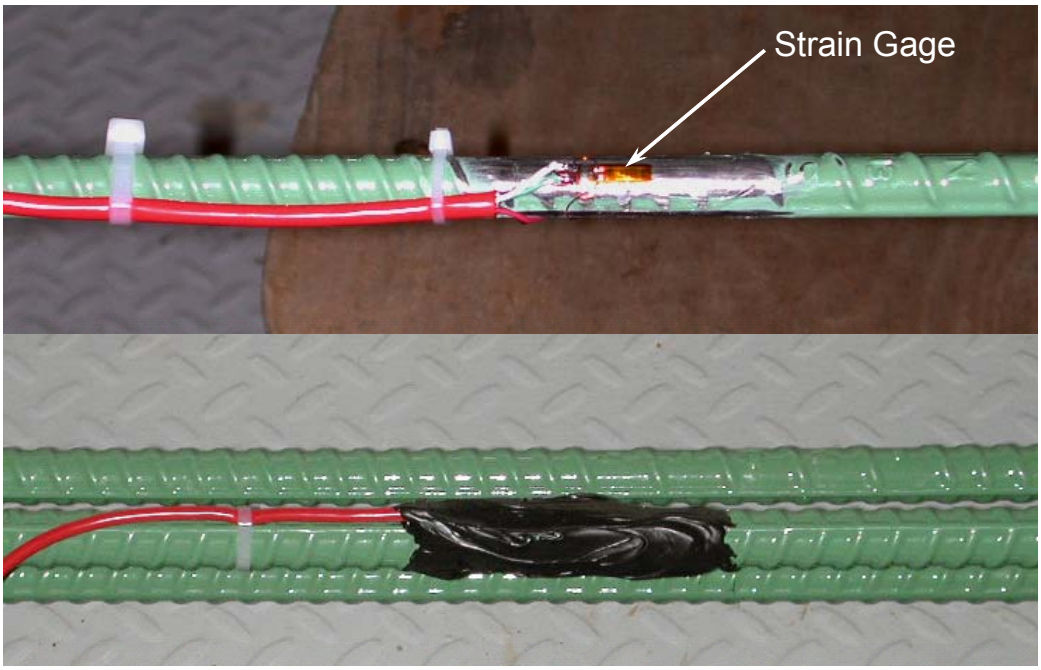

Figure 11 Strain gage bonded to the reinforcement before (top) and after (bottom) environmental protection

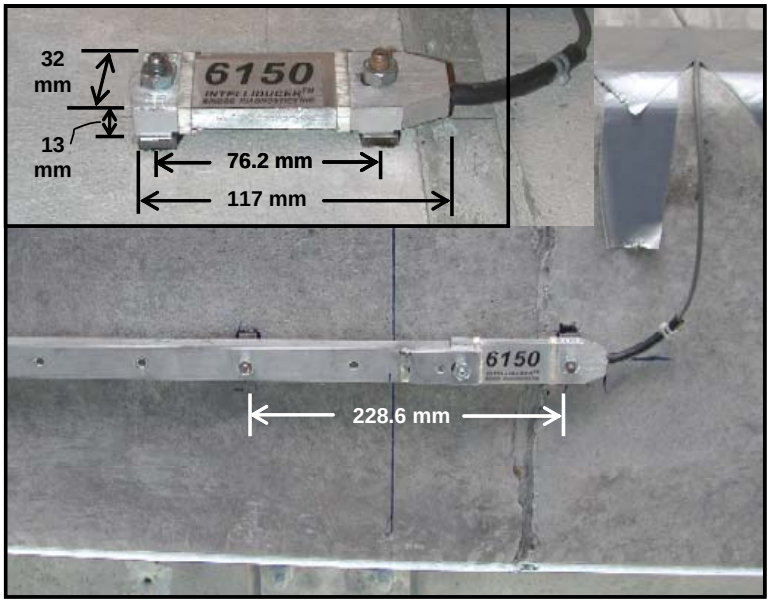

Figure 12 Intelliducer™ mounted on bottom of girder; Inset: Dimensions

Data Acquisition System

Each bridge site required an independent data acquisition system to store and transfer data. Each system consisted of a single data acquisition unit, two multiplexers, supporting circuitry, a 12-volt battery connected to a solar panel through a regulator, and a radio unit connected to an antenna. The CR5000 data acquisition unit, AM16/32 multiplexers, AVW1 vibrating wire conversion unit, and RF400 spread spectrum radios were manufactured by Campbell Scientific, Inc. Solar panels, batteries, regulators, and the radio antennas were purchased from other sources. A weather-resistant steel enclosure was used to house the data acquisition computer, radios, multiplexers, and other peripheral circuitry. Figure 13 shows the various components housed within each of the data acquisition boxes at each bridge site.

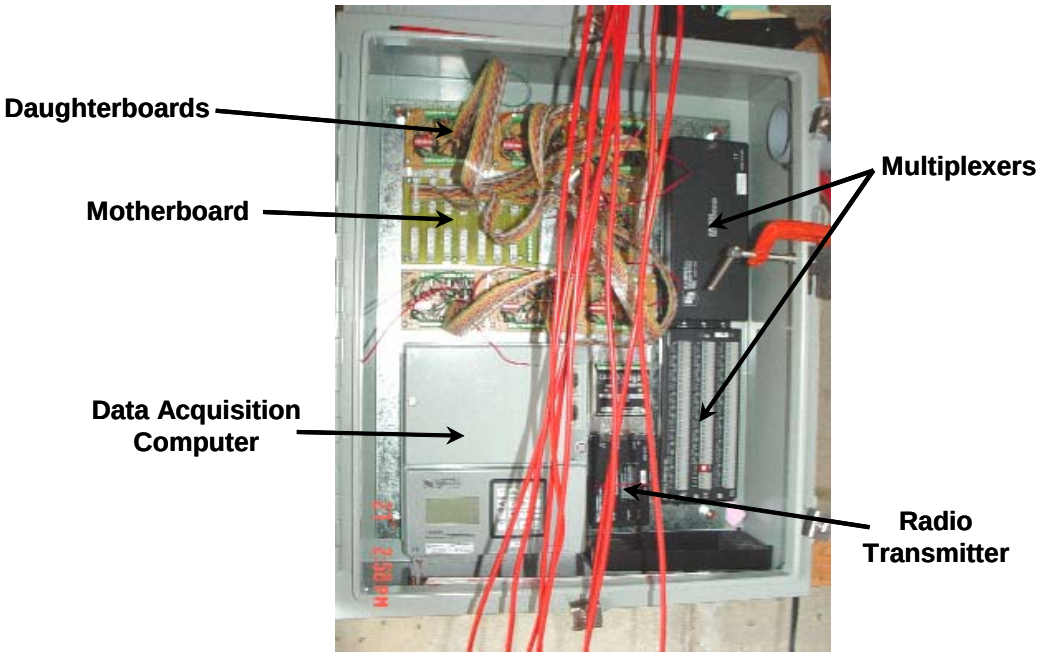

Figure 13 Various components within a data acquisition enclosure

Data Acquisition Unit

The CR5000 measurement and control system from Campbell Scientific, shown mounted in the box in Figure 13, is a rugged, high-performance data acquisition system. This data acquisition unit was selected for its durability, wide range of temperature operation, and internal computing and storage capabilities. Some of its other features include:

- a graphical display,
- low power draw,
- twenty differential (40 single-ended) input channels,
- 16 bit measurement resolution,
- 5-volt and 12-volt terminals to power sensors,
- 1,000,000 data point storage capacity
- a maximum throughput of 2000 to 5000 measurements per second (depending on configuration), and
- An operable temperature range of -40° to +85° C

The CR5000 data acquisition system uses a proprietary computer code to operate. A computer program was written to control data collection activities at the bridge site. Prior to installing the final program on the data acquisition computers, the program was tested at MSU to ensure that it was working properly. For long term monitoring, the program was generally written to deliver excitation voltage to each of the sensors at preset intervals (i.e., each hour), capture each sensor's response and store that information in internal memory. Collected data was transferred on command to MSU

using an Internet connection via the RF400 radios, discussed later in this chapter. For live load testing, a different program was required. This program was designed to record only the bonded-foil and embedded gages at a higher rate of speed (~50 Hz) during each test. Data sets collected during testing were transferred and stored on-site to a laptop computer.

Multiplexers

Multiplexers are used to expand the number of sensors that can be monitored by a datalogger. As previously mentioned, the datalogger can only accommodate 20 differential inputs. The AM16/32 multiplexer, seen in Figure 13, accommodates 32 differential measurement channels. It acquires data at a slow rate (approximately 1 Hz) by switching through its channels while logging the data through a single port on the face of the datalogger.

Two multiplexers are required at each bridge site to accommodate 16 vibrating wire gages, 16 temperatures, and 30 resistance strain gages during long term monitoring. The remaining resistance gage measurements are connected directly to the front face of the data logger. In this case, the advantage of using multiplexers is the increase in the number of available data ports without the expense of purchasing a second datalogger; the disadvantage is the relatively slower acquisition speed compared to a datalogger alone.

Communication and Power

During live load testing, data was transferred onsite via a direct link to a laptop computer. However, for long-term monitoring, a spread spectrum radio (RF400) was used to transfer data remotely to and from each of the bridges. As shown in Figure 14, antennas connected to the radio at each bridge communicate at 900 MHz to a single receiving antenna collocated with a weather station installed for the Saco Bridge Project atop the Saco Public School (less than 1 mile from the bridges). Information is then transferred from the school to MSU via the Internet. The antennas near the bridges are attached to a pole along with the solar panel.

Power components consist of a 12 Volt battery and a 60 Watt solar panel, interconnected by a regulator to maintain a specific battery voltage. Each solar panel measures approximately 1.1m by 0.5m and is rigidly connected to a wooden pole near the southeast corner of each bridge. Deep-cell 12-volt batteries are used for power storage because they are able to resist voltage decay during cold weather. Each bridge requires one battery, which is housed under the bridge, atop the pile cap near the data acquisition cabinet. Each battery has approximately two weeks of life in the event the solar panel malfunctions or is damaged. Wiring for the communications and power are run through conduit and buried in soil to protect them from varmints and the environment. In addition, a lightning rod is connected to this pole to provide lightning protection.

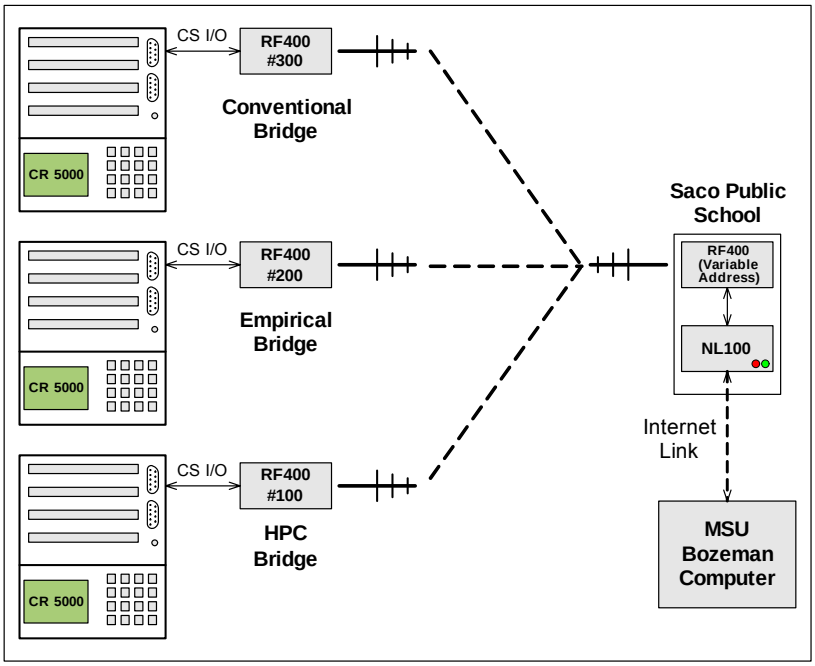

Figure 14 Communication path during long-term monitoring

Supporting Circuitry

Each bridge deck contains 35 resistance gages bonded to the reinforcement, 9 embedment gages, and 20 vibrating wire strain gages. The components used to support operations of the vibrating wires were discussed above. The circuitry used to service the resistance and embedded strain gages utilizes the Wheatstone Bridge circuit, discussed below. Overall, there are seven identical circuit boards such that each board contains six Wheatstone Bridge circuits, which service five resistance strain gages and one embedment strain gage. These seven boards are referred to as "daughterboards," since they complete the necessary circuitry for the strain gages and relay the final output to the datalogger through the "motherboard." This connection scheme allowed for rapid and more accurate reconfiguration of the system, notably for the short turnaround time

between live load tests on the three bridges. Due to limitations on the available number of connection points on the face of the datalogger, two different arrangements were required based on the unique needs of the long-term and the live load testing. These two arrangements will be discussed in further detail below.

Wheatstone Bridge. The Wheatstone Bridge arrangement is useful for detecting small changes in resistance elements, such as strain gages. Three of the four gage types employed in the instrumentation system for this project operate using a Wheatstone Bridge arrangement.

In its simplest form, the Wheatstone Bridge is composed of four resistors, as depicted in Figure 15. A voltage E_{in} is applied to the circuit; for this project, +5V was used. If the resistances in the upper arms of the bridge are identical (i.e., R1 = R2), the voltage-divider theory dictates that the voltage at point A will be exactly half of the input voltage (i.e., +2.5V). The same relationship holds true for the lower arm. Therefore, if R1 = R2 and R3 = R4, points A and B have equal voltages. Thus, the bridge is perfectly *balanced*, and E_{out} equals zero volts. However, a change in resistance in any one of the four arms of the bridge (i.e., if one of the arms is a strain gage) results in a voltage difference between points A and B. The resulting imbalance is detectable using sensitive voltage-reading equipment. Using theoretical calculations, the resistance change may be calculated using E_{out}. The resistance change is proportional to the strain experienced by the gages and may be converted to a real strain using the manufacturer's published gage factor.

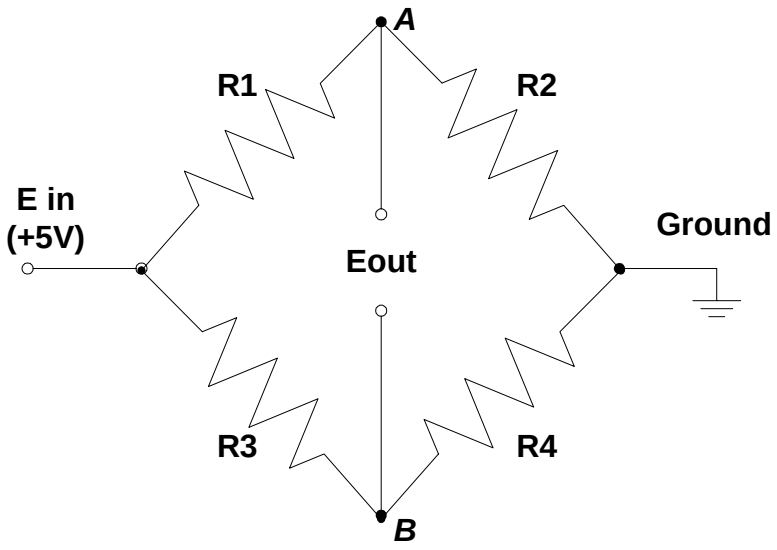

Figure 15 Ideal Wheatstone Bridge circuit arrangement

For this project, only the magnitude of axial strain is desired from the rebar strain gages. Thus, it is important that any effects due to bending be negated. This function is electrically possible by using the arrangement shown in Figure 16 (a) for all reinforcement gages. Notice that the two strain gages applied to the rebar are electrically in series, and occupy one arm of the bridge. If any bending is present in the bar, bending strains of opposite sign occur at the top and bottom of the bar. Due to the symmetrical location of the gages about the neutral axis of the bar, these strains have an equal magnitude, but opposite sign. The tensile strain due to bending in one gage cancels out the equal bending compressive strain in the other gage. For that arm of the bridge, the net result yields only the amount of axial strain in the bar.

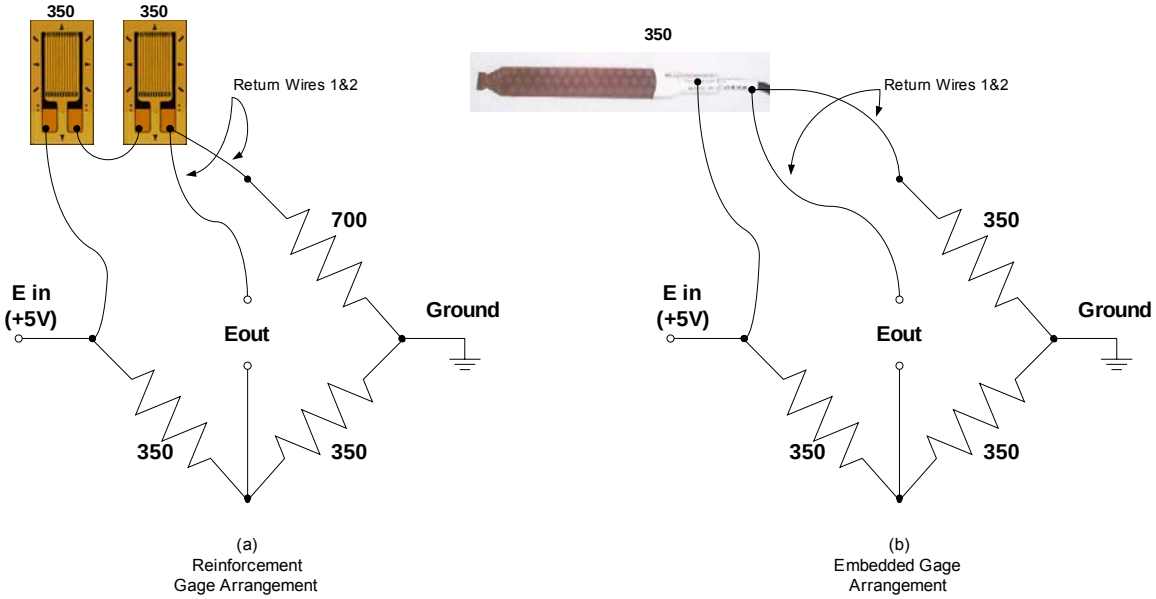

Figure 16 Wheatstone Bridge arrangements employed for Saco bridges

Practically, this arrangement is termed a "quarter bridge": only one arm of the bridge is occupied by strain gages, with the other three arms occupied by stable resistors. The arm with the strain gages is balanced by the 700Ω resistance arm. Although other arrangements of the Wheatstone Bridge also negate bending effects, this particular arrangement experiences the least sensitivity to changes in temperature – an important consideration for long-term monitoring. The two resistors comprising the 700Ω resistance arm were *unmatched* precision resistors, having a tolerance of ±0.01%, manufactured by Micro-measurements Group. The two 350Ω resistors used in the two lower arms of the Wheatstone Bridge were a matched pair, having a tolerance of ±0.005%.

A second notable feature of this Wheatstone Bridge arrangement is the use of the three-wire system. This technique was employed to compensate for the resistive imbalance in the circuit due to the long lengths of the gage lead wires. If only a single

wire was used, that wire would be susceptible to an unknown change in resistance under temperature changes, affecting the resistance of the gaged arm of the bridge. By adding a second wire of identical length to the other 700 Ω arm any temperature effects in the wire are present in both arms and the bridge remains balanced.

Quarter-Bridge Wheatstone Bridge circuits, shown in Figure 16 (b), are also used with the embedded gages. The fundamental theory and operation are the same, except all arms of the bridge are 350 Ω. The three-wire system is also used here.

Before recording strains in the bridge decks, baseline voltage measurements were recorded, which were subsequently subtracted from all readings to zero out the initial strain. A process called shunt calibration was employed to calibrate the relationship between the voltage output from the bridge and the strain sensed by the gage. Essentially, this process involves applying a very large resistance (176 kΩ) in parallel with the 700 Ω arm of the Wheatstone Bridge. The resulting resistance change is calculable as approximately 1900 με. The output voltage at this point is then the upper bound of a linear ratio measurement.

The circuitry described above was assembled on each daughterboard to accommodate six gage locations: five resistance strain gage locations and one embedment gage location, in the configuration shown in Figure 17. Thus, seven daughterboards are required to accommodate 35 bonded and 7 embedment gages. A single +5V voltage regulator (LM78L05) is used to ensure that a low-noise constant supply voltage is provided to the six Wheatstone Bridges on each board.

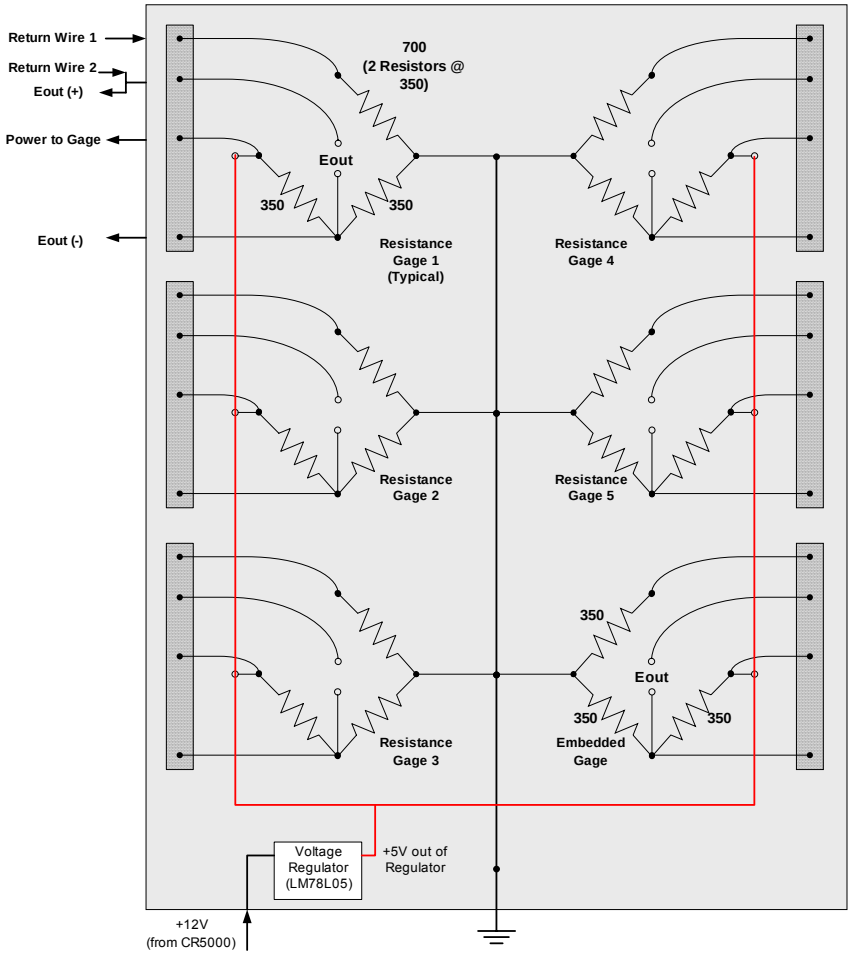

Figure 17 Diagram of daughterboard configuration

Circuit Alternatives and Testing. All of the Wheatstone Bridge arrangements require that a differential (two-wire) measurement be made to determine E_{out}. The CR5000 data acquisition unit used for this project is limited to 20 differential measurements on its face. To accommodate the number of measurements required for this project, a multiplexer is generally used. However, multiplexers require additional cost, are relatively slow, and create one more connection through which noise may be introduced to the signal. Therefore, in the early stages of the project, an attempt was made to streamline the data acquisition process. As shown in Figure 18, an instrumentation amplifier may be used to

convert differential analog outputs (a two-wire system) to single analog outputs (a one-wire system). By regulating one output arm of the instrumentation amplifier at 0V (i.e., datalogger ground), the other terminal can be read as a single-ended signal. This setup was attractive because the face of the datalogger can accommodate 40 single-ended measurements, thereby doubling its capacity compared to differential readings. However, based on the preliminary testing described below, this arrangement was *not* used in the final design.

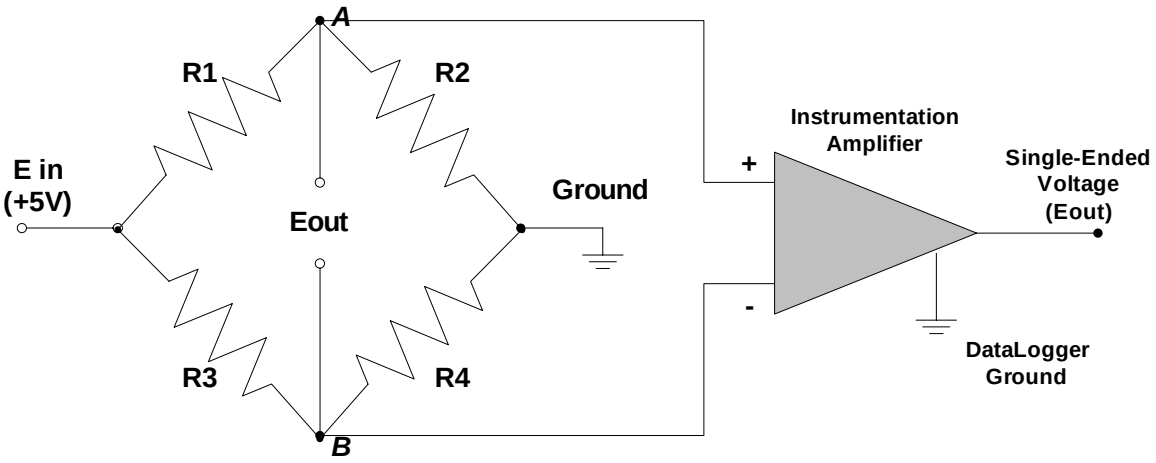

Figure 18 Alternative circuit design for employing single-ended measurements

Items of concern regarding both types of circuitry (differential and single-ended) included: accuracy of outputs compared to theoretical calculations, electronic stability over time and temperature variation, and noise abatement. Initial tests found that the gage output from both circuit arrangements matched the theoretical predictions reasonably well, and that noise was generally controllable using various modifications to the circuits and datalogger programming.

To further investigate the relative performance of the two wiring configurations, a small-scale, reinforced concrete test beam (.25 m deep by .15 m wide by 1.52 m long) was designed and fabricated in the MSU laboratory. In addition to testing the strain gage circuitry in a more realistic setting, this beam also afforded researchers an opportunity to evaluate the durability of the gage installations on the reinforcing steel. Other issues tested with this beam included: gage survivability during construction, cabling issues, and durability of the gages under loading.

To test gage durability, the gages at one location in the beam were purposefully abused during the construction process. All of the strain gages survived construction, confirming the durability of the installation procedure. Initial testing of the relative gage response found that the output matched the theoretical predictions reasonably well, and that noise was generally controllable using various circuits and programming modifications. However, it was difficult to assess electronic stability for long periods of time and at various temperatures due to the cumbersome nature of the concrete beam. A small segment of rebar was instrumented at two locations along its length to further study the electrical stability, accuracy and reliability of the strain gage circuitry for longer periods of time and under more controlled conditions. One gage location was connected to a differential circuit and the other to a single-ended circuit. Over a period of several days, a constant weight was suspended from the bar and the stability of the constant measurements evaluated against one another.

The single-ended circuit arrangement offered a significantly refined signal, with a low electrical noise band. This refinement was attributed to the filtering characteristics of the

instrumentation amplifier. However, performance of the single-ended voltage was too erratic over time for the long-term monitoring purposes of this project. The ground of the datalogger was being used as the ground; it was found that minor fluctuations in the electric potential of this ground proved to be quite significant when compared to the magnitudes of the recorded signal.

It was concluded from these laboratory experiments that the differential analog circuitry offered better stability and accuracy than the single-ended circuitry with sufficient noise abatement for the purposes of this project. Note also that additional time and cost would have been required to convert to single-ended measurements. Therefore, the final circuit design employed the differential outputs with a multiplexer.

Long-Term Monitoring Arrangement

For the long-term monitoring portion of the experiment, the available ports on the datalogger were inadequate to service all the necessary gages. As mentioned previously, multiplexers were employed to expand the number of gages that could be monitored at hourly intervals. Using the daughterboard-motherboard arrangement seen in Figure 19, the voltage signals for the reinforcement and embedded gage readings were transferred to the CR5000 either directly or via the multiplexer. All of the vibrating wire readings were accommodated using a second multiplexer in conjunction with the AVW1 vibrating wire conversion unit. This daughterboard-motherboard arrangement offered flexibility for performing zeroing/calibration activities without the need for rewiring. Five of the daughterboards are used to monitor long-term strains only, as they are routed through the multiplexer. The remaining two daughterboards are connected directly to the face of the

datalogger, allowing the gages wired into these boards to be logged at a relatively rapid rate. Events involving the passage of large trucks are being recorded on each of the bridges using the 12 gages wired through these two boards.

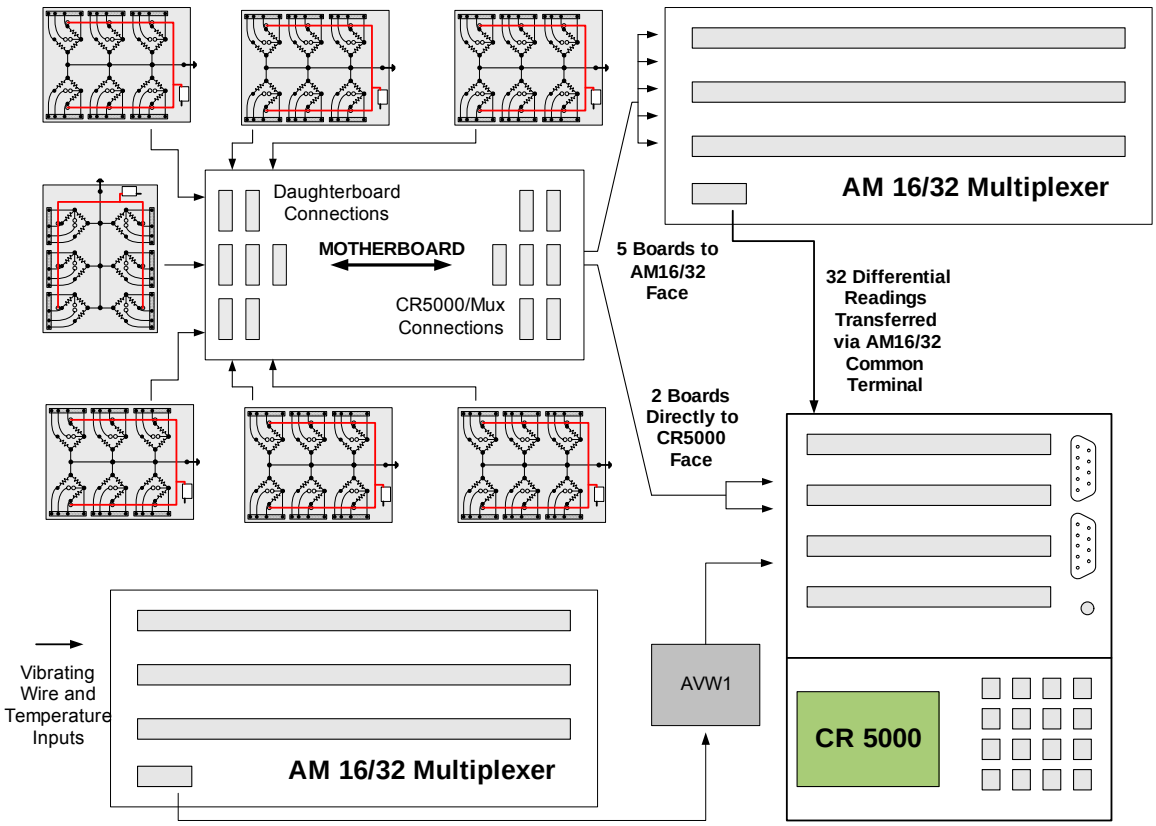

Figure 19 Data acquisition layout – long-term monitoring arrangement

Live Load Testing Arrangement

During the live load testing, the instrumentation system was temporarily reorganized to accommodate a large number of sensors operating at the higher acquisition speeds necessary during the live load passes. As previously mentioned, the multiplexers could not be used during these tests due to limitations on how rapidly they can switch between

instruments. As such, all resistance gage measurements were connected directly to the loggers. Due to capacity limitations on the input panels of the dataloggers, all three CR5000's were used together on each bridge to simultaneously log 53 differential channels for that bridge during its live load testing, as shown in Figure 20.

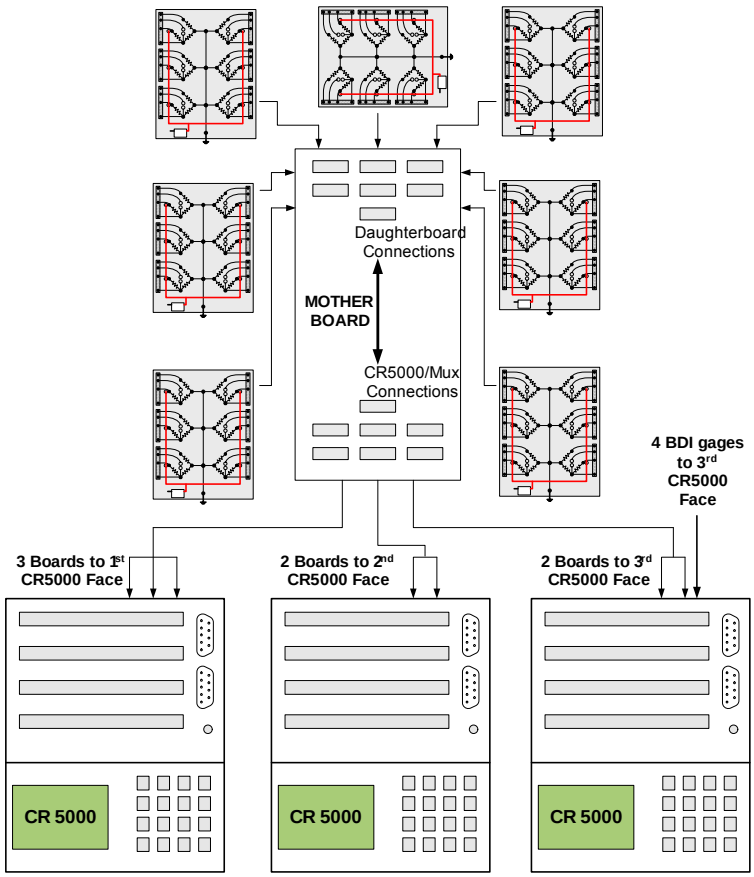

Figure 20 Data acquisition layout – live load testing arrangement

For the live load tests only, gages from Bridge Diagnostics, Inc. (BDI) were used to monitor strains at the bottom of the girders under the gaged section of each bridge; these gages were also directly connected to the face of the dataloggers. Vibrating wire strain gages were *not* monitored during live load due to their slow acquisition speeds. Once

again, the daughterboard-motherboard interface allowed speedy transitions during live load testing by reducing the amount of physical rewiring required to modify the system to acquire data by datalogger only (without multiplexers).

CHAPTER 5

LIVE LOAD TESTING

The objective of the live load testing of the Saco bridge decks is to determine how each type of deck structurally transfers wheel loads from their point of application to the supports. It is also important to determine the magnitudes of stresses and strains that develop in the decks as they perform this function. This information is used to understand whether the current deck design methods reasonably represent actual structural behavior, with respect to both the load-carrying mechanism and the stress levels generated in the system. Information obtained from live load testing is also useful for assessing the likelihood of immediate and/or long-term crack development in the decks from vehicle loads. The primary focus of the live load tests is the manner in which wheel loads are locally transmitted from the decks into the bridge girders. The manner in which the decks participate globally with the girders to longitudinally transfer vehicle loads into the abutments and piers is not the thrust of this research.

Live load tests were conducted on the three bridges approximately six weeks after placing the bridge deck concrete, during the week of July 28, 2003. The testing was conducted prior to opening the bridges to traffic, but the decks were grooved and sealed and the bridge approaches were paved at the time of testing. The vehicles used in these tests were 3-axle dump trucks, provided by MDT. Most test runs were conducted with a single truck traversing the bridges, at both low and high speeds; additional tests were conducted using two trucks traveling side-by-side at low speed.

Test Vehicles

Calculations were performed prior to live load testing to establish desirable truck weights (Cuelho, et al. 2004). The design moments for the deck were determined by using an AASHTO standard HL-93 truck configuration (3-axle truck) with a 145 kN single axle, positioned to generate the highest possible transverse moment in the deck. To test the bridges as close as possible to their design capacity, the trucks to be used in the 2003 live load tests had a proposed load on the tandem axles of 112 kN per axle (GVW 300 kN). At this load, transverse moments in the deck (carried locally by the deck spanning between the girders) are equal to approximately 90 percent of those from the design load (a 145 kN single axle, as mentioned above). Also, under these increased loads, the longitudinal moment demand (carried by the composite action of the girders and the deck) is 104 percent of the longitudinal moment generated by the HL-93 design vehicle.

Using a heavier vehicle for the live load tests pushes the decks closer to their design demands and may better reveal differences in deck behavior between the empirical and conventional reinforcement designs. A review of prior research found that other researchers have utilized heavy 3-axle dump trucks with wheel loads on the same order of magnitude as the proposed heavier load set (Yang and Myers 2003; Stallings and Porter 2003; Nassif, et al. 2003). Alternate vehicle configurations were also investigated (i.e., grain trucks, farm tractors, etc…) but they offer little advantage over 3-axle dump trucks with respect to maximizing demands on the deck. In light of this situation, the bridges were tested using the heaviest 3-axle dump truck that the MDT Bridge Bureau and truck

operator were comfortable with, but not to exceed the 300 kN GVW and 112 kN tandem axle weights presented above. The weights and dimensions of the Sterling and Volvo trucks used in the live-load experiments are summarized in Figures 21 and 22, respectively. Scaled drawings also show the contact footprint of the tires. Figure 23 shows a side-view of the Sterling truck, which was used for all the single truck tests.

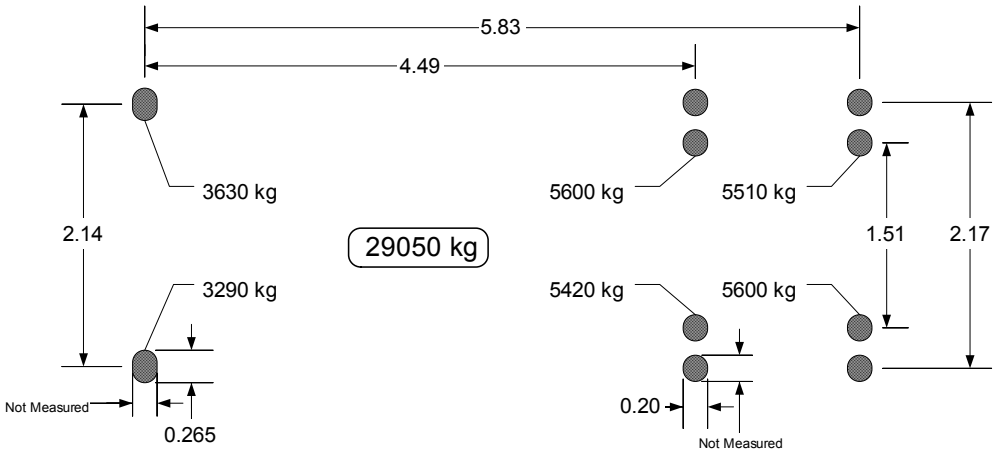

Figure 21 Dimensions and weights of the Sterling 3-axle dump truck (lengths in meters)

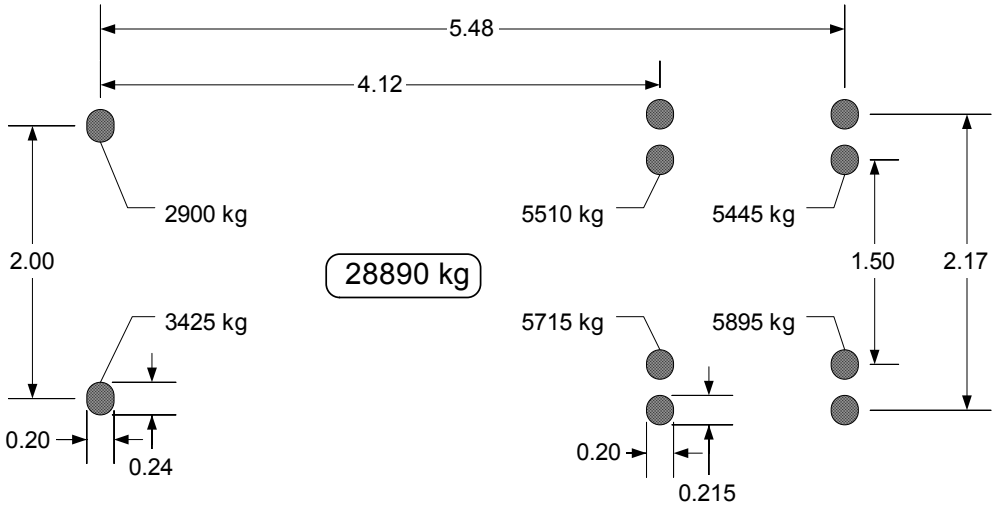

Figure 22 Dimensions and weights of the Volvo 3-axle dump truck (lengths in meters)

Figure 23 Side view of the Sterling 3-axle dump truck

Testing Procedure

Live Load Testing Regimen

An identical regimen of live load tests was performed on each of the three Saco bridges. Each bridge was subjected to 15 test runs: 8 low speed single-truck tests, 5 high speed single-truck tests, and 2 low speed two-truck tests. Throughout the remainder of this document, low speed single-truck tests will be referred to simply as 'Single Truck' (ST) tests; high speed single-truck tests will simply be referred to as 'High Speed' (HS) tests; low speed two-truck tests will simply be referred to as 'Two Truck' (TT) tests.

Prior to conducting the live load tests, nine longitudinal truck paths were painted on the bridge deck. These nine longitudinal truck paths were used to guide the truck as it traversed the bridge. The positions were labeled R, S, T, U, V, W, X, Y, and Z, as shown

in Figure 24. To record the longitudinal position of the truck as it crossed the bridge, transverse lines were also painted on the deck at two-meter intervals. A hand-held button was connected to all three data loggers to synchronize strain measurements with the position of the truck. As the truck traversed the bridge during slow-speed tests (ST and TT), the hand-held button was depressed to electronically record each time the front axle of the truck reached each successive two-meter mark.

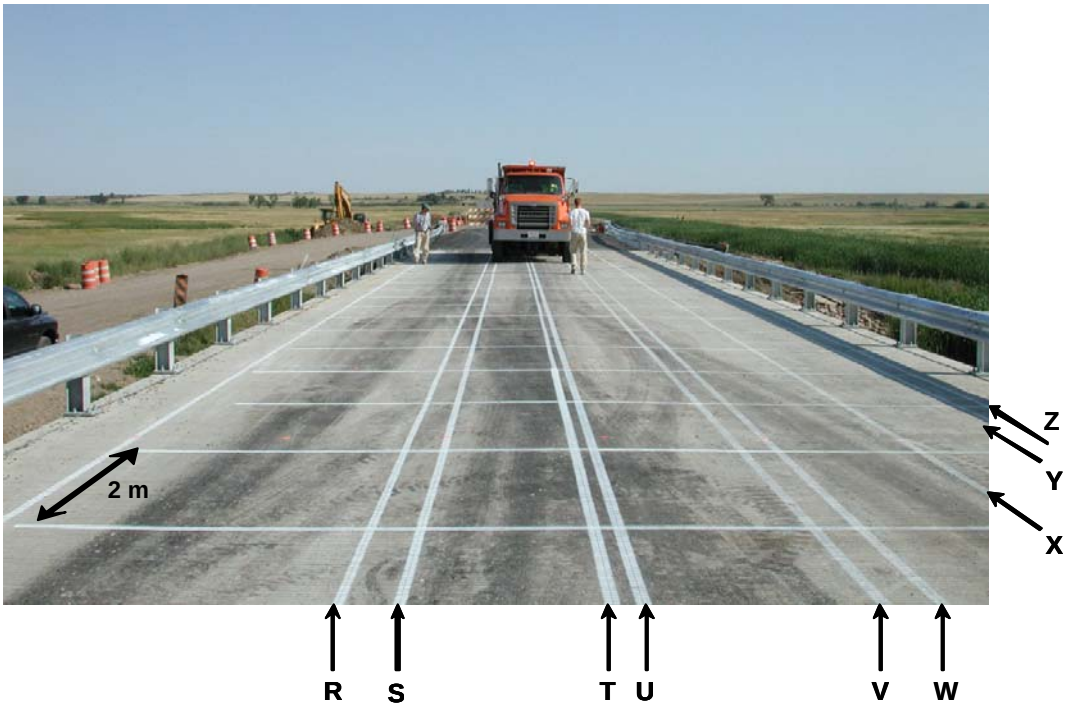

Figure 24 Photograph of lines used for truck positioning during live load testing

The nine truck positions were selected to characterize deck response under the most critical loading combinations. Generally, tire loads are positioned to either be directly over a girder or at the midspan between girders, as shown in the cross-section views of Figure 25. Truck paths U and X are exceptions to this general rule, positioning the center of the truck directly over a girder, such that the tires symmetrically straddle the girder.

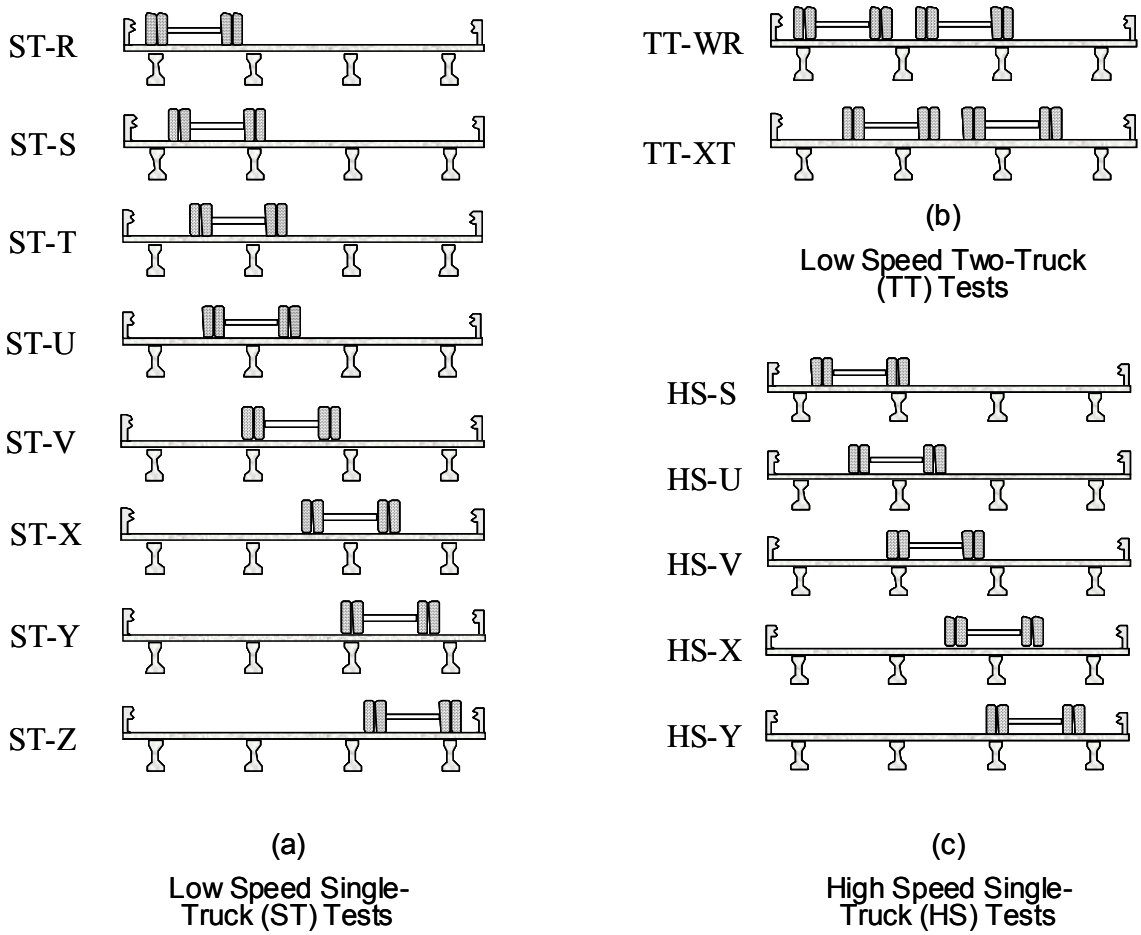

Figure 25 Cross-section views of truck tire placement for live load tests

Most live load tests performed by others have utilized static placement of the trucks. In this case, a crawl test was used, allowing all longitudinal truck positions to be captured as the truck traverses the length of the bridge. This approach is more efficient and provides more complete live load response information than static placement at discrete locations. At the slow speeds used for these tests, dynamic effects are minimal. The disadvantages of using a crawl test are the potential for minor imprecision in the truck

position during testing, and the inability to use certain gages (i.e., vibrating wire strain gages) in lieu of static or quasi-static conditions.

During the low speed single-truck (ST) tests, the Sterling dump truck was driven along each of the 8 selected longitudinal truck paths, as shown in Figure 25 (a). Notice that each of these tests is denoted as a 'Single Truck' (ST) test, followed by the letter of the appropriate truck path (e.g., ST-R represents a low speed single-truck test along the R truck line). These tests were performed at a speed of approximately 3 miles per hour. Figure 24 shows the driver's-side front tire of the Sterling truck following Line V and the 2-meter transverse line spacing to mark the position of the truck's front wheels. During the slow-speed tests (ST and TT), one person to the left side of the vehicle marked the position of the front wheels using the hand-held button while the other guided the truck along the proper longitudinal path.

For the low speed, two-truck (TT) tests, both the Sterling and Volvo dump trucks were driven across the bridges side-by-side at a speed of approximately 3 miles per hour. Two unique combinations of longitudinal truck paths were used on each bridge: truck lines W and R, and truck lines X and T, as shown in Figure 25 (b). As mentioned above, a similar procedure was followed for guiding the two trucks and electronically marking their longitudinal positions with the hand-held button.

Finally, for the high speed single-truck (HS) tests, the Sterling truck was driven across the bridge at a speed of approximately 60 miles per hour along each of the five selected longitudinal lines shown in Figure 25 (c). Due to the relatively short duration of these tests and the high speeds involved, no correlation between strain response and truck

position was electronically recorded. Note that only five HS tests were conducted. Truck lines R and Z place the truck very close to the guardrail and were omitted due to safety concerns. Because of the high speeds involved, the actual positioning of the truck was relatively imprecise (within approximately 1 foot). As such, truck lines T and W were omitted due to their close proximity to other test lines.

Data Processing

To facilitate analyses of the live load data, it was manipulated to output deck response as a function of vehicle position, rather than a function of the elapsed time (which was how the data was recorded). Notably, due to differences in the travel speeds of the vehicle during the various tests, the data arrays from all the tests were difficult to correlate. Utilizing the position stamps created by the hand-held push button, a routine was written to estimate, from the time histories, the strain data at specific longitudinal truck positions. In this way, all data sets consisted of strain response information at identical spatial positions of the truck. Additionally, it was determined that minimal changes occurred over the short duration of each test (less than 2 minutes) due to changes in ambient conditions (i.e., temperature variation). As such, all strain histories were shifted as necessary so that initial strains were zero for each experiment.

CHAPTER 6

RESULTS AND OBSERVATIONS

Objectives

The live load test data can be used to develop a fundamental understanding of how each bridge deck reacts to vehicle loads. Simple observations in this regard allow for useful comparisons to be drawn between the performance of the three decks when more complex behaviors arise. Comparisons between the reported data and expected responses derived from basic strength of materials concepts are also useful in this process. To analyze the live load test results, an attempt was made to isolate the deck's behavior from the contributions of other structural elements in the bridges. In this regard, the current investigation focused specifically upon the transverse deck response, since it was believed to be most significantly affected by the configuration of each bridge deck. Thus, the following analysis of the live load data focuses on strains recorded by transverse reinforcement gages.

The primary goal of the entire Saco Bridge Project is ultimately to compare the relative performance of the three bridge decks. While the analysis presented here does reveal some subtle behavioral differences between the three decks under vehicle loads, these differences are relatively "small" at this point. It is too early to assess what these differences indicate with regard to the overall durability and structural efficiency of each

deck type. The significance of these differences in behavior on performance may become clear as additional data is collected over the next few years.

The following sections present an analysis of several fundamental behaviors that have been observed in three Saco bridge decks to date. Each behavior offers valuable insight about the baseline condition of each deck and how they performed compared to one another. Aspects of bridge deck behavior that are discussed include:

- longitudinal cracks,
- in-plane stresses,
- the manner in which each bridge carries load,
- transverse deck integrity over the girders, and
- general non-linear behavior.

These behaviors are examined using the transverse reinforcement strain data. This data obviously provides a direct measurement of the level of the strain experienced in each deck. It also can be used to determine the height of the neutral axis within the deck, the relative magnitude of the bending moments experienced by the decks, and the validity of superposition for calculating deck demands under multiple vehicle events. These various items are indicative of deck condition relative to stiffness, cracking, and non-linear behavior.

General Behaviors

Before proceeding with detailed analyses of the data, it is critical to validate that behavioral responses reported in the data match the direction and relative magnitude of

the expected response. One unique aspect of this project is the availability of several live load tests on three different bridges. Certainly, some behavioral differences are expected between the three decks, which will be examined later in this chapter. Nonetheless, general behaviors are expected to be similar. These similarities build confidence in the data and what it can reveal. The response patterns and magnitudes can also be compared with published data from other bridge live load tests to validate that it is "reasonable".

Presumably, the longitudinal bridge response is best understood conceptually. Under a truck load, the loaded span deflects downward (as shown in Figure 26) and positive moments (compression top, tension bottom) are generated in the center of the span. Under the same load, the curvature reverses over the interior bents, creating negative moments (tension top, compression bottom) over the bent and in adjacent spans.

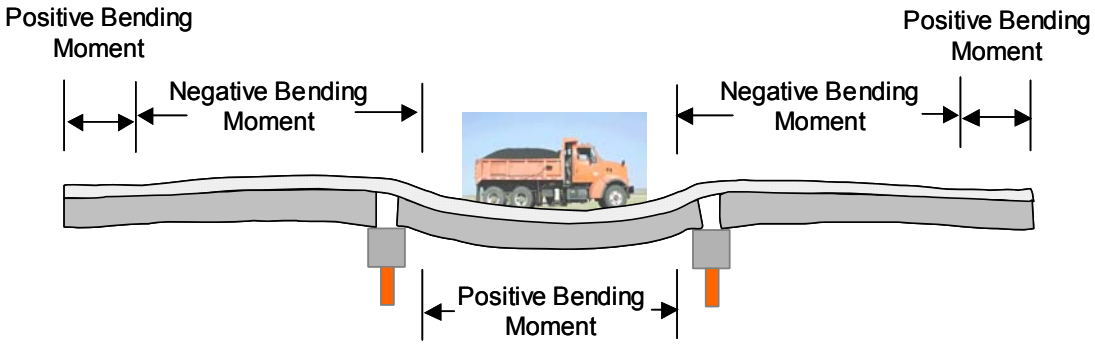

Figure 26 Depiction of expected global longitudinal behaviors

The longitudinal strain history at the longitudinal quarter-span (Gage Location D-3) is shown in Figure 27. For this style of plot, the positions denoted along the horizontal axis refer to the position of the truck's front tire as it traverses the bridge. The strain trace is the record of the strain at a single, stationary gage location when the truck is at the

various longitudinal positions along the deck. Thus, for example, the peaks corresponding to the tandem axles are later in the strain history than the front axle (i.e., the front axle passes over the fixed gage location first, followed by the tandem axles about 5m later). The "Finish" line indicates the point at which the front axle of the truck leaves the south end of the deck; the rear tandem axles remain on the deck for approximately five more meters.

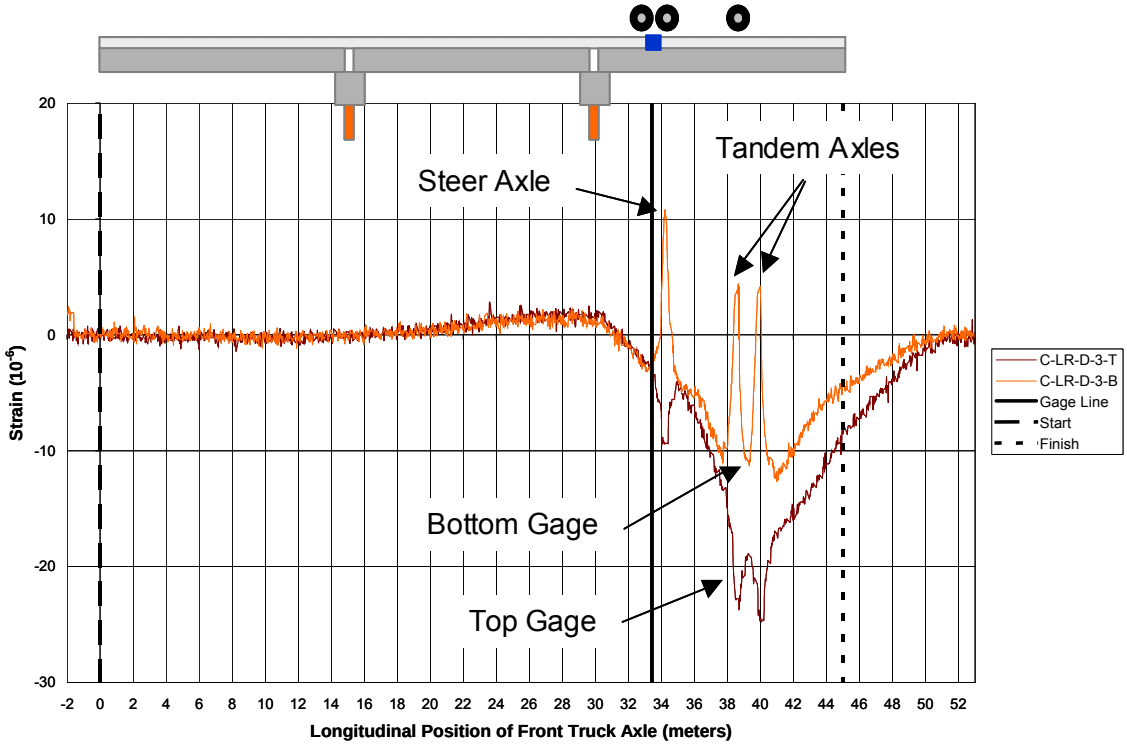

Figure 27 Strain history - Conventional deck longitudinal Gage Location D-3 (ST-T test)

Returning to Figure 27, when the truck loads the middle span of the bridge (15m-30m, adjacent to the gaged span), negative moments in the instrumented span are apparent in the nominal tensile strains at Gage Location D-3 (refer to Figure 4 for gage location). As the truck tires subsequently enter the instrumented third span, the response

quickly changes to the expected positive bending moment response. The shape of the longitudinal cross-section includes the girders (forming a T shaped cross-section), with the neutral axis expected to be below the deck. This is consistent with the data shown in Figure 27: under positive moment, the top and bottom gages are both in compression, with the top gage more severely so. Also notable is the sharp positive moment peak in the gage response when each axle passes over the gage line. This characteristic response is caused by the local positive moment in the deck in the immediate vicinity of each tire footprint (i.e., a small 'dish' is formed around each tire footprint). These behaviors match the expected behavior for this location in the bridge deck, considering that Gage Location D-3 is not immediately over a girder, which allows a local dish to form immediately under each tire. The shape and magnitude of this deck response are also similar to longitudinal deck strains observations by Stallings and Porter (2002) (see Figure 1). The longitudinal response at this location (D-3) for all three bridges is shown in Figure 28. Notably, all the bridges exhibit similar shapes and magnitudes of response, building confidence in the data.

Figure 29 shows the longitudinal deck strain response over the bent. The strain history in Figure 29 is recorded from the Empirical deck longitudinal Gage Location F-1, positioned immediately over Bent 2. In contrast to the strain histories at Gage Location D-3 (Figures 27 and 28), a negative bending moment dominates the response of Gage Line F (tension top, compression bottom). Due to global bending behaviors, the negative moment is expected at this location in the deck. It should be noted that only the deck is continuous across the bent; the girders are not continuous over the internal bents. Thus,

at this gage location the available cross-section is simply that of the deck, not the composite deck and girder section. The sharp reduction of the moment output when the tandem axles of the truck are directly over Gage Line F (front axle at approximately 35-36m) is also noteworthy. At this position, only the front axle is loading the deck away from the bent, so the negative moment over the bent is greatly diminished.

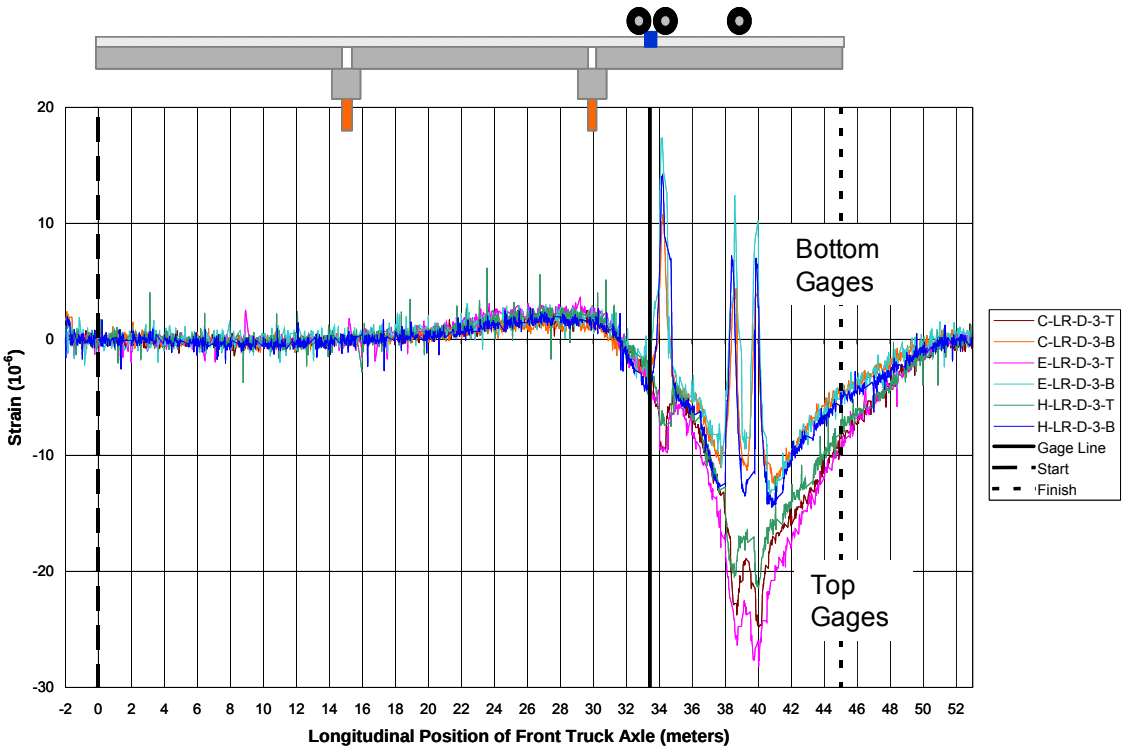

Figure 28 Strain history - all three decks longitudinal Gage Location D-3 (ST-T test)

Strain histories for all three bridges at Gage Location F-1 are shown in Figure 30. Initial inspection would indicate that the three deck responses are remarkably different. However, a closer inspection reveals that each deck is performing similarly, with a distinct negative moment at this point in the deck. For each deck, the strain in the top gage is relatively more tensile than the strain in the corresponding bottom gage, and the

magnitude of the bending moment is similar for each deck (i.e., the difference between the strains of the top and bottom gages). The primary difference between the three bridges arises from the magnitude and direction of in-plane axial forces at this point in the deck. The Empirical deck response (see also Figure 29) shows very little axial strain, and most obviously reveals the negative bending moment. Although the Conventional deck traces reveal a net tension in the continuous deck over the bent, the negative moment is also evident here. The HPC deck also reveals the negative moment, despite having a net compression across the cross-section at this point. The accuracy of these differing responses was verified using co-located embedment gages. It is suggested that these differences in response are indicative of variations in the presence and restraint of longitudinal forces in each bridge. Despite the uniqueness of the specific response over the bent in each bridge, the recorded responses still verify that the expected behavior (i.e., negative bending moment) is present in each of the decks at magnitudes that are 'reasonable'. All of the remaining longitudinal gages also show behavioral similarity among the three decks. This consistency in response further builds confidence in the accuracy of the data.

Strain histories from the transverse direction are the focus of the remainder of this analysis. The transverse gages were installed, conditioned, and recorded in the same manner as the longitudinal gages; thus, the corresponding strain histories should be valid. As observed for the longitudinal strains above, the measured transverse responses in all three bridges were generally similar in shape and magnitude under corresponding vehicle tests (several of these traces are presented and discussed in detail in the following

sections of this thesis). These observations validate that it is reasonable to proceed with more complex analyses and begin drawing conclusions about deck behaviors from the data.

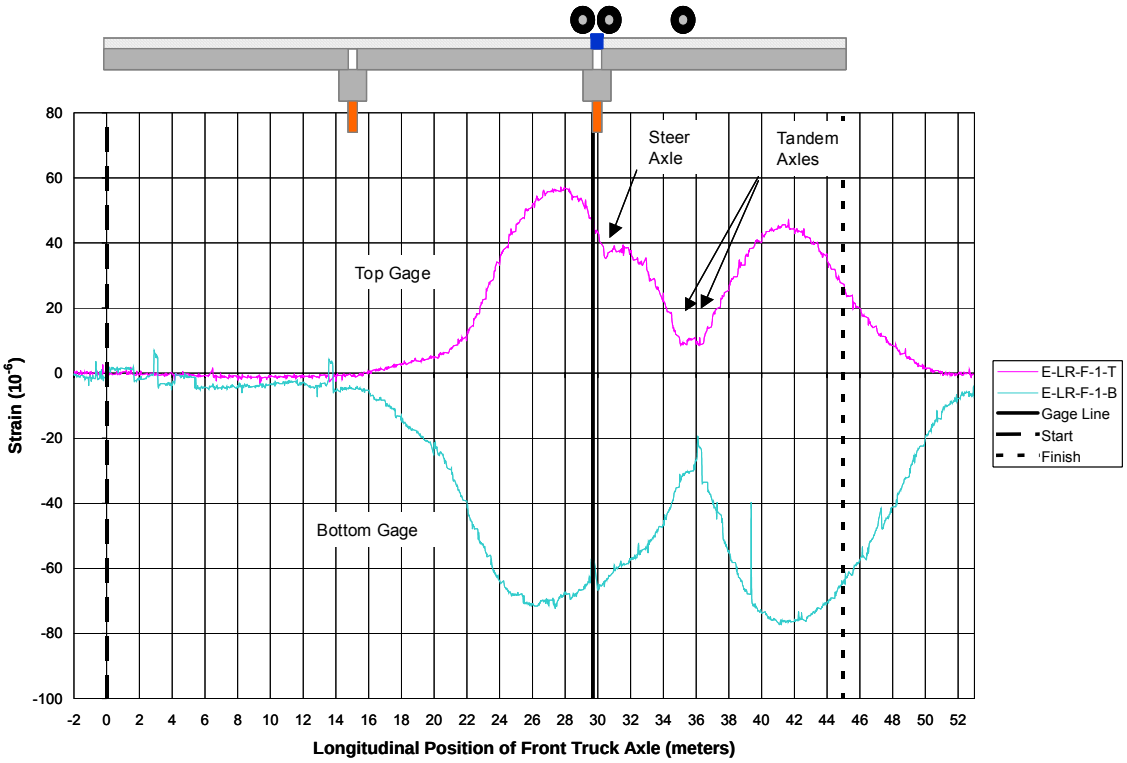

Figure 29 Strain history - Empirical deck longitudinal Gage Location F-1 (ST-T test)

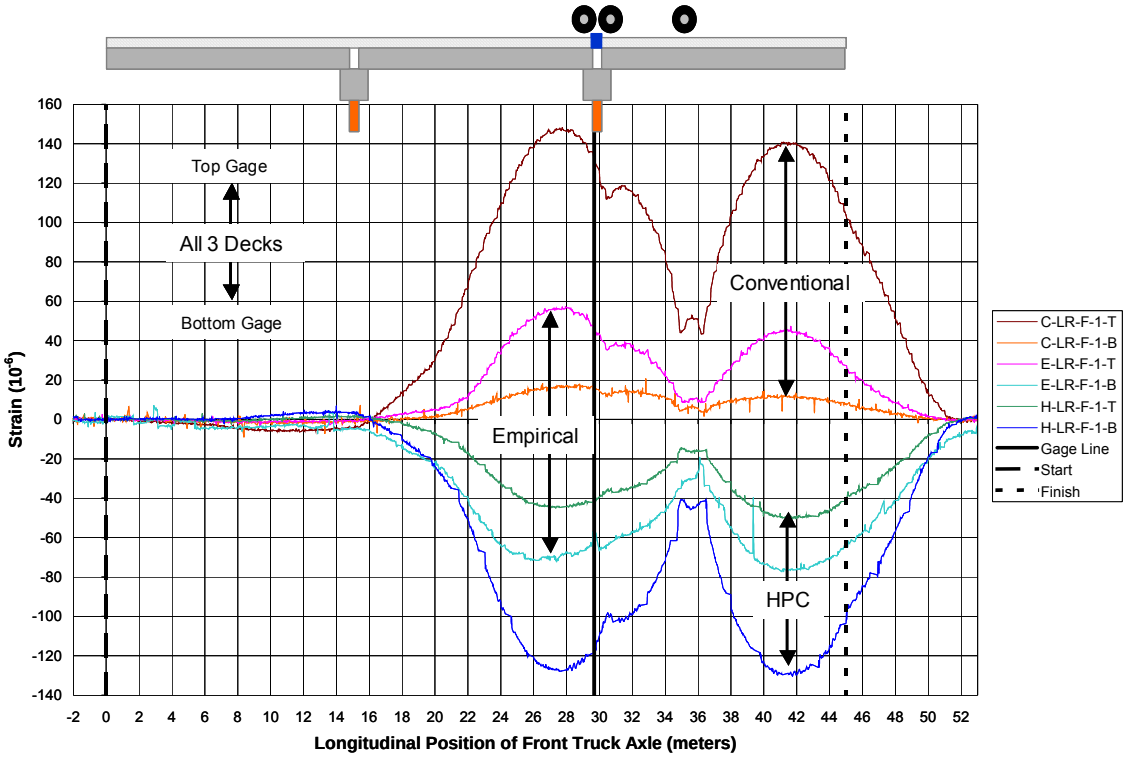

Figure 30 Strain history - all three decks longitudinal Gage Location F-1 (ST-T test)

Deck Cracking and Axial Strain Analysis

A brief review of the standard theories for bridge deck behavior is presented here to establish a foundation for interpreting the live load data. Recall that AASHTO (2000) traditionally represents a bridge deck as a continuous beam in the transverse direction, supported by rigid girders below. This approach is reportedly based upon the work of Westergaard, which was conducted in 1930 (Csagoly and Lybas 1989; Cao 1996). The deck transmits applied tire loads transversely to the girders. Westergaard's treatment of the bridge deck as a continuous beam over rigid girders makes qualitative predictions of behaviors relatively easy to form. However, actual load carrying mechanisms are more

complex in nature and require a more sophisticated representation of the deck-girder system to identify subtle differences in behavior between the three decks. The assumption Cao (1996) made is that the girders more reasonably act as springs rather than fixed supports. Thus, the deck is simultaneously engaged in both longitudinal and transverse bending behaviors, thereby making analysis of the live-load data complicated. Even so, the representation of the deck as a continuous beam, spanning transversely across rigid or flexible girders, will provide a useful foundation for several of the behavioral observations made here.

Admittedly, AASHTO (2000) has recognized that the primary load supporting mechanism in the transverse direction of bridge decks is internal arching action combined with a small flexural component, providing justification for the empirical design method. This load-carrying mechanism occurs in scenarios of high stresses. However, this load-carrying mechanism manifests itself only after the bottom of the deck has cracked (AASHTO 2000; Csagoly and Lybas 1989; Fang, et al. 1990; Fenwick and Dickson 1989). The competency of the cracked region is then dependent upon the restraint provided by surrounding regions of concrete and other supporting elements, such as girders or diaphragms. As discussed in the literature review, the deck concrete surrounding the area of loading experience compressive membrane forces. However, Fang, et al. (1990) performed testing on Texas bridge decks with Ontario design and observed that the deck remained in the linear elastic region under service loads and overloading (three times the AASHTO design load). Additionally, tensile membrane forces were observed in the deck up to the point of cracking in the positive moment

regions; compressive membrane forces were only apparent after the occurrence of cracking. Thus, it will be useful to determine if any of the Saco bridge decks shows evidence of cracking or internal arching behavior.

Before engaging in a detailed analysis of deck cracking, it is noteworthy that longitudinal cracking is not expected to occur at the strain levels observed in the Saco bridge decks during the live load tests. The maximum transverse tensile strain recorded during live load testing was approximately 50 με at Gage D-4-Bottom during the ST-U test. A strain of 50 με in the lower mat of reinforcing steel corresponds to a strain of 75 με at the lowest extreme fiber of the concrete. The transverse deck strains are below the magnitude that would suggest concrete cracking. While there is no consensus on how the cracking strain of a particular concrete can be determined, it generally is expected to be in the range of 78 to 136 με (*Annex* 1997). In the case of the Saco decks, expected cracking strains of approximately 100 με were calculated, based on the elastic modulus and the peak tensile strength for the concrete in each deck.

It is commonly accepted that strains in the bridge deck are dominated by environmental temperature changes (Hughes, et al. 2000; Boothby and Laman 1999). These strains can easily be on the order of magnitude that would induce cracking. In fact, the transverse temperature-induced strains in these decks have been as high as 100 με in tension. If cracking of the deck had occurred due to changes in ambient conditions, it should be evident in some aspects of the deck response under live load demands. No visible longitudinal cracking was evident during the live load tests. This observation

certainly does not preclude the possibility of micro-cracking, which could have similar effects on deck behavior as macrocracking, although not to the same extent.

The initial investigation of axial strains within the deck was primarily focused upon determining the possible presence of internal arching behaviors. However, in later stages of the analysis, it became apparent that the investigation of axial strains could provide additional insight into deck behaviors, independent of the presence of arching action. Furthermore, in light of Fang's observation, it was unlikely that load levels in the Saco tests were high enough to create this behavior (Fang, et al. 1990). This portion of the analysis will serve as a baseline for evaluating future live load testing results, to determine if the internal arching mechanism has become more or less pronounced.

To observe transverse deck behaviors, the five transverse gages along Gage Line D are very valuable; these five gages are circled in Figure 31 (a). The superstructure cross-sectional shown in Figure 31 (b) indicates the position of each gage with respect to features of the deck. These five gages are used throughout the analysis to characterize transverse deck behaviors.

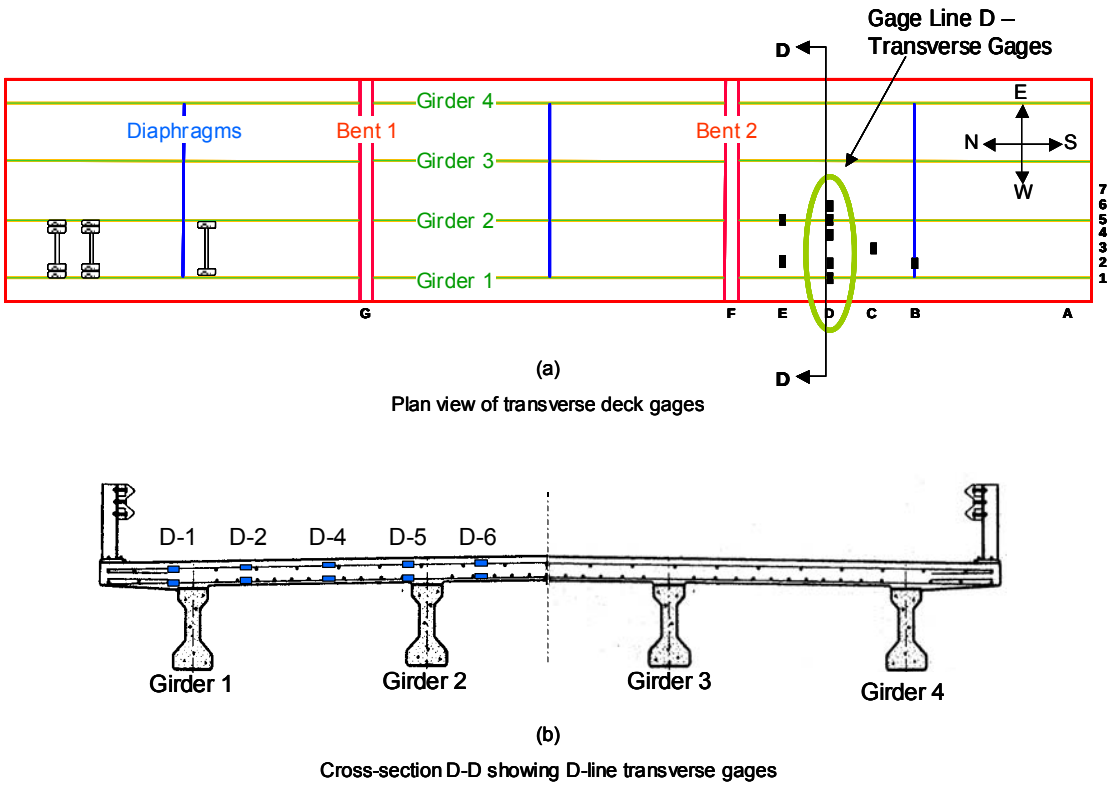

Figure 31 Transverse gages of interest (Gage Line D)

Deck Neutral Axis Position

One attribute of the deck response that reflects the presence of cracking or any in-plane axial stress in the deck is the height of the neutral axis within the deck. The *neutral axis* of a beam is simply the height within its cross-section at which it experiences zero normal stress. In this analysis the neutral axis was determined from strain data, and is referred to as the *actual* neutral axis throughout the reminder of this thesis. More specifically, the *bending* neutral axis is the height of the beam's neutral axis under pure bending (i.e., no axial forces present). For beams composed of homogeneous materials, the height of the bending neutral axis can be determined from the geometry of the cross section. Using the first moments of areas, the bending neutral axis of a full rectangular

cross-section is predicted to lie exactly at mid-depth, through the centroid, as shown in Figure 32 (a).

For composite materials such as reinforced concrete, the relative amount, location, and stiffness of the two materials each factor into the position of the bending neutral axis. The standard procedure to locate the bending neutral axis is to apply the Method of Transformed Areas. This method converts the actual area of steel to a theoretical area of concrete that would provide equivalent flexural resistance. Thus, the transformed cross-section is composed of a homogeneous material; the location of the bending neutral axis is then determined by taking the first moments of area (Wang and Salmon 1985).

In typical design practice, it is common to neglect all of the tensile concrete when determining the position of the bending neutral axis. However, the material research of Gopalaratnam and Shah (1985) and Fenwick and Dickson (1989) indicate that concrete does, in fact, provide a substantial contribution in the tensile regions of the cross-section. Specifically for bridge decks, Fang, et al. (1990) observed that under service loads, the deck remained uncracked. Thus, in the following analyses, the tensile contribution of the concrete will be included as part of the cross-section when calculating the bending neutral axis. However, it is important to realize that the integrity of the concrete could greatly affect the position of the bending neutral axis, and if for any reason significant cracking is expected to have occurred, this assumption should be revisited.

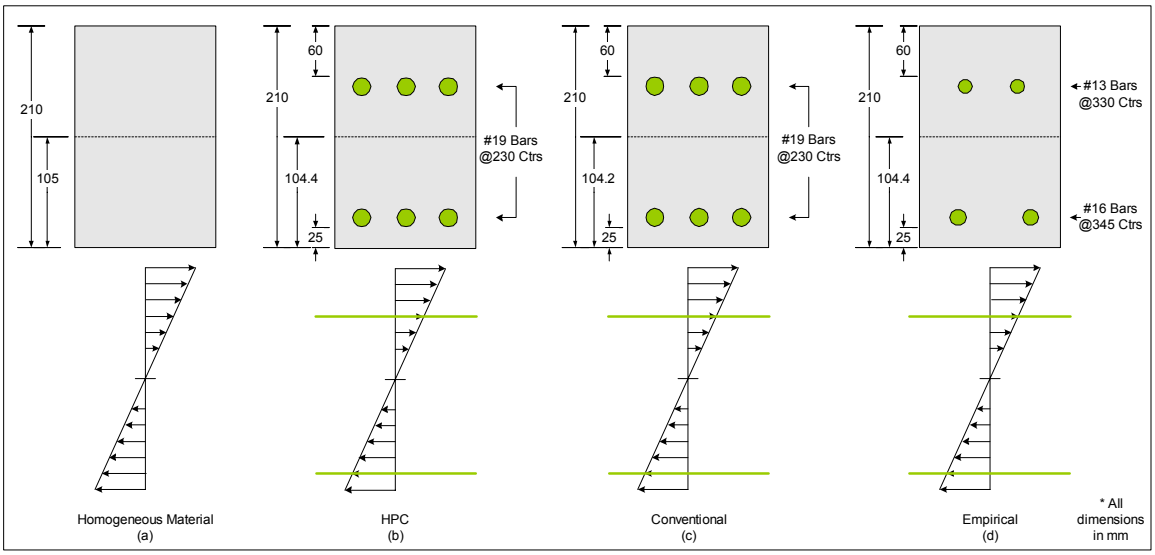

Figure 32 Deck cross-section geometries with calculated bending neutral axes and expected bending strain profiles (uncracked)

Predicted Bridge Deck Bending Neutral Axes. Assuming that the concrete is uncracked, the expected location of the bending neutral axis was calculated for each deck using the method just described (Method of Transformed Areas). All three decks had a specified thickness of 210mm. For both the Conventional and HPC decks, the size (19mm diameter) and distribution (230mm on center) of the transverse steel is identical in the top and bottom reinforcing mats. However, the mats are not symmetrically located in the depth of the cross-section; the clear cover on the top surface (60mm) is larger than at the bottom (25mm).

Taking into consideration the different concretes in the two decks, the bending neutral axes for the Conventional and HPC decks were calculated to be at nearly the same height, lying just below mid-depth, at 104.2mm and 104.4mm above the bottom fiber of the deck, respectively (Figure 32 (b) and (c)). As the reinforcing steel was laid out identically in these two decks, the ratio of strains in the bottom steel versus strains in the

top steel were also predicted to be similar: 1.92 for the Conventional deck and 1.94 for the HPC deck. Although strains recorded in the rebar will have different magnitudes, strains in the concrete at the extreme fibers of the deck should have approximately equal magnitudes under pure bending, but be opposite in sign.

The Empirical deck cross-section has a slightly different geometry from the Conventional and HPC decks: the transverse steel in this deck is *not* identical in the upper and lower mats, as shown in Figure 32 (d). Although the specified clear covers are the same as the other two decks, the bottom mat of transverse rebar has larger diameter bars (16mm), which are spaced less densely (345mm on center) than the top mat (13mm diameter bars at 330mm on center). Despite this difference, the bending neutral axis for the uncracked Empirical deck was also predicted to lie relatively close to mid-depth, at 104.4 mm. Although the bending neutral axis was nearly identical to those of the Conventional and HPC decks, the predicted ratio of bottom rebar strains to top rebar strains is 1.82. This difference stems from the smaller bar sizes in the Empirical deck – given the same clear cover, the smaller bars place the mid-plane of each bar farther from the neutral axis. Again, the concrete strains at the extreme fibers will have approximately the same magnitude, with opposite sign.

Actual Neutral Axis Determination. Strains recorded during live load testing were used to locate the height of the actual neutral axis in each deck during testing. Differences between the actual neutral axis and the predicted bending neutral axis were subsequently used in explaining deck behaviors observed under the live load events. The ST-S test strain histories at Gage Location D-4 in all three bridge decks are shown in

Figure 33. Before looking at the specific neutral axis position, it is informative to review what these gages indicate relative to general behavior of the deck at this location during test ST-S. As expected, this truck position induces a positive moment on the deck at Gage Location D-4 (top compression, bottom tension). The bottom mat gages report tensile strains approximately twice as large in magnitude as the compressive strains in corresponding top gages, generally consistent with bottom-to-top strain ratios predicted above for pure bending in the decks. This general behavior is evident in all of the free-span areas under the influence of positive moments. This basic behavior is also indicated by strains reported from co-located concrete embedment gages at mid-depth and in the plane of the upper mat of reinforcing steel (not shown). For situations where positive moments are imparted, tensile strains are reported by the mid-depth gages, which qualitatively support the assertion that the actual neutral axis is nearer to the top mat of steel than to the bottom.

The live load strains from each truck test were used to calculate the position of the actual neutral axis at each gage location. These calculations were accomplished using the recorded strains and the geometric cross-section depth at which those strains were recorded (bar depths), and assuming a linear strain distribution across the depth of the deck, as shown in Figure 34. The point of intersection of the linear profile with the zero-strain-axis revealed the actual neutral axis position, as indicated by point AA in Figure 34. The angle φ in Figure 34 describes the interior angle formed between the internal linear strain profile and the vertical zero-strain-axis. Coincidently, the value of φ is approximately equivalent to the strength-of-materials value of curvature, κ. The φ value

is proportional to the bending moment, indicating both the sign and the relative magnitude of the moment (i.e., larger φ indicates larger magnitude moment, assuming the stiffness remains unchanged). Positive values of φ are counterclockwise and indicate positive moment, while negative values of φ indicate negative moment.

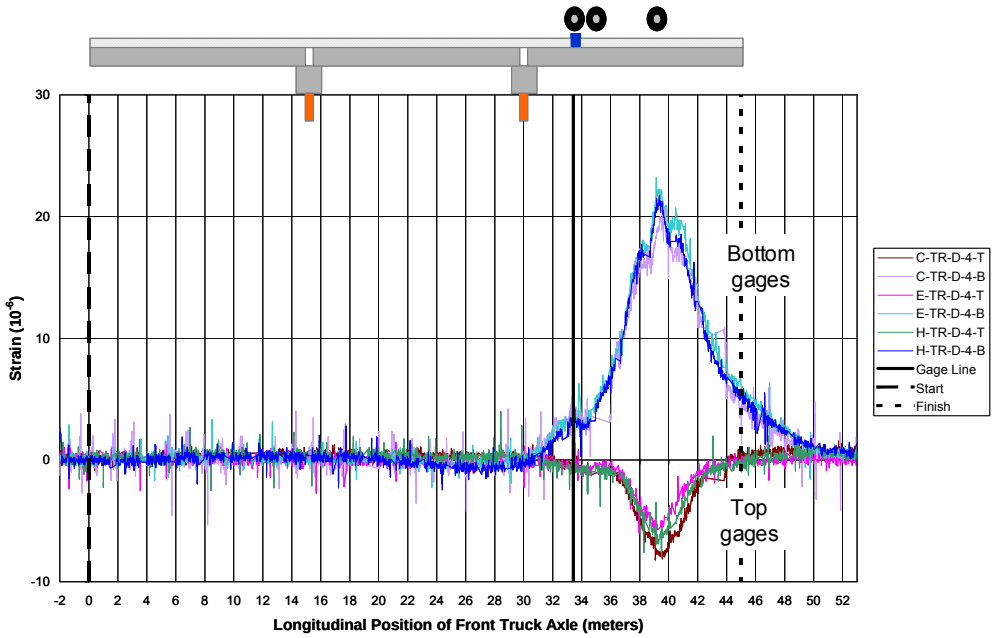

Figure 33 Typical positive moment response (Gage Location D-4, ST-S test)

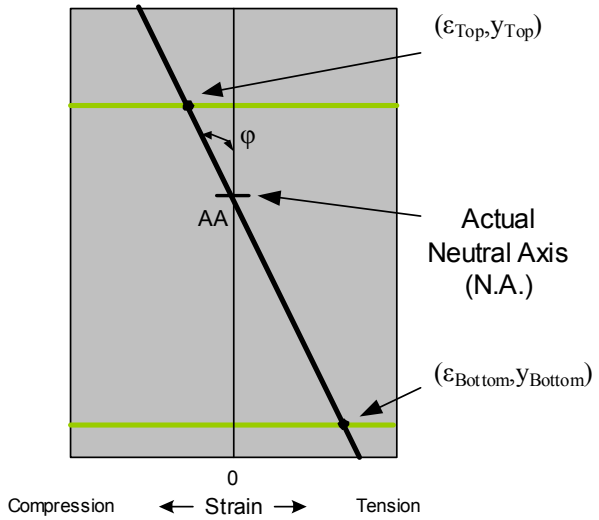

Figure 34 Determination of actual neutral axis height

The actual neutral axis positions, determined from the live load data for each live load test on the Conventional, Empirical, and HPC decks, are given in Table 2, Table 3, and Table 4, respectively. All values are the height in millimeters (mm) of the actual neutral axis above the bottom fiber of the deck concrete; shaded cells indicate negative moment is present. The neutral axis values have been reported for strains recorded at two separate truck positions along the strain history. The first truck position locates the front axle at 40m, leaving the back tandem axle of the truck directly at Gage Line D, as shown in Figure 35. The second truck position marks the progression of the front axle to 42m, moving the back tandem axles two meters away from Gage Line D. As might be expected, distinct behaviors were sometimes observed in the immediate vicinity of the concentrated wheel loads (evident in the 40m response), relative to the global effects observed away from the vicinity of the wheel loads (observed in the 42m response).

Table 2 Actual neutral axis heights – Conventional deck

Truck Position	Gage Location	Single-Truck Tests *								Two-Truck Tests *	
		ST-R	ST-S	ST-T	ST-U	ST-V	ST-X	ST-Y	ST-Z	TT-XT	TT-WR
40m	D-1	-299	-3	48	35	30	56	103	18	50	-22
	D-2	117	109	120	123	71	90	99	129	118	159
	D-4	111	111	102	104	132	91	101	105	107	115
	D-5	204	144	39	28	125	88	99	100	73	830
	D-6	79	169	122	118	120	118	111	114	120	120
42m	D-1	252	-4134000	-178	-178	-72	49	100	16	-121	-150
	D-2	142	141	141	139	-49	86	94	141	166	177
	D-4	137	126	114	115	118	56	93	97	120	129
	D-5	132	120	110	112	110	-106000	93	97	116	121
	D-6	202	136	130	122	120	127	102	109	125	126

* All measurements in mm above bottom fiber of concrete
Shading indicates negative moment

Table 3 Actual neutral axis heights – Empirical deck

Truck Position	Gage Location	Single-Truck Tests *								Two-Truck Tests *	
		ST-R	ST-S	ST-T	ST-U	ST-V	ST-X	ST-Y	ST-Z	TT-XT	TT-WR
40m	D-1	-237	-19	36	46	56	66	112	130	29	-50
	D-2	126	118	121	125	94	102	108	116	131	190
	D-4	120	121	117	118	141	105	113	113	122	126
	D-5	775	172	82	78	159	101	113	101	91	39
	D-6	86	207	126	122	123	65	120	119	123	125
42m	D-1	337	322	-283	-299	40	33	102	130	-280	-704
	D-2	144	138	134	150	33	95	112	110	283	187
	D-4	141	135	130	130	130	84	107	103	143	140
	D-5	162	142	129	128	126	-110500	104	88	136	144
	D-6	270	144	131	133	128	137	114	113	133	139

* All measurements in mm above bottom fiber of concrete
Shading indicates negative moment

Table 4 Actual neutral axis heights – HPC deck

Truck Position	Gage Location	Single-Truck Tests *								Two-Truck Tests *	
		ST-R	ST-S	ST-T	ST-U	ST-V	ST-X	ST-Y	ST-Z	TT-XT	TT-WR
40m	D-1	-225	-20	25	19	35	129	282	406	36	-77
	D-2	113	107	114	117	80	97	104	111	107	167
	D-4	109	115	111	112	141	106	117	118	112	118
	D-5	247	155	73	69	148	98	107	105	90	41
	D-6	96	227	124	123	122	130	116	117	121	125
42m	D-1	312	277	441	-1979	-178	88	141	406	847	794
	D-2	131	128	131	129	-1344	81	96	107	141	176
	D-4	114	128	124	126	126	85	117	111	128	136
	D-5	139	126	117	118	117	35	99	100	123	127
	D-6	353	145	121	130	128	173	109	110	129	133

* All measurements in mm above bottom fiber of concrete
Shading indicates negative moment

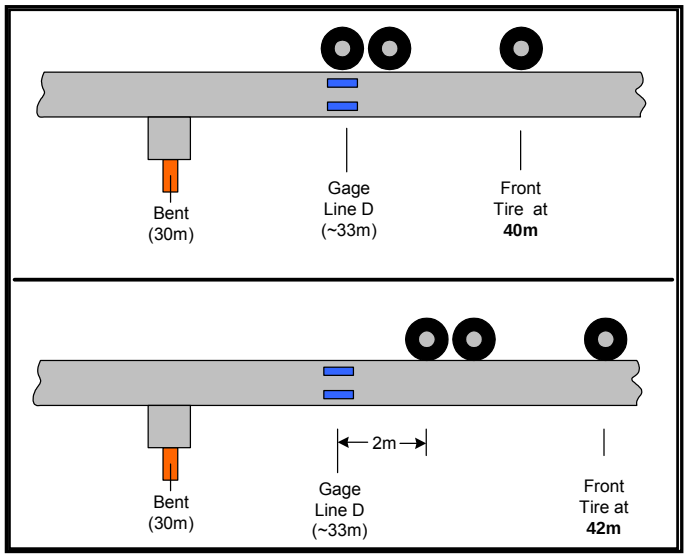

Figure 35 Distinction between 40m and 42m truck positions, relative to Gage Line D

In many cases, the actual neutral axis locations reported in Tables 2, 3, and 4 are quite different from the predicted bending neutral axis position of approximately 104mm. In general, in the presence of positive bending moments, the actual neutral axis is *higher* than the bending neutral axis. This observation is statistically supported by a one-sided t-test, with 104mm as the null hypothesis and using the mean of all positive moment neutral axis heights as the test statistic. A statistical t-test was also used to investigate differences *between* mean neutral axis heights of different decks. The mean neutral axis height of the Empirical deck under positive moment was found to be significantly higher than the mean neutral axis height of the Conventional deck under positive moment ($\alpha = 0.05$). The mean neutral axis height for the HPC deck under positive moment rests somewhere between the means of the other two decks, but it is not statistically different from either of them. Excluding the Two Truck tests values, a second comparison between mean neutral axis heights under positive moment found that the means for both the Empirical and HPC decks were significantly higher than the mean neutral axis height of the Conventional deck, at an $\alpha = 0.025$ significance level.

The neutral axis positions reported under negative moment were scattered, with many outliers both higher and extremely lower than the predicted bending neutral axis (see Tables 2, 3, and 4). These outliers made it difficult to assess trends in these positions with any confidence. In general, most of the negative moment neutral axis heights for the Conventional deck were below the predicted value of 104mm; most of the Empirical and HPC values were above 104mm. Nonetheless, in the presence of negative bending

moment, the actual neutral axis heights appear generally *lower* than for the positive moment.

Comparing the localized effects and the more generalized global effects, the 42m neutral axis heights seem generally higher than those at 40m, although this observation does not appear to be consistently supported with statistical significance. Additionally, the neutral axes obtained during Two-Truck tests appear about the same or nominally higher than the Single-Truck experiments, in most cases.

Perhaps the most important conclusion that can be drawn is that the actual height of the neutral axis differs from the predicted height of the bending neutral axis. This difference in the neutral axis location could be the result of either of two distinct phenomena (or a combination of both): 1) a geometric shift of the bending neutral axis due to cracking or other irregularities in the cross-section, and 2) the presence of in-plane axial tension or compression forces.

Two separate analyses were conducted to investigate which of these phenomena is most dominant. Due to the different transverse locations of the gages across the deck, they are difficult to compare head-to-head. Therefore, each gage location is considered separately, based on the surrounding geometry and presumed behaviors at that point. The most conclusive evidence used to evaluate each bridge deck for cracking and axial effects is found in the data of Gage Locations D-4 and D-1, respectively. Specific evidence from these two gage locations is presented below. Data obtained from the remaining three gage locations (D-2, D-5, and D-6) corroborate and support the evidence from the other two gages, but they do not offer any unique insights.

Deck Cracking Analysis

An investigation was conducted to determine whether deck cracking was responsible for shifting the bending neutral axis, using the values presented in Tables 2, 3, and 4. To begin this investigation, it is necessary to establish whether the actual neutral axis heights are reasonable. To offer some basis of comparison, Table 5 presents heights of bending neutral axes predicted under three different theoretical conditions, also represented graphically in Figure 36: uncracked (refer to Figure 32), cracking up to the lower mat of steel, and all tensile regions of concrete cracked. In all cases, the indicated values were determined using positive moments. When the concrete cracks in the bottom fibers due to a positive moment, the cross-section geometry changes and the neutral axis is expected to shift upward in the cross-section, as indicated in Table 5 and shown in Figure 36.

Table 5 Hypothetical bending neutral axis locations at various cracking levels under positive moment

Deck	Uncracked	Cracking up to Lower Rebar Mat	All Tensile Concrete Cracked
Conventional	104.2 mm	120.0 mm	166.2 mm
Empirical	104.4 mm	120.0 mm	175.7 mm
HPC	104.4 mm	120.5 mm	170.1 mm

The middle column of bending neutral axis heights in Table 5 was calculated with cracks extending just up to the bottom mat of rebar. Many of the actual neutral axes fall reasonably close to this theoretical 120mm bending neutral axis height, potentially suggesting that the decks might be cracked. Such cracking might not be visually pronounced and could have gone unnoticed during the live load tests. Further investigation was warranted and discussed below. On the other hand, cracking of all

tensile concrete to the neutral axis height (approximately 85% of the cross-section height) would probably have been noticed.

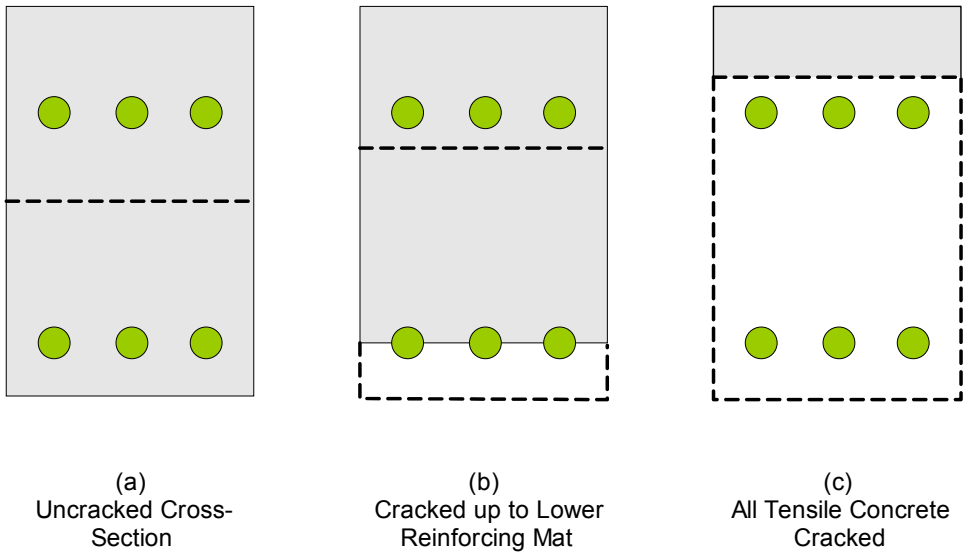

Figure 36 Representations of theoretical cracking scenarios

Gage Location D-4 offers the best location for investigating deck cracking because it is positioned relatively close to the midspan between Girder 1 and Girder 2. At this location, the expected behaviors are presumably the best understood, with the deck behaving most like a beam spanning between the adjacent girders.

Relative to seeing evidence of cracking under positive moment, consider the hypothetical case of a partially cracked cross-section, as shown in Figure 37 (a). This crack may either be stable or unstable. An unstable crack propagates under increased positive moment (Figure 37 (b)), while a stable crack remains the same length (Figure 37 (c)). The propagation of the unstable crack changes the geometry of the cross-section, resulting in a relatively higher neutral axis position (Figure 37 (b)). For the stable crack,

the geometry of the cross-section remains the same, leaving the neutral axis at the same height (Figure 37 (c)). In either case, the neutral axis height is never expected to shift lower, given a larger magnitude positive moment.

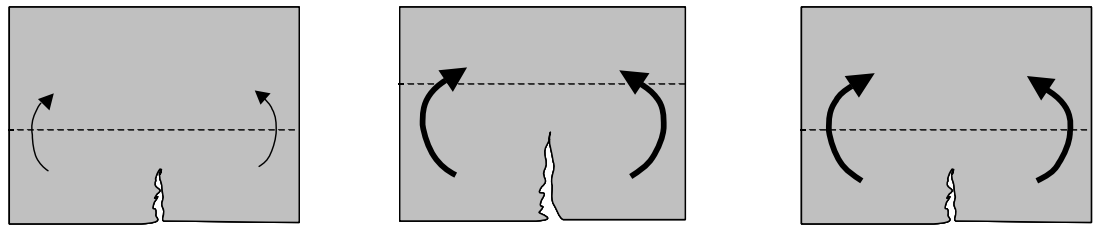

Figure 37 Hypothetical behavior of partially-cracked cross-section

To compare magnitude of positive moments, several values of φ are shown in Table 6, taken from Gage Location D-4 of each bridge deck, for truck tests ST-R, ST-S, ST-T, and ST-U. Based on these φ angles, the positive moments experienced at Gage Location D-4 are higher during the ST-T and ST-U tests than during tests ST-R and ST-S (assuming the stiffness is unchanged). In fact, the positive moments observed at Gage Location D-4 during ST-T and ST-U are the largest of all the live load tests. If any cracking had occurred, it would be most pronounced in these live load tests. However, the actual neutral axis heights in these tests do not support the occurrence of cracking. The actual neutral axis heights from Gage Location D-4 in all the decks during tests ST-R, ST-S, ST-T, and ST-U are presented in Table 7. Notably, the reported neutral axis heights are lower for tests ST-T and ST-U than for the corresponding ST-R and ST-S tests, with a minor exception for the HPC deck. Thus, in the Saco decks, higher positive

moments are associated with lower neutral axis heights. For a partially cracked cross-section, recall that lower neutral axis positions are not expected under higher positive moments. This expected behavior is not supported by the data presented here. Thus, it is unlikely the bottom of any of the decks has cracked.

Table 6 Values of φ at Gage Location D-4

Londitudinal Position	Deck	ST-R*	ST-S*	ST-T*	ST-U*
40m	Conventional	15.9	15.0	31.2	30.6
	Empirical	15.2	14.0	29.5	29.5
	HPC	16.6	14.5	30.3	31.4
42m	Conventional	5.6	7.6	11.8	11.3
	Empirical	6.0	7.3	10.2	10.9
	HPC	7.2	7.5	10.4	12.7

* All values measured in degrees; All values indicate positive moment

Table 7 Actual neutral axis heights at Gage Location D-4

Londitudinal Position	Deck	ST-R*	ST-S*	ST-T*	ST-U*
40m	Conventional	111	111	102	104
	Empirical	120	121	117	118
	HPC	109	115	111	112
42m	Conventional	137	126	114	115
	Empirical	141	135	130	130
	HPC	114	128	124	126

* All measurements in mm above bottom fiber of concrete

Similar to the evidence just presented above, larger positive moments are induced at the 40m truck position than at the 42m truck position, confirmed by the φ values in Table 6. Physically, with the front axle at 42m (refer to Figure 35) the truck is moving away from the vicinity of the gages of interest (Gage Line D), so the positive moments are reduced. Consequently, neutral axis heights are expected to be higher for the 40m

positions. However, the neutral axis heights at 40m in Table 7 are lower than corresponding neutral axis heights at 42m. This is further evidence that the relationship between moment and neutral axis is different from what was expected for a partially cracked cross-section under pure bending.

In light of these two observations regarding the relationship between positive moment and the actual neutral axis, it is unlikely that cracking occurred in the bottom fibers of the freespan regions of any of the three decks during live load testing. It is important to qualify that the absence of cracking is conclusive only within the specific cross-section containing the strain gages. However, it is assumed that the gages are located at critical response points, and that it is reasonable to infer that the other positive moment regions of the deck are also cracked.

While the actual neutral axis has shifted in the decks relative to the predicted bending neutral axis, cracking does not appear to be responsible. Since cracking is not causing the shift, some mechanisms other than pure bending must exist.

Axial Force Analysis

In the preceding discussion, a logical analysis of the strain data from the decks indicated that none of the decks had cracked. In the following discussion, a similar approach is used to investigate the possibility that changes in neutral axis height are caused by the presence of in-plane axial forces and associated strains.

If an uncracked deck section is assumed, axial forces acting in conjunction with the moment may explain the neutral axis shift. In the event of pure bending, no net axial stress exists, and the strain profile for each deck should look much like those shown in

Figure 32 (b),(c),(d). In the event that axial forces *do* exist, the effects are superimposed on the effects of pure bending. As such, the strain profile remains parallel to the predicted profile, but is shifted horizontally along the strain-axis, as shown in the two cases of Figure 38.

Notice that the presence of uniform axial force effectively changes the height of the actual neutral axis (i.e., the difference between the bending neutral axis Point A and the actual neutral axis, Point AA, in Figure 38). The strain profile of Figure 38 (top) represents the rise of the actual neutral axis when a positive moment acts in conjunction with an axial tension field. The strain profile of Figure 38 (bottom) represents the lowering of the actual neutral axis when a negative moment acts in conjunction with an axial tension field. The opposite movement of the neutral axis would be realized in a uniform axial compression field (not shown).

The uniform axial strain necessary to cause such a shift was calculated for all truck runs on each bridge. The results of these calculations are presented in Table 8, Table 9, and Table 10 for each live load test performed on the Conventional, Empirical, and HPC decks, respectively. To calculate this axial strain shift, the live load data was used to determine the slope of the reported linear strain profile at each gage location (refer to Figure 34). Rebar strains for pure bending were then predicted by drawing a parallel profile through the theoretical uncracked bending neutral axis (the light grey profile shown in Figure 38). The amount of superimposed axial strain necessary to shift the strain profile to the actual neutral axis was simply the numeric strain difference between the pure bending profile and the actual profile (Figure 38). In Tables 8, 9, and 10, a

positive sign indicates a tensile axial strain, while a negative sign indicates a compressive axial strain. Once again, shading indicates the presence of negative moment.

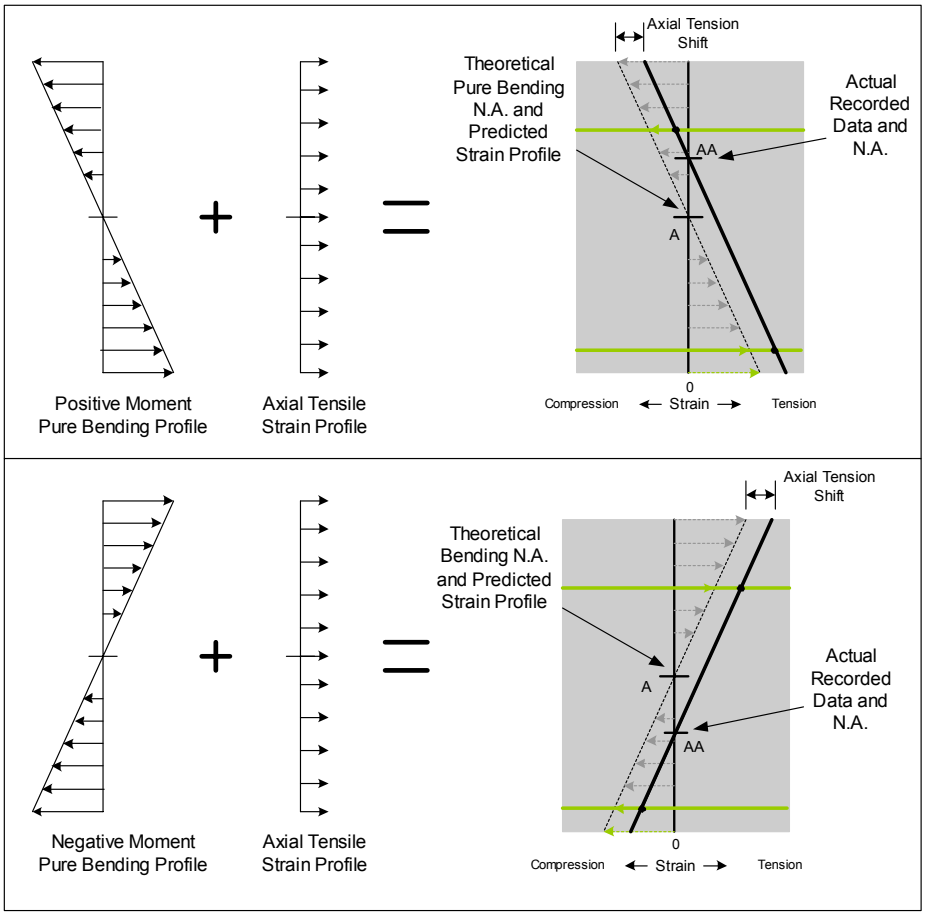

Figure 38 Addition of axial strains to bending strains, with resulting neutral axis shift

Table 8 Calculated axial strains – Conventional deck

Truck Position	Gage Location	Single-Truck Tests*								Two-Truck Tests*	
		ST-R	ST-S	ST-T	ST-U	ST-V	ST-X	ST-Y	ST-Z	TT-XT	TT-WR
40m	D-1	5.3	7.2	4.0	4.3	1.6	0.9	0.0	-3.6	4.7	7.8
	D-2	2.4	2.0	1.5	1.2	1.5	0.9	0.3	-0.9	1.9	4.4
	D-4	1.9	1.8	-1.1	-0.2	1.4	0.9	0.2	-0.1	1.2	3.2
	D-5	4.7	5.1	4.8	4.9	2.8	1.7	0.4	0.4	6.0	6.8
	D-6	1.2	2.5	7.3	4.8	5.2	0.8	-0.7	-1.3	7.6	7.2
42m	D-1	2.8	3.9	2.7	2.9	1.7	1.1	0.1	-3.4	3.2	5.5
	D-2	3.0	3.6	2.6	1.9	2.0	1.0	0.5	-1.0	3.4	4.6
	D-4	3.2	3.0	2.0	2.1	1.3	0.9	0.6	0.4	3.2	4.4
	D-5	2.5	2.3	1.5	1.8	1.1	1.0	0.6	0.5	2.6	3.9
	D-6	1.8	2.3	5.5	3.7	3.8	1.9	0.1	-0.5	6.2	4.7

* All values reported in με ; Positive = Axial Tension; Negative = Axial Compression
Shading indicates negative moment

Table 9 Calculated axial strains – Empirical deck

Truck Position	Gage Location	Single-Truck Tests *								Two-Truck Tests *	
		ST-R	ST-S	ST-T	ST-U	ST-V	ST-X	ST-Y	ST-Z	TT-XT	TT-WR
40m	D-1	5.6	5.9	3.9	3.2	1.1	0.3	0.0	-0.2	5.6	7.3
	D-2	3.7	4.8	0.9	0.6	0.4	0.1	-0.2	-0.5	2.4	4.6
	D-4	4.4	4.2	7.1	7.7	1.4	-0.1	-0.5	-0.4	7.6	6.3
	D-5	4.2	4.8	2.7	3.0	4.2	0.2	-0.5	0.2	2.7	5.5
	D-6	1.2	2.6	8.6	5.9	5.4	-0.8	-1.7	-1.7	8.2	8.1
42m	D-1	2.5	2.6	2.5	1.8	0.9	0.6	0.0	-0.2	4.2	4.4
	D-2	3.0	3.4	2.0	2.2	0.9	0.4	-0.2	-0.2	4.4	4.8
	D-4	3.8	3.9	4.5	4.9	2.0	0.5	-0.1	0.1	6.1	5.9
	D-5	2.5	3.1	3.4	3.2	2.8	1.0	0.0	0.6	4.5	5.0
	D-6	2.1	2.7	5.0	5.3	4.7	1.0	-0.7	-0.7	6.4	5.7

* All values reported in με ; Positive = Axial Tension; Negative = Axial Compression
Shading indicates negative moment

Table 10 Calculated axial strains – HPC deck

Truck Position	Gage Location	Single-Truck Tests *								Two-Truck Tests *	
		ST-R	ST-S	ST-T	ST-U	ST-V	ST-X	ST-Y	ST-Z	TT-XT	TT-WR
40m	D-1	5.6	5.7	4.0	3.8	1.2	-0.2	-0.5	-0.6	4.3	7.0
	D-2	1.6	0.9	0.9	1.0	0.8	0.4	0.0	-0.2	0.4	3.5
	D-4	1.4	2.9	3.7	4.8	1.2	-0.1	-0.7	-0.6	3.4	4.0
	D-5	4.4	4.8	3.4	3.7	2.9	0.7	-0.2	0.0	3.5	5.3
	D-6	0.6	2.5	8.6	7.4	5.7	0.9	-1.2	-1.6	7.6	8.8
42m	D-1	2.5	2.3	1.9	2.0	1.3	0.1	-0.1	-0.6	2.1	3.9
	D-2	1.9	2.6	1.8	1.5	1.4	0.7	0.3	-0.1	2.1	3.2
	D-4	1.2	3.1	3.6	4.9	1.7	0.4	-0.4	-0.3	3.6	4.0
	D-5	2.4	2.4	2.3	2.4	1.8	0.9	0.3	0.3	3.1	3.7
	D-6	1.2	2.5	3.1	5.0	4.4	1.9	-0.3	-0.5	5.4	4.8

* All values reported in με ; Positive = Axial Tension; Negative = Axial Compression
Shading indicates negative moment

Notably, most of the axial strains calculated from the live load data were tensile. With respect to their magnitudes, they are "small" but not insignificant. Many of the negative moment regions also reveal axial tension strains, which again are small but not insignificant in magnitude. With a minor exception in the Conventional deck, the only axial compressions noted were in regions experiencing negative moment, primarily test runs ST-X, ST-Y, and ST-Z. All the decks reveal fairly similar magnitudes and directions of axial strains, although the Empirical deck appears to show generally higher strains than the other two decks. A statistical one-sided t-test was performed to compare

the means of axial strains in the three decks under positive moment only. The mean of the axial tension strains in the HPC deck under positive moment are statistically higher than the mean of the Conventional deck ($\alpha = 0.05$). The Empirical deck has a statistically higher mean axial tension strain in positive moment regions than the means of both the Conventional and HPC decks ($\alpha = 0.025$).

Originally, it was not necessarily expected that axial tensions would be generated in the decks under vehicle loadings. If anything, a little compression was possibly expected due to internal arching. In this regard, however, recall that Fang, et al. (1990) observed no deck cracking and observed in-plane tension membrane stresses in the decks up until cracks occurred at three times the AASHTO service load. Also recall the statements by AASHTO (2000), Csagoly and Lybas (1989), and Fenwick and Dickson (1989), which indicate that cracking of the bottom of the deck is a critical prerequisite to the internal arching phenomenon. Therefore, in the absence of cracking, no compressive dome action is expected.

The source of the observed axial tension is not entirely clear, but a suggested behavioral description of this phenomenon is offered here. As the truck nears the region of the gages, the deck deforms like a plate in flexure, also tending to "draw in" toward the tire location. Due to the lateral restraint provided by the girders, diaphragms, and surrounding deck concrete, the "drawing" action is resisted and axial forces and strains are present in the deck section. This is similar to the behavior exhibited by a beam or plate, pinned at both ends and subjected to flexural load. A simply supported member, without restraint, is allowed to deform along its axis as needed. By contrast, the lateral

restraint in a pinned-pinned member resists those deformations, lengthening the bending neutral axis and resulting in axial stresses and corresponding axial strains. This behavior can occur in a linear-elastic fashion if the beam has already transversely deflected under the action of other loads (i.e., self-weight of the member). Cuelho, et al. (2004) performed finite element analysis confirm the validity of this "unexpected" axial tension. An uncracked model of the Conventional deck was subjected to truck loads, revealing in-plane axial tension within the deck.

For the Saco bridge decks, the data reported at Gage Location D-1 presents compelling evidence that axial forces are present. Recall that this gage is located in the overhang, just outside Girder 1 (Figure 31 (b)). Many of the actual neutral axes for Gage Location D-1 (shown in Tables 2, 3, and 4) fall outside of the geometric limitations of the cross-section. This phenomenon is physically impossible without the presence of axial forces. For example, the diagram presented in Figure 39 shows a strain profile in net tension, resulting from a positive bending moment occurring in a uniform axial tension field. Note the position of the neutral axis above the upper fiber of the cross-section.

The net tension in the deck at Gage Location D-1 is obvious in the transverse strain profile recorded from all three bridges at 40m (truck tires in the vicinity of Gage Line D) for test ST-S, as shown in Figure 40. The moments induced at Gage Location D-1 are relatively small, as indicated by small φ angles. As such, bending and/or cracking effects are not expected to be very dramatic here. Therefore, it is reasonable to conclude that axial effects are the predominant factor affecting the position of the actual neutral axis at Gage Location D-1, in the overhang.

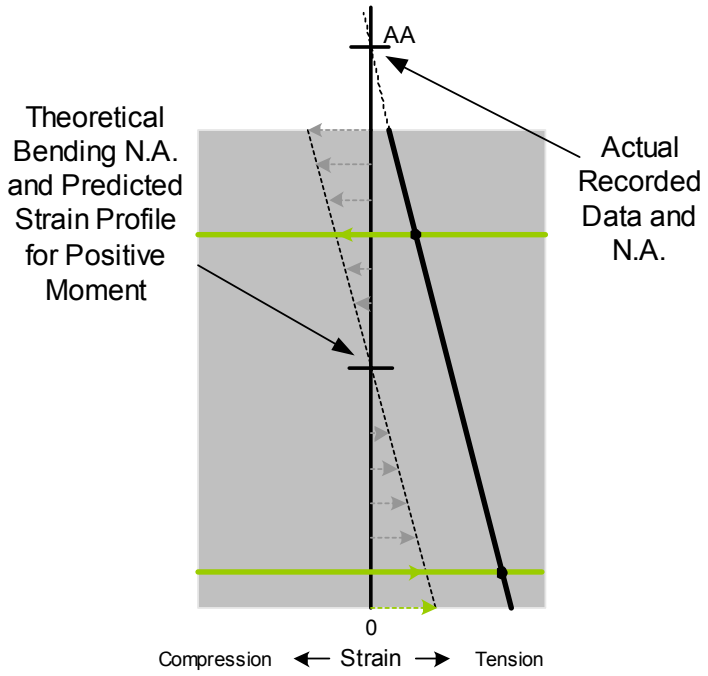

Figure 39 Representation of axial tension behavior at Gage Location D-1

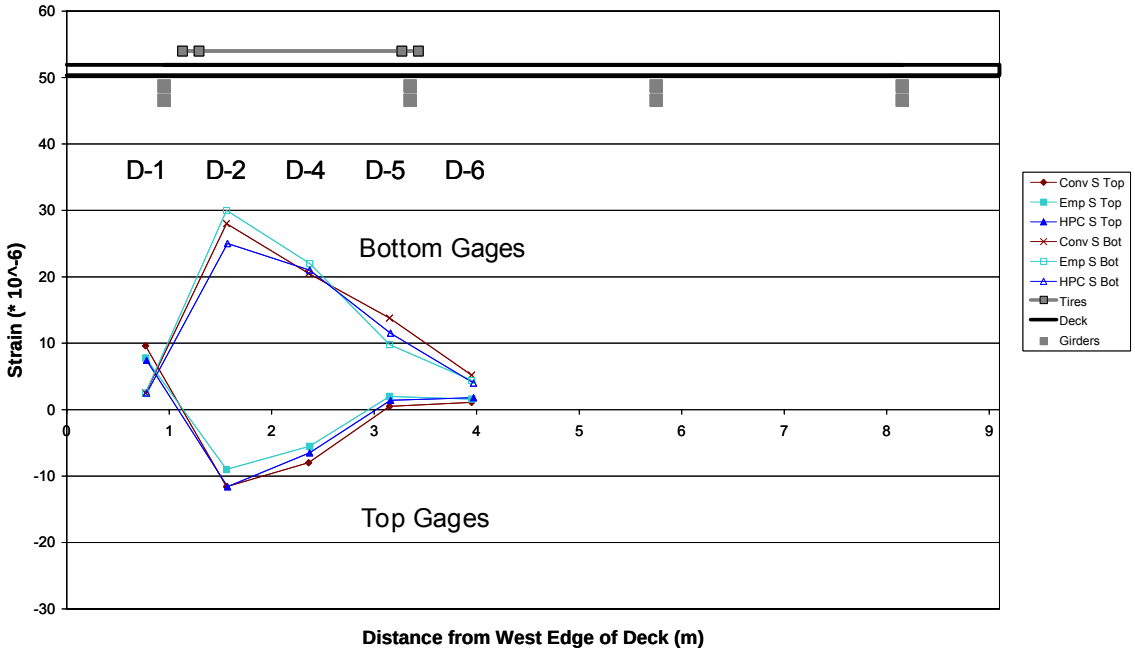

Figure 40 Transverse strain profile reveals axial tension (ST-S test at 40m)

A similar net tension is also evident at Gage Locations D-5 and D-6 in the transverse strain profile in Figure 40, further supporting the evidence of obvious in-plane axial tension in the bridge decks. Although less obvious, calculation of the axial strains for this truck run at Gage Locations D-2 and D-4 are also shifted in tension (Tables 8, 9, and 10). In light of the preceding discussion, it is evident that in-plane axial forces are present in all of the bridge decks, and that these axial forces are responsible for shifting the neutral axis.

Conclusions

The presence of axial forces is a more likely explanation than deck cracking with regard to the noticeable shift in the height of the neutral axis from its position predicted from pure bending. The evidence from Gage Location D-4, supported by the other locations, presents a consistent picture that cracking has *not* occurred in any depth of the deck. With this cause for the observed neutral axis shift ruled out, the in-plane axial forces are most likely the cause. Convincing evidence was found to support this conclusion in the data of Gage Location D-1 and others. Undeniably, certain anomalies do exist in the data, which limit the development of patterns or predictive models regarding these axial effects. However, in light of the data analysis, supported by finite element analysis evidence and results observed by other authors, it is reasonable to conclude that cracking is not present, and that in-plane axial forces are the behavior driving the neutral axis shift throughout the deck. Finally, instead of observing axial compression strains indicative of the internal arching mechanism, axial tension was

observed in a majority of the readings, indicating that arching action is *not* occurring in any of the bridge decks at live load stress levels.

Deck Integrity Over Girders

When considering the transverse behavior of the bridge deck, the integrity of the concrete located over the girders is of great concern. When the tires of a truck transversely straddle a girder, a negative moment is induced over the top of that girder, inducing tension in the upper fibers of the deck. If the strains are large enough, the deck surface may crack parallel to the girders. These cracks can have two detrimental effects on deck performance, namely, corrosion of the reinforcing steel and direct freeze-thaw damage of the deck concrete. Therefore, determining whether cracking at this location is imminent or has already occurred is of interest for evaluating relative deck performance.

This particular live load distress is expected to be the most critical during truck tests that position the truck tires to straddle a girder, namely ST-T and ST-U, in which the truck tires straddle Girder 2 (Figure 25). In this case, negative moments are expected over the top of the girders. Figure 41 presents the transverse strain history captured during test ST-U from the Conventional bridge deck at Gage Location D-5, off the western face of Girder 2. Negative moments were generated here, as evidenced by tension in the top gages and compression in the bottom gages, but the negative moments are relatively small in magnitude, with maximum tension in the top gage being less than 10 με. A strain of 10 με in the top reinforcing mat corresponds to approximately 30 με in

the upper concrete fiber. Strains of this small magnitude suggest that this live load distress is not as critical as originally expected.

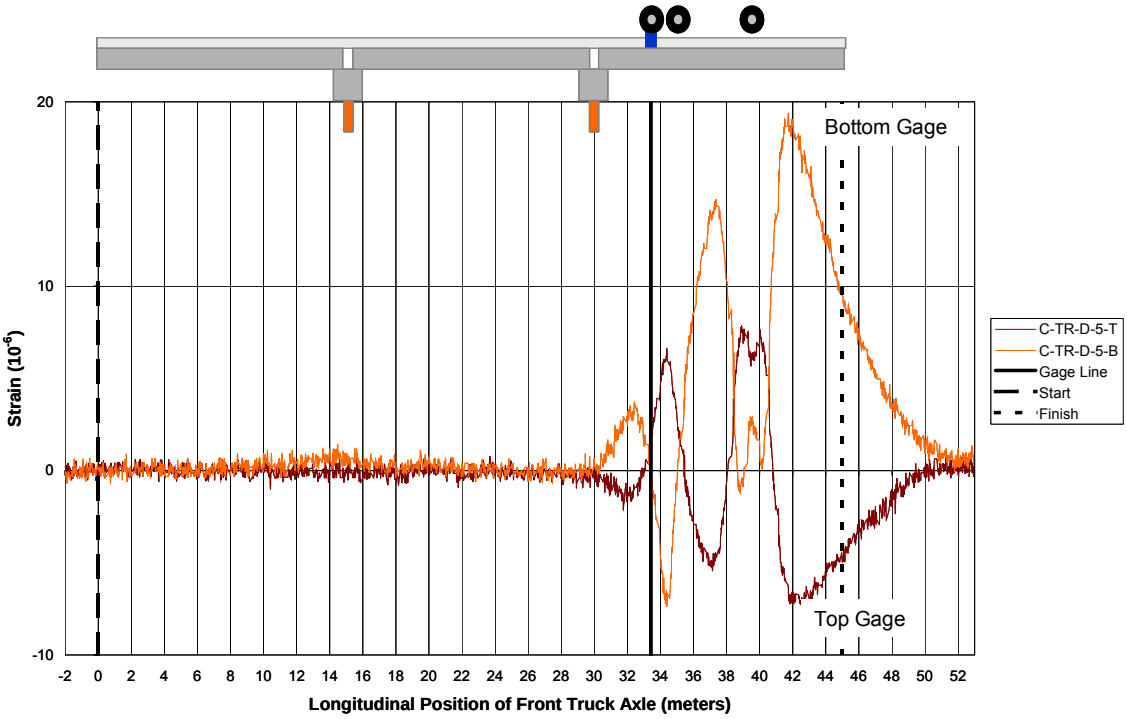

Figure 41 Strain history at Gage Location D-5 during ST-U test (Conventional deck)

The strain histories from Gage Location D-5 during test ST-U for all three decks are shown in Figure 42. A comparison of the three strain histories reveals that all three decks responded similarly to this load case. A chronological description of the strain history shows that a positive moment begins forming at a truck position of about 30m, similar to the trace of Gage Location D-4 (Figure 33). At this point, the front axle passes Bent 2 and enters the third longitudinal span (the instrumented span). At 34m, the front axle passes over Gage Line D, causing a reversal of the moment. As the front axle continues downstream, Gage Line D is between the front and rear axles of the truck, so the moment is again positive. As the front axle nears 40m, the rear tandem axles pass over Gage Line

D, again imposing a net negative moment. As the truck proceeds further downstream, the tandem axles leave the vicinity of Gage Line D, and a positive moment is again present, with its peak at around 42m. This positive bending moment effect tapers off as the truck nears the end of the test and finally exits the north end of the bridge. Similar strain histories were observed for the ST-T, TT-XT, and TT-WR tests.

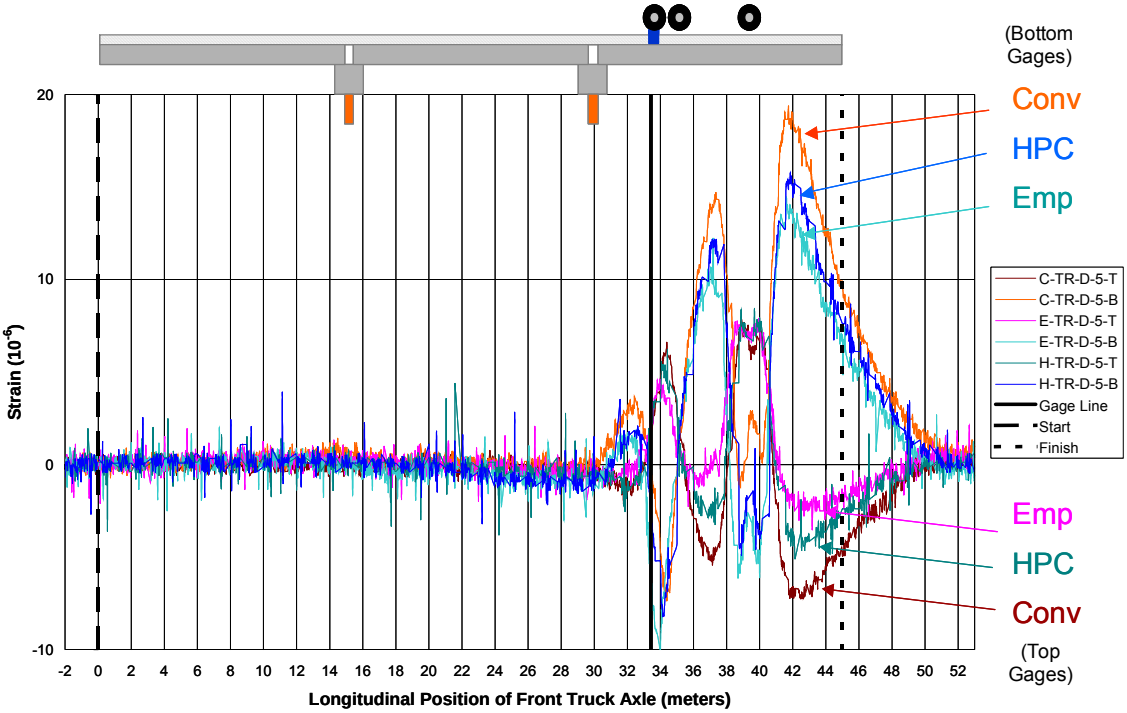

Figure 42 Strain history at Gage Location D-5 during ST-U test (all three decks)

The net response that was just described may be behaviorally separated into a *global response* and a *local response*, as illustrated in Figure 43. The global response is a large 'dish', indicative of a positive bending moment produced by the presence of the truck, most obvious at the 42m truck position (Figure 43 (b)). The local response is the negative bending of the deck over Girder 2, in the immediate vicinity of the truck tires, captured at the 40m truck position (Figure 43 (c)). Notice the position of Gage Location

D-5 over Girder 2, which is in positive curvature at 42m, with superimposed local negative curvature occurring at 40m.

The distinct presence of the global positive moment and the local negative moment in the deck response at Gage Line D are best seen in the strains measured at the 42m and 40m truck positions, respectively. Transverse strain profiles for the Conventional deck at Gage Line D for these two longitudinal truck positions are shown in Figure 44, for the ST-U test (truck straddling Girder 2). The solid points show the transverse strain profile when the tandem axle was away from Gage Line D (42m), revealing the global positive moment effect (Figure 43 (b)). The dashed points show the transverse strain profile when the rear tandem axle was at Gage Line D (40m), reflecting the local bending effect in the immediate vicinity of the axle and tires (Figure 43 (c)). Especially notable in the 40m (dashed) profile of Figure 44 is the local negative bending moment of over Girder 2, superposed atop the global positive bending moment. The net result of these superposed moments is a relatively small net negative bending moment over Girder 2 (top tension, bottom compression). In the clear span region (Gage Location D-4), the tires increase the positive moment, resulting in a relatively higher net positive moment (top compression, bottom tension) than observed for the global 42m response.

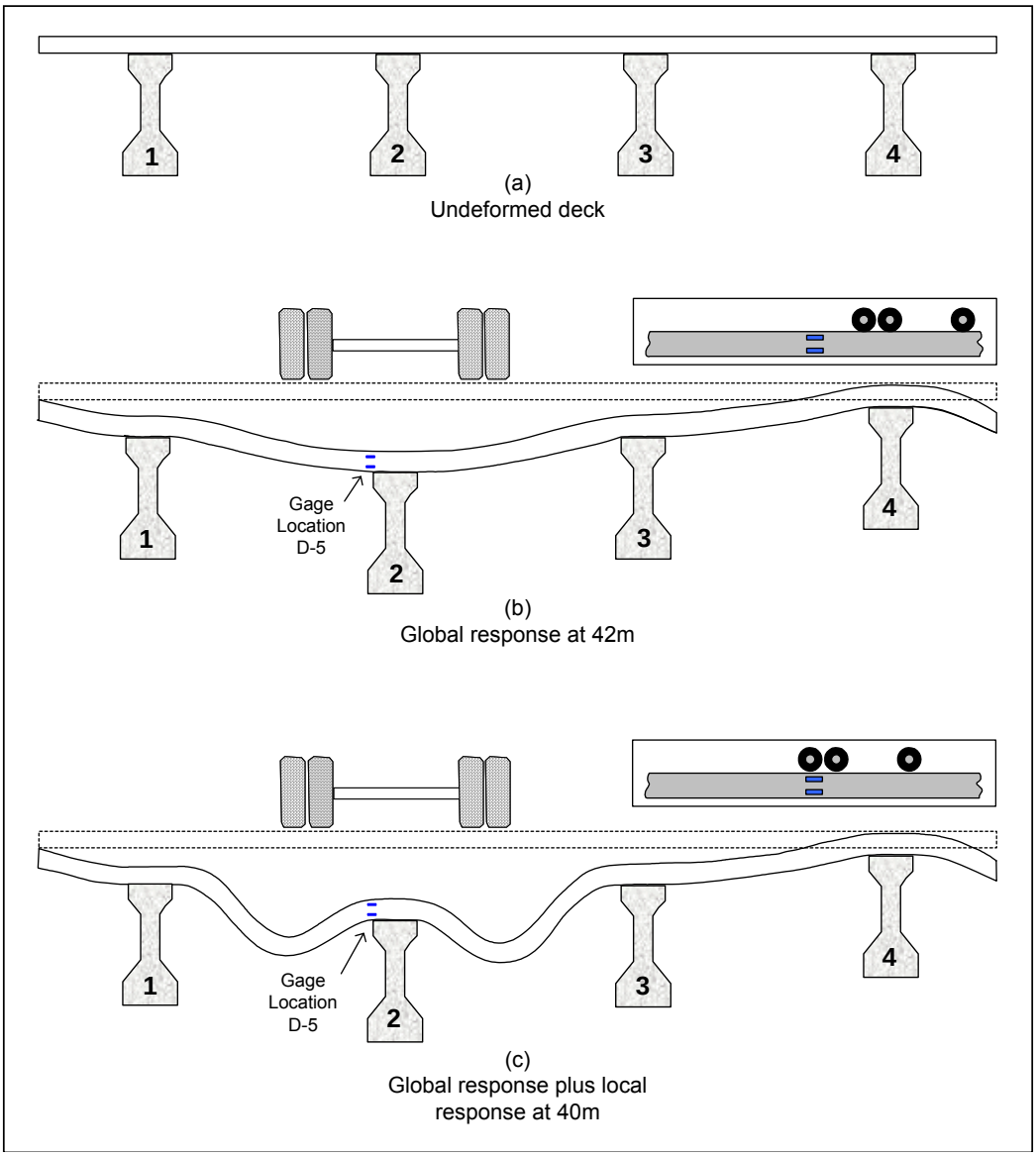

Figure 43 Exaggerated depiction of Global (42m) and Local (40m) responses

To determine if the upper fibers of the deck concrete are cracked, a similar analysis to that used for the Deck Cracking section of this chapter was followed using the strains measured at Gage Location D-5. To make these arguments, a partially-cracked cross-section is assumed, with a partial crack in the top fibers of concrete, quite similar to the argument presented using Figure 37. Compared to the positive moment regions, negative

moment regions exhibit distinctly different bending strain behaviors. Such differences are most evident in the gaged areas (the southbound lane, near Girder 1 and Girder 2, see Figure 31), when the test truck loads the bridge from the northbound lane, near Girders 3 and 4 (i.e., ST-X, ST-Y, and ST-Z). Truck loads from the northbound lane impart global negative moments (tension top, compression bottom) on the gaged portion of the deck. Figure 45 shows the strain profile for all three decks at 40m during the ST-X test. The strain profiles for these loadings appear relatively more symmetric than the profiles from positive moment loading. These shapes and magnitudes are typical for the ST-X, ST-Y, and ST-Z tests.

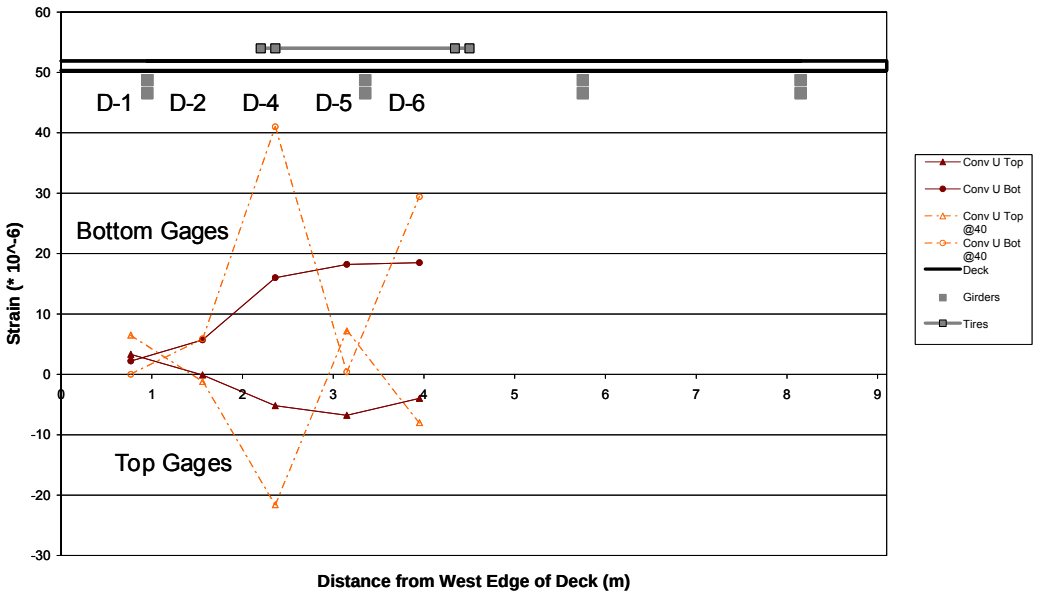

Figure 44 Transverse strain profiles 42m (solid) & 40m (dashed) - Conventional (ST-U)

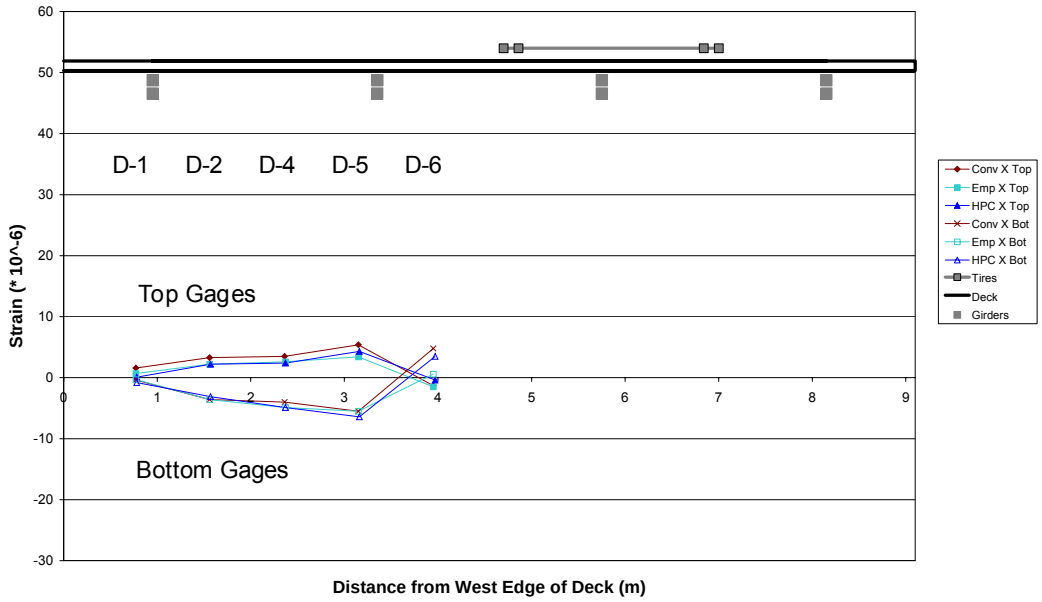

Figure 45 Transverse strain profile reveals tensile shift under negative moment (ST-X test at 40m)

From the bending neutral axis calculations for an uncracked cross-section (Figure 32), a negative moment is expected to impart compressive strains in the bottom reinforcing steel that are approximately twice as large as the tensile strains in the top mat. The transverse strain profile seen in Figure 45 is consistent with the actual neutral axis being higher than the uncracked bending neutral axis because the top strains and bottom strains are approximately equal in magnitude and opposite in sign. If the section were actually partially cracked in the top tension zone, however, the bending neutral axis would have shifted downward. Thus, it is unlikely that there are any cracks in the upper fibers of the deck. Rather, neutral axis shifts are the results of in-plane axial forces, as reported in Tables 8, 9, and 10.

In light of this evidence and the relatively small tensile strains (less than 10 με) resulting from negative moment over the top of Girder 2 under vehicle loads, it is highly

unlikely that the upper fibers of the bridge deck are cracked. It is also unlikely that the decks will crack in the future due to vehicle loads. Other researchers have discussed this phenomenon. Cao (1996) proposed that the current AASHTO bridge deck design was too conservative, because it assumes that the girders provide rigid support in the calculation of the negative transverse moments in the deck over the girders. This traditional calculation is based purely on flexure of the deck over rigid supports and over-designs the deck slab. Cao (1996) observed during testing that the negative moment over the girders was reduced due to girder deflection, which also appears to be the case for the Saco bridges.

It does not appear that cracking is imminent under vehicle loads in the concrete over the top of the girders, but this location should receive close continued observation. Based upon the data presented, it is unlikely that the bridge decks have cracked over the top of the girders.

Deck Stiffness

Nominal differences in the magnitudes of the transverse strains measured from different decks at the same gage locations under the same test events may possibly be related to differences in the deck stiffnesses. Referring to the strain histories reported in Figure 42, for example, the responses have similar waveforms for all three bridges, but their magnitudes are noticeably different. The most obvious difference occurs in the global positive moment (42m) portion of the strain history, where the Conventional deck appears to show a larger positive moment than the HPC deck, and both of them appear larger than the Empirical deck. However, the behaviors of greatest interest for this

analysis are the behaviors in the immediate vicinity of the truck tires, as represented by the strains at 40m. This truck position better emulates a transverse section of the deck as a continuous beam (deck) with applied point loads (tires). The relative magnitudes of the strains at 40m in Figure 42 suggest that a larger magnitude negative moment is present in the Empirical deck, relative to the other two decks. The φ values reported for the ST-U test are provided below in Table 11. Recall that φ is approximately equivalent to curvature (κ) for beams. Curvature is related to both the bending moment (M) and flexural stiffness of the beam cross-section by the following relationship: $\kappa = M / EI$, where E is the elastic modulus of the material and I is the cross-section moment of inertia. Thus, different values of φ could indicate one of two things: 1) given equal stiffness, a higher φ indicates higher moment, and 2) given equal moment, a higher φ indicates lower stiffness. Thus, comparisons of φ values between the different decks should be made cautiously, if the deck stiffnesses are different.

Table 11 Values of φ at 40m during ST-U test

Deck	D-1*	D-2*	D-4*	D-5*	D-6*
Conventional	-3.51	3.83	30.57	-3.67	19.43
Empirical	-3.16	1.81	29.49	-6.40	19.07
HPC	-2.54	4.42	31.36	-5.87	21.33

* All values measured in degrees
Shading indicates negative moment

The relative stiffness (EI) of the three decks in the transverse direction was calculated for each deck; they are summarized in Table 12. The cross-section moment of inertia (I) was calculated using an uncracked cross-section and the dimensions presented in Figure 32. The transverse flexural stiffness of the Empirical deck is noticeably lower than the

other two decks, as might be expected based upon the relative reduction in the amount of steel used in the Empirical deck. The differences noted in the φ values of Table 11 correlate closely with the differences in stiffness shown in Table 12.

Table 12 Summary of calculated transverse stiffness for each deck

Deck	Concrete Elastic Modulus E (GPa)	Deck Cross-Section Moment of Interia I (cm^4)	EI (10^6 N*m^2)
Conventional	39.2	18470	7.24
Empirical	32.1	18180	5.84
HPC	49.0	18290	8.96

Girder Distribution Factor. The stiffness of the decks in the transverse direction also has an effect on the manner in which the bridge carries load longitudinally. Bridge engineers and analysts characterize the stiffness of the bridge superstructure using a parameter called the Girder Distribution Factor (GDF). The GDF value is often expressed as a percentage, indicating how much of the applied load is carried by each girder in the superstructure. The specific manner in which the applied load is shared by the girders is dependent upon the transverse stiffness of the decks relative to the longitudinal stiffness of the girders. Because of the composite interaction between the girders and the composite deck in the longitudinal direction, this load sharing is also influenced by the longitudinal rigidity of the deck. Conceptually, the stiffness of the deck may be correlated with the GDFs in the following manner. Lower longitudinal deck stiffness will result in an overall softer longitudinal response. A softer longitudinal stiffness results in more severe girder deflection near the truck. As a particular girder

deflects further downward, adjacent girders begin to carry more of the load. The degree to which the load is shared with adjacent girders is dependent (among other things) on the transverse stiffness of the deck. As the transverse stiffness of the deck increases relative to the longitudinal stiffness of the girder-deck system, more uniform load sharing results. Thus, more uniform load sharing in a bridge results from either a stiffer deck or softer girders.

Cuelho, et al. (2004) calculated the GDFs for the three Saco decks. The results reported in Table 13 represent the worst-case, single-truck loading scenario for an exterior girder with a single truck loading (the ST-R test line; refer to Figure 25). Referring to Table 13, the most uniform load sharing between girders occurs for the Empirical deck. Based upon a cursory review of the bridge configurations, this situation implies that the Empirical deck is stiffer in the transverse direction than the other two decks, since the longitudinal girders used in the bridges are identical. The previously calculated flexural stiffnesses (EI) in Table 12, however, indicate that the Empirical deck is the softest of the three decks in the transverse direction, as would be expected. Thus, a closer look at the longitudinal stiffness of the bridges is merited.

Relative to the other two decks, the Empirical deck has less longitudinal steel over the bents, in addition to the deck-wide reduction in the transverse steel. The removal of the steel over the bents greatly reduces the longitudinal stiffness of the whole deck. This softening was also confirmed by investigating several longitudinal gage responses. Due to the lower longitudinal stiffness, the GDF values make the Empirical deck appear stiffer in the transverse direction than the other two decks. Thus, the Empirical deck is softer

both longitudinally and transversely, which was expected from the reduction in steel volumes for this deck design.

Table 13 GDFs for longitudinal midspan, worst case for exterior girder

Deck	Girder 1	Girder 2	Girder 3	Girder 4
Conventional	60%	37%	16%	6%
Empirical	50%	32%	20%	18%
HPC	55%	36%	15%	14%

Evaluation of Linear-Elastic Behavior

A simple check on whether or not the Saco bridge decks are behaving linear elastically was made by determining if the Principle of Superposition is valid for these structures. The Principle of Superposition essentially states that in a linear system the effects caused by combined loadings may be predicted by the summation of individual effects due to each unique load in the combination. This principle has been used in scientific and engineering applications ranging from heat transfer to simple beam theory. AASHTO states that this principle also applies to the presence of multiple vehicles on a bridge deck. The validation of superposition should verify that the bridge decks are operating in the linear elastic realm.

To verify the applicability of the Principle of Superposition, the three Saco bridges were tested using two heavily loaded three-axle dump trucks, traveling side-by-side along the length of the bridge, as seen in Figure 46. If superposition is valid, strains calculated by adding together the strains measured during two single-truck (ST) events should

match the strains measure during a corresponding two-truck (TT) event. A minimum of (2) Two-Truck live load tests was conducted on each bridge. Each of the three bridges was subjected to a Two-Truck X-T (TT-XT) experiment and a Two-Truck W-R (TT-WR) experiment (refer to Figure 25 (b)).

Beginning with an actual two-truck event, the transverse strains measured during a TT-XT test at Gage Line D with the truck at the 40m position are presented in Figure 47. Figure 48 shows the same profile after the truck progressed farther along the bridge to the 42m truck position. To facilitate comparison between the 40m and 42m truck positions, Figure 49 shows an overlay of both the 40m (dashed) and 42m (solid) profiles for only the Conventional deck, which is typical of all three decks.

Figure 46 Test trucks preparing for a Two-Truck test

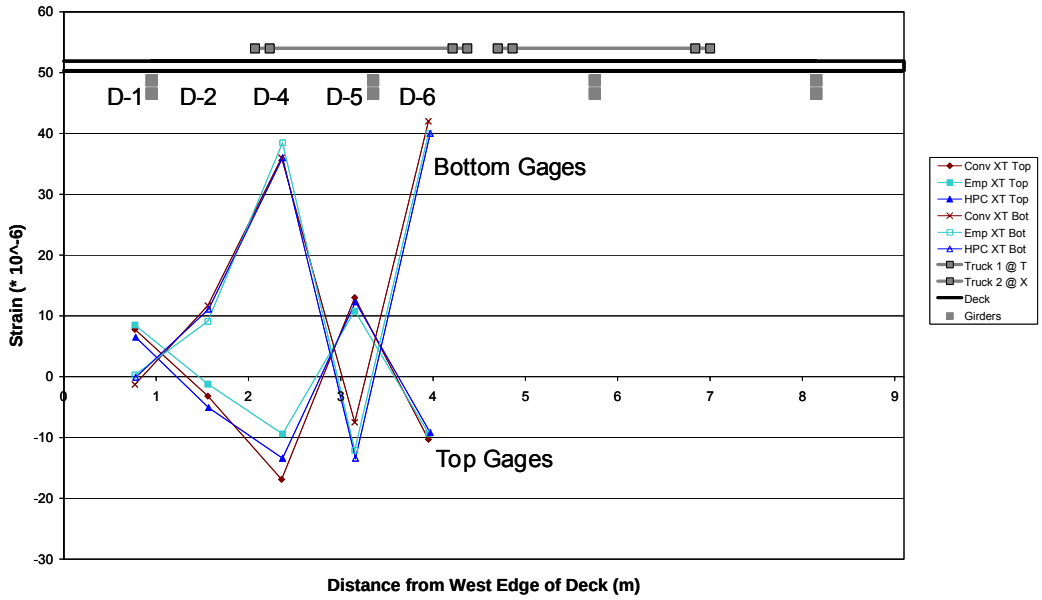

Figure 47 TT-XT transverse strain profile at 40m – All three decks

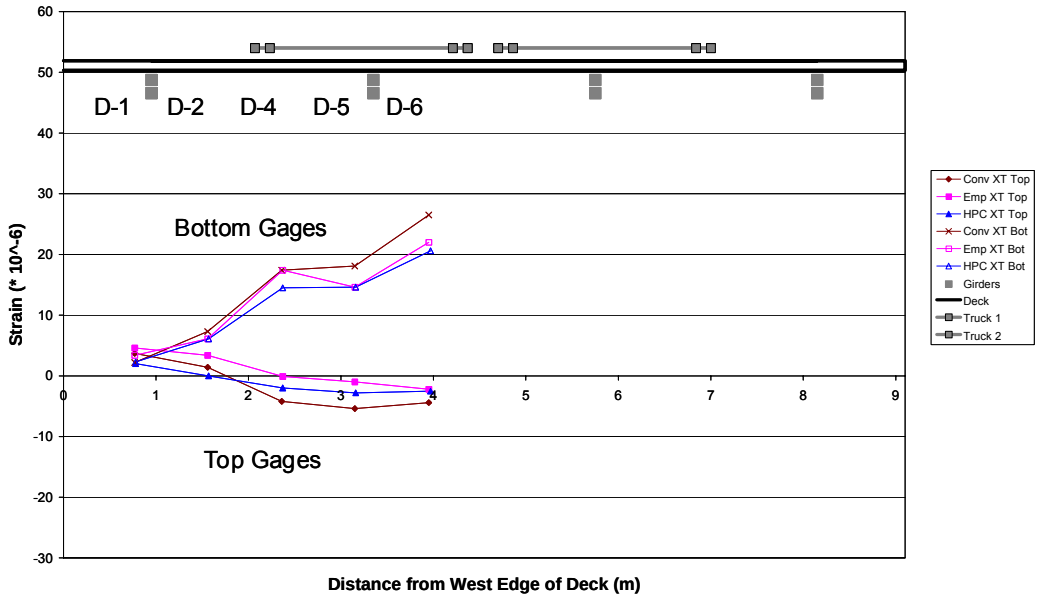

Figure 48 TT-XT transverse strain profile at 42m – All three decks

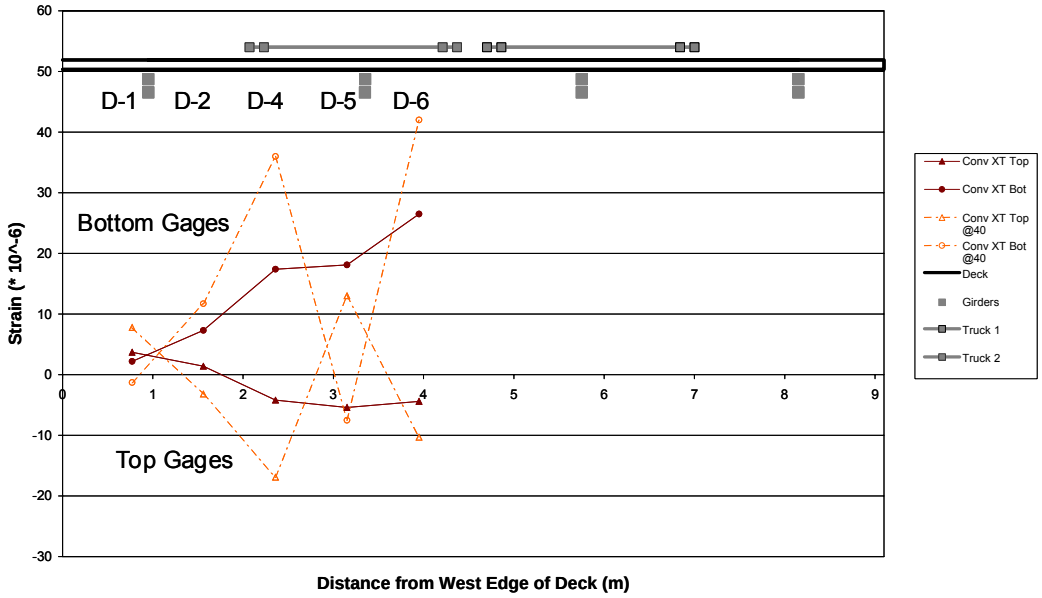

Figure 49 Conventional Deck TT-XT 40m (dash) profile overlaid on 42m (solid) profile

One notable phenomenon in the TT-XT test data is the relative reduction in the positive moment at Gage Location D-4, as compared to Tests ST-T or ST-U alone (which have very similar responses; see Figure 44). The φ values shown in Table 14 confirm that the positive moment at Gage Location D-4 is indeed lower in the Two-Truck experiments. Essentially, the presence of the second (east) truck induces negative moment in the instrumented lane of the first (west) truck, thereby reducing the positive moment induced by the first (east) truck in the instrumented section. However, this reduction in global positive moment accentuates the effect of the local negative moments over the girders in the presence of the truck tires. The result is a higher net negative moment at Gage Location D-5 than seen in the ST-T or ST-U tests alone at 40m. The maximum tensile value recorded in the top reinforcement gages at this point is only 13

με, corresponding to approximately 38 με in the top fiber of concrete. This strain is still relatively small compared with expected tensile cracking strains.

Table 14 Values of φ (in degrees) at Gage Location D-4

Londitudinal Position	Deck	ST-T	ST-U	TT-XT
40m	Conventional	31.24	30.57	26.52
	Empirical	29.49	29.49	23.44
	HPC	30.28	31.36	24.99
42m	Conventional	11.78	11.31	11.52
	Empirical	10.16	10.86	9.00
	HPC	10.42	12.66	8.85

Returning to superposition, strain data gathered from separate Single-Truck experiments (ST-T and ST-X) was added together and compared to the data gathered during the TT-XT Two-Truck experiment (Figures 47, 48, and 49). Figure 50 and Figure 51 display a typical comparison between the TT-XT test and the superimposed ST-T + ST-X experiments, for the 40m and 42m truck positions, respectively. With regard to shape and magnitude, the two transverse profiles look very similar overall, indicating superposition is valid.

The largest differences are observed at Gage Location D-2, but even these are nominal. In the presence of the truck tires (40m), the maximum difference between TT-XT and the superposition values for all three bridges was 8.1 με at Empirical gage D-2-Bottom. After the tandem axle had left the vicinity of Gage Line D (42m), the maximum difference between testing and superposition was 2.3 με on Conventional D-2-Bottom. It is unclear why these differences are so much larger than the other gage locations. Gage Location D-2 may be near the point of curvature reversal in the deck, and thus is greatly

influenced by minor variations in the specific locations of the tires. Moreover, the observed strain magnitudes are relatively small and thus more sensitive to minor test variations than comparatively larger strain magnitudes.

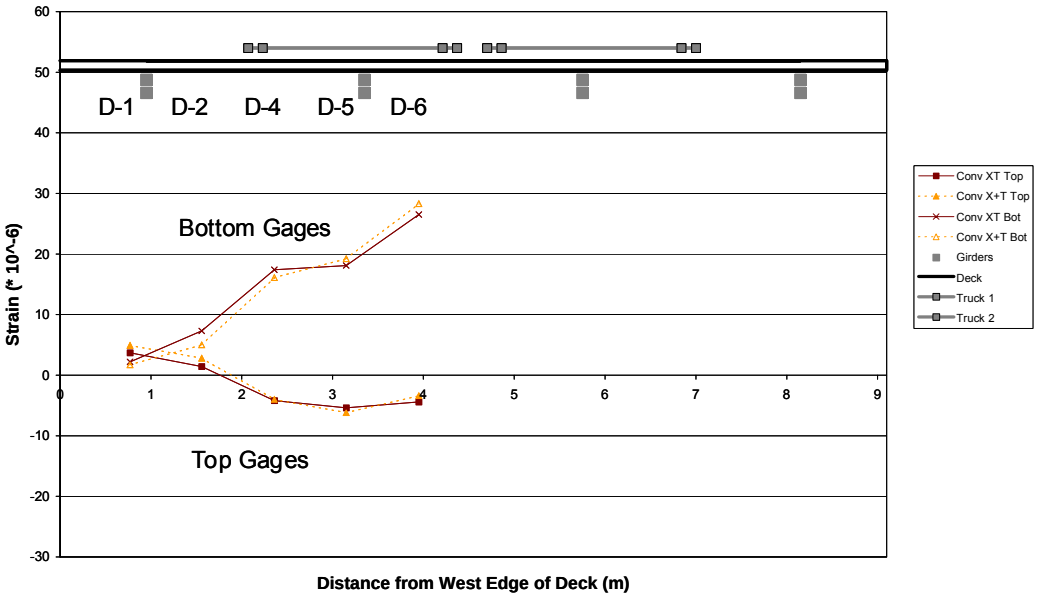

Figure 50 Typical TT-XT linear superposition comparison (Conventional deck at 42m)

Based on the evidence of the TT-XT testing, superposition works equally well for all three bridges. There are no apparent differences in performance between the three bridges. Similar results were obtained upon comparison of the TT-WR test response to the results obtained by adding ST-R and ST-V. In this case, ST-V was used to approximate position W, as no Single-Truck W test was conducted. Figure 52 and Figure 53 show the comparison between the actual TT-WR test data and the superposed single truck responses on the Conventional deck at the 40m and 42m truck positions, respectively. Considering the absence of data from a Single Truck W Test, superposition appears to work reasonably well on all three decks for the TT-WR testing, with little

difference observed between the response of the three decks. These results indicate that none of the decks is exhibiting non-linear response.

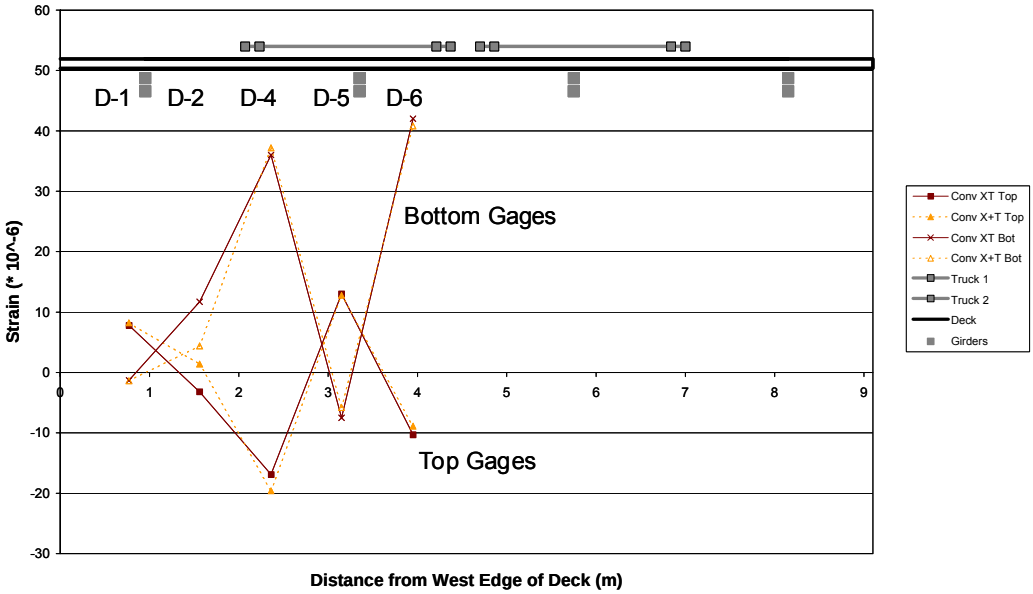

Figure 51 Typical TT-XT superposition comparison (Conventional deck at 40m)

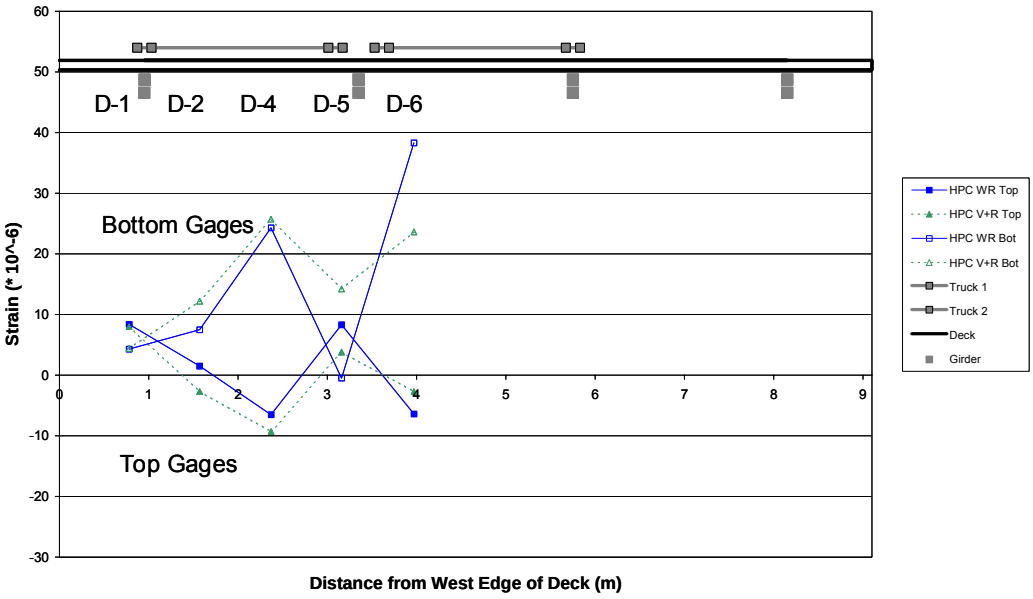

Figure 52 Typical TT-WR superposition comparison (HPC deck at 40m)

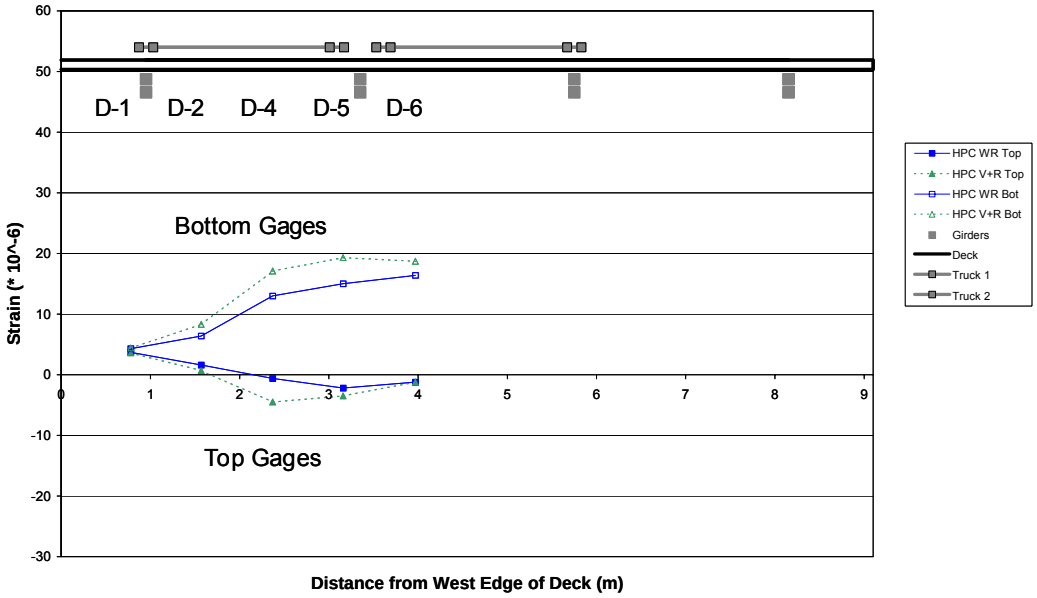

Figure 53 Typical TT-WR linear superposition comparison (HPC deck at 42m)

Review of Analysis Observations

Throughout the preceding analyses, several conclusions were arrived at through engineering judgment and analysis of the live load testing data. To briefly summarize:

- All three decks exhibit similar global longitudinal behaviors, and these behaviors are in agreement with expected behaviors.
- No longitudinal cracking of the concrete is evident from the strain data in the positive moment regions (lower concrete fibers) of any of the decks.
- The presence of in-plane axial forces are inferred from the strain data from each of the decks. Most of the reported axial strains are tensile and of relatively small magnitude (less than 10 με). Finite element analysis also confirmed the presence of axial tension in an uncracked deck.
- No internal arching is evident in any of the decks because none of the decks is cracked and little evidence of in-plane compression exists.
- No longitudinal cracking is evident from the strain data in the negative moment regions (upper concrete fibers) over the top of the girders of any of the three decks, nor is such cracking imminent

- Negative bending over the girders is not critical under live load demands.

- The Empirical deck is softest, both longitudinally and transversely, despite classic interpretation of the Girder Distribution Factors (GDFs), which gives the appearance that the Empirical deck is stiffer in the transverse direction.

- Linear superposition works well for all three bridge decks, indicating that all three decks are behaving linear-elastically.

- For the parameters analyzed in this thesis, no difference in performance (i.e., occurrence of cracking, non-linear behavior, or possible indication of accumulating damage) was observed between the three decks.

CHAPTER 7

SUMMARY, CONCLUSIONS, AND RECOMMENDATIONS

Summary

The deterioration of bridge decks in Montana prompted the Montana Department of Transportation (MDT) to investigate some possible solutions for mitigating this problem. Specifically, MDT was interested in evaluating procedures that reduce concrete cracking and the steel corrosion that results from corrosive agents accessing the steel via those cracks. Three new bridges with identical geometries being constructed near Saco, Montana within one mile of each other along the same roadway afforded an excellent opportunity for such an investigation. The bridges were built by the same contractor and the decks were poured within two weeks of each other. The only difference between the three bridges was the composition of the reinforced concrete deck. One bridge was designed using a conventional deck design, which is the standard design used by MDT, with a conventional concrete and conventional layout of reinforcement. The second bridge was built with an empirical deck, designed according to the AASHTO empirical deck design, allowing for a reduction in the volume of steel throughout the deck; thus, conventional concrete was used with a modified reinforcement layout. The third bridge deck was built with a High Performance Concrete (HPC) with the conventional reinforcement layout.

Prior to pouring the deck concrete on each bridge, a suite of strain and temperature sensors was installed in the decks. Concrete embedment strain gages and vibrating wire

strain gages were both used to monitor strains in the deck concrete; bonded-foil resistance strain gages were used to monitor strains in the reinforcing steel. Deck temperatures were recorded from thermistors built into the vibrating wire gages. During live-load testing only, four temporary strain transducers were mounted to the bottom surface of the concrete girders. A data acquisition system consisting of a datalogger, two multiplexers, supplemental Wheatstone Bridge circuitry, communication radios, and power components was assembled and located beneath the bridge to record, store, and transmit data from the sensors.

Prior to opening the bridges to regular traffic, live load testing was performed on each bridge. A series of eight low speed single-truck tests, five high speed single-truck tests, and two low speed two-truck tests was performed on each bridge. For this thesis, only the data sets from the low speed experiments were analyzed.

Strains recorded during the live load testing were analyzed to evaluate structural behaviors for each deck. Strain data recorded from longitudinally-oriented gages during these tests was analyzed to establish the validity of the measured response relative to expected direction and magnitude. Strains from transversely-oriented reinforcement gages were subsequently used to investigate deck behaviors unique to each deck design. This analysis investigated several aspects of the deck behavior, including longitudinal cracking, in-plane axial forces, deck integrity, relative deck stiffness, and general non-linear behaviors.

Conclusions

The primary conclusion from the live load data analysis is that all three bridge decks are behaving in a similar fashion. The shape and magnitude of strain response under vehicle loads matches expected behavior and is similar in the three decks. No evidence of concrete cracking in the deck was inferred in the live load data. Particularly, there was no evidence of cracking of the top of the decks over the girders, nor was there any indication that cracking will occur over the girders due to vehicle loads. Neither was there any evidence that cracking had occurred in the bottom of the deck at the time of live load testing. Moreover, there was no evidence of non-linear behavior in any of the three decks, as determined by examining strains via superposition; this implies that the decks are behaving linear-elastically.

During live load data analysis the height of the actual neutral axis within the cross-section was determined from strain data and used as a tool to evaluate whether deck cracking had occurred. After determining that cracking had not occurred in any of the decks, further investigation into shifts of the actual neutral axis height revealed in-plane axial forces acting in all of the decks. In-plane axial tension forces were inferred from the strain data in all of the tests, implying that traditional deck models derived from flexural beam bending do not fully capture true behaviors. In the absence of both cracking and in-plane axial compression forces, it was determined that no internal arching had begun to occur in the decks at the time of the first live load tests, which was expected at these load levels, based on the results of other research.

Although the behavior of all three decks was similar in nearly all respects, a few nominal differences were observed between them. These differences are merely behavioral differences noted during the analysis, which do not necessarily indicate any differences in the performance of each deck relative to long-term durability, cracking or corrosion. Longitudinal behavior over the bent was different between the three bridges, indicating differences between the three decks in the in-plane axial forces at this location. The stiffness of the three decks was also found to be different, both longitudinally and transversely. The Empirical deck was determined to be the least stiff in both directions, which was expected based upon the reduced steel volume throughout the entirety of this deck.

The analysis presented in this thesis serves as a baseline for the relative condition of the three bridges before any exposure to demands from traffic and the environment. Data obtained from long-term monitoring and the second live load test will provide a more complete body of evidence from which to make judgments about which deck design is "better".

Recommendations for Future Research

- Conduct the second live load experiment (already scheduled for summer 2005) and compare its results with the findings of this analysis. A few minor modifications to the test procedure are recommended:
    - Perform a Single-Truck W test to more precisely validate superposition.
    - While the truck is on the deck, carefully examine the upper and lower surfaces of the deck for cracks that would not be visible with the load removed. This will help to more conclusively validate the conclusions made from the strain data about cracking and internal arching.

  - Develop a system for indicating truck position on the deck during high-speed tests. At least provide some electronic mark when the truck enters and leaves the deck. Correlating the position of the truck with the recorded deck strains is valuable during interpretation.

- Analyze long-term data to evaluate differences in durability of the three decks due to variations in ambient conditions (mainly temperature). Watch for signs of cracking from temperature-induced stresses. Investigate any differences in structural behavior that might be a direct result of long-term stresses.

- Calibrate a finite element model of the bridge deck to provide predictive power and investigation of hypothetical load scenarios. Based on the results of this thesis analysis, the use of a linear elastic, uncracked model of the deck (in the transverse direction) is warranted until future data suggests that this is no longer true.

- Pursue laboratory testing on a representative model (i.e., beam between two girders) to correlate and evaluate in-the-field deck performance with lab testing. Favorable results from this type of testing could lead to a less demanding live load test regimen.

- Pursue a laboratory test that compares the relative behavior of three plates or beams with configurations simulating the three bridge decks. Of greatest interest is the internal arching behavior and how it differs between the three decks. Although prior research has proven the existence of the internal arching mechanism in the context of relatively large loads and ultimate failure, little has been done in the context of an already-cracked cross-section. This research might prove useful for decks cracked by fatigue, temperature-induced stresses, or some other mechanism.

  - This could be tested as a simply-supported beam with axial confinement, similar to the work of Fenwick and Dickson (1989).

  - A second test type re-creates the continuous nature of the deck over the girders by building a longer beam (i.e., deck strip).

- Investigate the occurrence of in-plane axial membrane forces in the deck via laboratory testing. Compare the membrane behaviors of: 1) a perfectly straight beam, 2) a beam with some upward camber, and 3) a beam with some downward sag. Most realistically, a bridge deck will begin with some small degree of downward sag, before any loading is applied. It is suggested that this initial deflection provides the shape change necessary to elongate the neutral axis of the beam, causing any added tire loads to easily induce in-plane axial tension without it being a non-linear response.

- Reduce the laboratory experimentation to a finite element analysis of the arching behavior, given the three different deck designs. This model would be required to represent cracking in the positive moment region of the beam, to initiate the arching behavior. Ideally, such a model would be calibrated against data from a laboratory experiment.

- For future live load bridge tests of this nature, create a strain gage to be embedded in the concrete that is not as susceptible to cracking as the embedded gages used in the current experiment, but allows for faster acquisition speeds than vibrating wires. Vibrating wire strain gages appear to resist damage in the presence of cracks, given their high survival rate even though located in regions known to be cracked.

REFERENCES CITED

AASHTO LRFD Bridge Design Specifications, 2nd ed. (2000 Interim). American Association of State Highway and Transportation Officials, Washington D.C.

Amer, A., Arockiasamy, M., Shahawy, M. (1999). "Load Distribution of Existing solid Slab Bridges Based on Field Tests", *Journal of Bridge Engineering*, ASCE, Vol. 4, No. 3, August, 1999, pp. 189-193.

Annex 1: Determination of Tensile Strain Capacity (1997). Publication number ETL 110-2-542, U.S. Army Corps of Engineering Internet Publishing Group, May 30, 1997. Retrieved April 24, 2004, from http://www.usace.army.mil/publications/eng-tech-ltrs/etl1110-2-542/annex1.pdf

Bakht, B., Al-Bazi, G., Banthia, N., Cheung, M., Erki, M., Faoro, M., et al. (2000). "Canadian Bridge Design code Provisions for Fiber-Reinforced Concrete Bridges", *Journal of Composites for Construction*, ASCE, Vol. 4, No. 1, February, 2000, pp. 3-15.

Bakht, B. and Lam, C. (2000). "Behavior of Transverse confining Systems for Steel-Free Deck Slabs", *Journal of Bridge Engineering*, ASCE, Vol. 5, No. 2, May, 2000, pp. 139-147.

Bakht, B. and Mufti, A. A. (1998). "Five Steel-Free Bridge Deck Slabs in Canada", *Structural Engineering International*, March 1998, pp. 196-200.

Boothby, T. E. and Laman, J. A. (1999). "Cumulative Damage to Bridge Concrete Deck Slabs Due to Vehicle Loading", *Journal of Bridge Engineering*, ASCE, Vol. 4, No. 1, February, 1999, pp. 80-82.

Cao, L. (1996). "Analysis and Design of Slab-on-Girder Highway Bridge Decks", PhD Dissertation. University of Colorado, August, 1996.

Cao, L., Shing, P. B., Allen, J., and Woodham, D. (1996). "Case Study of Concrete Deck Behavior Without Top Reinforcing Bars", *Proceedings of the Fourth International Bridge Engineering Conference, August 28-30, 1995, San Francisco, California*. pp. 100-109.

Csagoly, P. F. and Lybas J. M. (1989). "Advanced Design Method for Concrete Bridge Deck Slabs", *Concrete International*, May, 1989, pp. 53-63.

Cuelho, E., Stephens, J., Smolenski, P., and Johnson, J. (2004). "Evaluating Concrete Bridge Deck Performance: Interim Project Report", Expected completion May, 2004.

Fang, I. K., Worley, J., Burns, N. H., and Klingner, R. E. (1990). "Behavior of Isotropic R/C Bridge Decks on Steel Girders", *Journal of Structural Engineering*, ASCE, Vol. 116, No. 3, March 1990, pp. 659-678.

Fenwick, R. C. and Dickson, A. R. (1989). "Slabs Subjected to Concentrated Loading", *ACI Structural Journal*, V. 86, No. 6, Nov-Dec 1989, pp. 673-678.

French, D. L. (2002). "Finite Element Modeling of a Three Span concrete Slab on Stringer Bridge Deck to Determine Critical Instrumentation Locations", Professional Paper, Montana State University – Bozeman, June, 2003.

Gopalaratnam, V. S. and Shah, S. P. (1985). "Softening Response of Plain Concrete in Direct Tension", *ACI Journal*, May-June, 1985, pp. 310-323.

Hughes, G., Smith, J. S. C., and Kanagasundaram, S. (2000). "Remote Monitoring of Bridge Decks", *Concrete Engineering International*, May 2000, pp. 46-49.

Lenett, M. S., Hunt, V. J., Helmicki, A. J., and Aktan, A. E. (2001). "Instrumentation, Testing, and Monitoring of a Newly Constructed Reinforced Concrete Deck-on-Steel Girder Bridge – Phase III", *Report* # UC-CII 01/1, Cincinnati Infrastructure Institute, May 2001.

Mourad, S. and Tabsh, S. W. (1999). "Deck Slab Stresses in Integral Abutment Bridges", *Journal of Bridge Engineering*, ASCE, Vol. 4, No. 2, May, 1999, pp. 125-130.

Nassif, H., Suksawang, N., Gindy, M., Abu-Amra, T., and Davis, J. (2003). "Instrumentation and Field Testing of the Doremus Avenue Bridge", *Compendium of Papers CD-ROM of the 82nd Annual Meeting of the Transportation Research Board, January 12-18, 2003, Washington, D. C.*

Sargent, D. D., Ventura, C. E., Mufti, A. A., and Bakht, B. (1999). "Testing of Steel-Free Bridge Decks", *Concrete International*, August, 1999, pp. 55-61.

Stallings, J. M. and Porter, P. (2002). "Live Load Tests of Alabama's HPC Bridge", TE-036 Report, ALDOT Research Project 930-373, Auburn University Highway Research Center, 2002.

Tabsh, S. W. and Tabatabai, M. (2001). "Live Load Distribution in Girder Bridges Subject to Oversized Trucks", *Journal of Bridge Engineering*, ASCE, Vol. 6, No. 1, January/February, 2001, pp. 9-16.

Wang, C. K. and Salmon, C. G. (1985). *Reinforced Concrete Design* (4th Ed.). New York: Harper and Row.

Yang, Y. and Myers, J. J. (2003). "Live Load Test results of Missouri's First High Performance Concrete Superstructure Bridge", Paper No. 03-3717, *Compendium of Papers CD-ROM of the 82nd Annual Meeting of the Transportation Research Board*, *January 12-18, 2003, Washington, D. C.*